TECHNICAL REPORT SL-80-4

STRENGTH DESIGN OF REINFORCED-CONCRETE HYDRAULIC STRUCTURES

Report 6
ANALYTICAL STUDY OF THE ULTIMATE BEHAVIOR OF MODEL REINFORCED-CONCRETE CIRCULAR CONDUITS

by

Kurt H. Gerstle

Department of Civil, Environmental, and
Architectural Engineering
University of Colorado
Boulder, Colorado 80302

July 1987
Report 6 of a Series

Approved For Public Release; Distribution Unlimited

Prepared for DEPARTMENT OF THE ARMY
US Army Corps of Engineers
Washington, DC 20314-1000

Monitored by Structures Laboratory
US Army Engineer Waterways Experiment Station
PO Box 631, Vicksburg, Mississippi 39180-0631

my Corps
gineers

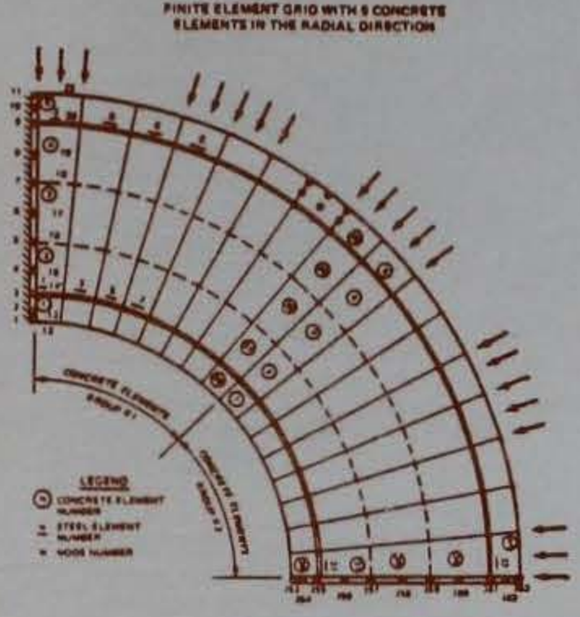

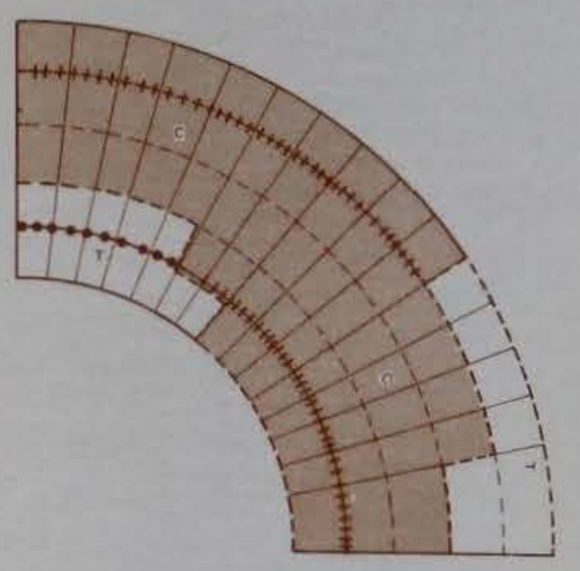

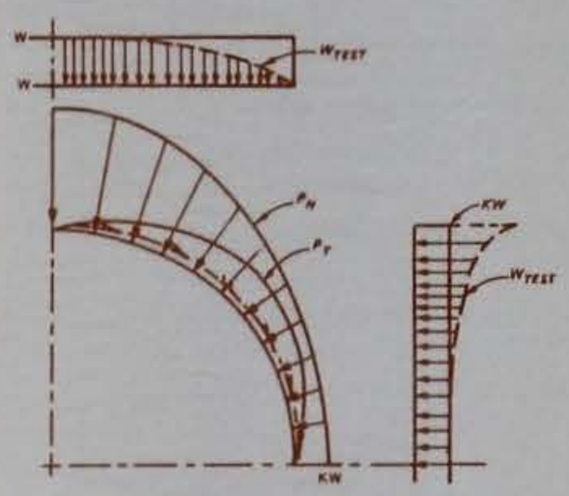

STRUCTURES LABORATORY

Unclassified
SECURITY CLASSIFICATION OF THIS PAGE

REPORT DOCUMENTATION PAGE

Form Approved
OMB No. 0704-0188
Exp. Date: Jun 30, 1986

1a. REPORT SECURITY CLASSIFICATION
Unclassified

1b. RESTRICTIVE MARKINGS

2a. SECURITY CLASSIFICATION AUTHORITY

2b. DECLASSIFICATION/DOWNGRADING SCHEDULE

3. DISTRIBUTION/AVAILABILITY OF REPORT
Approved for public release; distribution unlimited.

4. PERFORMING ORGANIZATION REPORT NUMBER(S)

5. MONITORING ORGANIZATION REPORT NUMBER(S)
Technical Report SL-80-4

6a. NAME OF PERFORMING ORGANIZATION
University of Colorado

6b. OFFICE SYMBOL (*If applicable*)

7a. NAME OF MONITORING ORGANIZATION
USAEWES
Structures Laboratory

6c. ADDRESS (*City, State, and ZIP Code*)
Boulder, CO 80302

7b. ADDRESS (*City, State, and ZIP Code*)
PO Box 631
Vicksburg, MS 39180-0631

8a. NAME OF FUNDING/SPONSORING ORGANIZATION
US Army Corps of Engineers

8b. OFFICE SYMBOL (*If applicable*)

9. PROCUREMENT INSTRUMENT IDENTIFICATION NUMBER

8c. ADDRESS (*City, State, and ZIP Code*)
Washington, DC 20314-1000

10. SOURCE OF FUNDING NUMBERS

PROGRAM ELEMENT NO.	PROJECT NO.	TASK NO.	WORK UNIT ACCESSION NO.

11. TITLE (*Include Security Classification*)
Strength Design of Reinforced-Concrete Hydraulic Structures; Analytical Study of the Ultimate Behavior of Model Reinforced-Concrete Circular Conduits

12. PERSONAL AUTHOR(S)
Gerstle, Kurt H.

13a. TYPE OF REPORT	13b. TIME COVERED	14. DATE OF REPORT (*Year, Month, Day*)	15. PAGE COUNT
Report 6 of a series	FROM _____ TO _____	July 1987	84

16. SUPPLEMENTARY NOTATION
Available from National Technical Information Service, 5285 Port Royal Road, Springfield, VA 22161.

17. COSATI CODES		
FIELD	GROUP	SUB-GROUP

18. SUBJECT TERMS (*Continue on reverse if necessary and identify by block number*)
See reverse.

19. ABSTRACT (*Continue on reverse if necessary and identify by block number*)

A series of tests of model reinforced-concrete rings simulating culvert sections under radial loads was carried out at WES. These tests are described in Report 5 of this series. The purpose of this study was to perform nonlinear finite element analyses of these models, to compare analytical results with test results, and to produce a realistic strength design methodology for these structures.

20. DISTRIBUTION/AVAILABILITY OF ABSTRACT
☐ UNCLASSIFIED/UNLIMITED ☒ SAME AS RPT. ☐ DTIC USERS

21. ABSTRACT SECURITY CLASSIFICATION
Unclassified

22a. NAME OF RESPONSIBLE INDIVIDUAL

22b. TELEPHONE (*Include Area Code*)

22c. OFFICE SYMBOL

DD FORM 1473, 84 MAR

83 APR edition may be used until exhausted.
All other editions are obsolete.

SECURITY CLASSIFICATION OF THIS PAGE

Unclassified

18. SUBJECT TERMS (Continued).

Circular concrete conduits
Load confinement
Model test
Nonlinear finite element analysis
Strength design
Ultimate behavior

Preface

This study was conducted during the period September 1984 through September 1985 by Department of Civil, Environmental, and Architectural Engineering, (CEAE), University of Colorado, under the sponsorship of the Office, Chief of Engineers (OCE), US Army. The Technical Monitors were Mr. Don Dressler and Dr. Tony Liu.

This work was conducted under the supervision of Messrs. Bryant Mather, Chief, Structures Laboratory (SL), and James T. Ballard, Assistant Chief, SL, and Dr. Jimmy P. Balsara, Chief, Structural Mechanics Division (SMD), SL. Mr. Vincent P. Chiarito, SMD, monitored the work. Dr. Robert L. Hall, SMD, coordinated the publication of the work. Valuable discussions were held with Messrs. C. Dean Norman, Concrete Technology Division, SL, and Stephen Wright, SMD.

Dr. Kurt H. Gerstle, CEAE, was the principal investigator. Mr. Thomas Stankowski, CEAE, implemented the nonlinear finite element program, SMART, which had been written by Dr. Kaspar William, CEAE. Messrs. Mohammed Ayari and Stankowski, graduate assistants, CEAE, provided technical assistance.

COL Dwayne G. Lee, CE, is Commander and Director of WES. Dr. Robert W. Whalin is Technical Director.

Contents

Conversion Factors, Non-SI to SI (Metric) Units of Measurement

Non-SI units of measurement used in this report may be converted to SI (metric) units as follows:

Multiply	By	To Obtain
Fahrenheit degrees	5/9	Celsius degrees or kelvins*
inches	25.4	millimetres
kip-inches	112.9848	newton-metres
kips (force)	4.448222	kilonewtons
kips (force) per square inch	6.894757	megapascals
pounds (force)	4.448222	newtons
pounds (force) per square inch	6.894757	kilopascals
square inches	6.4516	square centimetres

* To obtain Celsius (C) temperature readings from Fahrenheit (F) readings, use the following formula: $C = (5/9)(F - 32)$. To obtain Kelvin (K) readings, use: $K = (5/9)(F - 32) + 273.15$.

ANALYTICAL STUDY OF THE ULTIMATE BEHAVIOR OF MODEL REINFORCED-CONCRETE CIRCULAR CONDUITS

Introduction

Objective and Scope

1. In 1984, a series of tests of model reinforced-concrete rings simulating culvert sections under radial loads was carried out at the US Army Engineer Waterways Experiment Station (WES).* The purpose of this study was to perform nonlinear finite-element analyses of these models, to compare analytical results with test results, and to produce a realistic strength design methodology for these structures. These analyses, comparisons, and methodology were developed by the Department of Civil, Environmental, and Architectural Engineering (DCEAE) of the University of Colorado.

Redistribution of the Applied Loads

2. The printout of loads applied to these rings tested indicates that, particularly in the thin rings, it was difficult to maintain the specified load ratios. In general, the load ratio actually applied tended toward equal intensities of crown and springing load intensities, closer to hydrostatic loading. Fig. 1, for instance, shows that in Specimen 8-1 (R/H = 4.0, specified load ratio 3:1), the actual load ratio was closer to 2.2:1. This indicates that these rings tried to readjust their loads closer to a distribution that they were best able to resist (the smartness of the structure).

3. Even for the thicker rings, it appeared that close to failure (after progressive degradation of stiffness), the minor (springing) load tried to catch up with the major (crown) load. Fig. 2 shows that in Specimen 5-1 (R/H = 2.4) the load ratio during the last load increment decreased from the specified value of 3:1 to an actual value of 2.6:1. This redistribution would cause an apparent strength increase of the ring, leading to higher applied test loads than predicted by analysis (based on the specified load ratio).

---

* S. Wright and V. Chiarito. In preparation. "Strength Design of Reinforced-Concrete Hydraulic Structure: Report 5," Technical Report SL-87-4, US Army Engineer Waterways Experiment Station, Vicksburg, Miss.

4. Based on these observations, one might predict that buried concrete culverts will try, through soil-structure interaction (SSI), to redistribute the soil pressure in a beneficial way. Realistic strength prediction of such structures should be based on an analysis that includes the inelastic behavior of both the structure and soil so that this redistribution (SSI) is included.

Selection of Non-Linear Model

5. The finite-element analysis of the rings was carried out by use of the computer program SMART (Structural Matrix Analysis for Reactor Technology), developed by Dr. Kaspar Willam and Associates at the Institute for Statics and Dynamics, University of Stuttgart, Germany. This is an analysis program specifically developed for the nonlinear analysis of large reinforced-concrete structures. Its features are briefly discussed in the following paragraphs.

Material Formulation

6. Concrete is assumed to act elastically, following the general Hooke's Law for isotropic materials, until attainment of the elastic limit. The elastic modulus and Poisson's ratio for the elastic concrete were taken from Table 1.

7. In tension, the elastic limit will occur when the major principal tensile stress reaches the uniaxial tensile strength value f'_t, as specified in the current data from split cylinder tests. At this instance, a smeared crack forms across the element in a direction normal to the principal tensile stress direction, and all tensile strength is lost across this crack.

8. In compression, the elastic limit is determined by a Mohr-Coulomb failure criterion as shown in Fig. 3a. This failure condition can be specified by two quantities, the cohesion c and the angle of internal friction $\emptyset$. To determine these two quantities, a series of triaxial compression tests under different values of confining pressure is required. Since in the WES tests only the uniaxial compression strength f'_c was available, a standard value of $\emptyset = 43.6°$ C from the literature was used. From this and the uniaxial compression strength given in Table 1, the cohesion was calculated by

$$c = \frac{1 - \sin\phi}{2\cos\phi} \cdot f'_c$$

leading to values of c between 0.7 and 0.8 ksi.*

9. In principal stress space, $\sigma_1 - \sigma_3$, this failure envelope takes the shape shown in Fig. 3b. It is independent of the intermediate principal stress, σ_2.

10. Beyond the compressive elastic limit, the lesser compression stress, σ_3, is adjusted so that the stress state satisfies the Mohr-Coulomb failure envelope, as shown by the dashed Mohr's circle in Fig. 3a. The corresponding strain increments, $\Delta\varepsilon_3$, are computed from these stress increments, $\Delta\sigma_3$, according to elastic theory.

11. Steel is assumed to be uniaxially elastic-perfectly plastic, with elastic modulus and yield strength specified in Table 2. It was later observed from the detailed report of the steel tests that the measured yield strengths for the D1 and D3 reinforcement varied over a wide range, so the average values given in Table 2 might not be appropriate for all specimens reinforced with these bars.

Numerical Method

12. Program SMART follows the finite element method in its displacement formulation, assuming small deflection theory and material nonlinearities incorporated in appropriate isoparametric high-order elements. Material nonlinearities such as tensile cracking or compressive crushing are accounted for by the initial stress method: for each load increment an elastic analysis is performed, and those stresses that are incompatible with the current state of the material are cancelled out by superimposing opposite loads; for instance, stresses are rerouted around a new crack in the concrete in this fashion. This incremental-iterative process must be carried out for each element at each load step and is time-consuming, a typical feature of nonlinear analysis.

13. The DCEAE analysis considered only proportionally increasing loadings. Thus, it was unable to account for the redistribution mentioned earlier, which resulted in variable load ratio under increasing loads. Analyses that include this effect would be considerably more demanding and were considered outside the scope of this investigation.

---

* A table of factors for converting non-SI units of measurement to SI (metric) units is presented on page 3.

14. Both spatial discretization of the structure and the number of load steps needed to represent any load history should be investigated by means of a thorough convergence study using different degrees of fineness. Time and budget limitations prevented such a study, but DCEAE believes that the mesh and load steps selected are adequate for reliable results.

Output

15. Typical output for each load step consists of nodal deflections, reactive forces at constrained nodes, element stresses and strains, and indication of cracking or compressive crushing at element integration points. With loading histories consisting of 15 to 25 load steps, vast reams of output were obtained. Since no graphic postprocessor is attached to this program, data had to be manually transferred from this output for plotting or further processing.

16. The internal stress resultants at the crown and springing lines were computed by numerical integration of the recorded analytical reactions at these support sections of the quarter ring.

Analysis of Tested Structures

17. In this section, the results of the analyses of six specimens under loadings simulating those actually applied in test are presented. In the case of the thin rings, the specified load ratio differed from that actually applied. In such cases, the analysis is for the actual load ratio deduced from the record of the applied test loads. The material properties for these specimens were taken from Tables 1 and 2.

18. The analytical deflection and strain results at the different load levels are superimposed on the previously determined experimental load-deflection and load-strain curves.

19. Thrusts and moments at the crown and springing sections were computed by integration of the nodal reactions at these support sections of the quarter ring for various load levels. They were checked for satisfaction of equilibrium of the structure, and the thrust-moment combinations were then

superimposed on the thrust-moment strength envelopes for the different specimens obtained from Wright and Chiarito.*

20. The first concrete cracking, crushing, and steel yielding were recorded, and the damaged concrete regions at high load levels were mapped.

21. The format of the presentation of these analytical results will follow a uniform scheme for each specimen: comments regarding specimen, loading and results, finite-element mesh, load-deflection curves, and crack pattern near failure.

Specimens 2-1, 2-2, and 2-3

22. Specimens 2-1, 2-2, and 2-3 were thick (R/H = 1.5). Load ratio was variable, of values 2:1, 3:1, and 4:1. Specified and actual load ratios checked well. These three rings were modeled as shown in the finite-element mesh with 80 nine-node isoparametric concrete elements and 32 three-node steel elements for one-quarter of the ring.

23. The loads were distributed to model postulated uniform load distribution under the 2-1/2-inch-wide steel loading plates, Fig. 4. A total of 10 to 15 load steps to failure were used in the analysis, with smaller load steps under higher loads when pronounced nonlinearities occurred.

Specimen 2-1

24. In Specimen 2-1, the analytical deflection underestimated the measured deflections considerably. However, the actual strength was slightly overestimated.

25. Strains at crown and springing sections had no correlation between analytical and measured strains, Fig. 5.b. The experimental strain channels appear to have been mixed up, because very good correlation could be achieved by suitable relabeling, Fig. 7.

26. First cracking was indicated by analysis at a much lower load level than observed. The analysis predicted crushing at springing intrados, as observed.

---

* Wright and Chiarito, op. cit.

27. Moment-thrust combinations were computed at both crown and springing sections, Figs. 8 and 9, that were greatly in excess of the strengths predicted by the interaction curves. Fig. 10 displays the crack pattern for Specimen 2-1.

Specimen 2-2

28. In Specimen 2-2, measured deflections across the crown diameter were underestimated by the finite-element analysis, and those across the springing diameter were overestimated, Fig. 11. Instability of the structure was predicted at a value about 5 percent less than the test strength.

29. Reasonable correlation between measured and calculated strains in both steel and concrete was obtained Figs. 12 and 13. It should be noted that measured extrados concrete strains at the crown were much less than the extrados steel strains. Any theory, that assumes perfect bond would predict the opposite, as shown in the dashed curves.

30. Both cracking and crushing at the springing section was predicted to occur much earlier than was observed.

31. The section strength predicted by the interaction envelopes, Figs. 14 and 15, was exceeded considerably by the calculated values of thrust and moment at both the crown and springing sections. Fig. 16 displays the crack pattern for Specimen 2-2.

Specimen 2-3

32. Specimen 2-3, subject to a load ratio of 4:1, had more bending action and correspondingly less thrust at the critical sections than the earlier Specimens 2-1 and 2-2. This was indicated by the thrust-moment curves, which showed close to balanced failure.

33. The crown deflections were again underestimated by analysis, Fig.17. Strength checked very well.

34. At the crown section, extrados steel and concrete strains were well predicted, Figs. 18 and 19. Intrados steel strains were off, but there might well have been some lag in the recorded steel strains on this side.

35. At the springing section, conversely, much larger extrados steel strains are recorded than were predicted. Intrados steel and concrete strains showed reasonable agreement.

36. The moment-thrust paths, Figs. 20 and 21, show similar trends to the earlier specimens. These figures show initial coincidence with the linear solution labeled 2-D. Under higher loads, the figures indicated slight deviation at the crown toward increased moment, and at the springing section a deviation toward increased thrust. Failure was near balanced, under internal-force combinations considerably larger than predicted by the strength envelopes.

37. These analyses seem to predict both cracking and crushing at a much earlier stage than could be observed during test.

38. Computer output for this specimen was sent to WES prematurely and was unavailable to DCEAE to plot the failure mode.

Specimen 5-1

39. Specimen 5-1, as well as Specimen 6-2, was of intermediate thickness, R/H = 2.4 . The specified load ratio was followed during the test until the last load increment neared failure.

40. The same finite-element subdivision was used as in Specimen 2, consisting of 80 nine-node isoparametric concrete element, and 32 three-node steel bar elements.

41. The analysis underestimated both the structure deflections, Fig. 22, and overestimated the strength of the ring, by a considerable margin.

42. Reasonable correlation was obtained between predicted and measured strains at crown and springing, although the intrados springing concrete strain was underestimated by a wide margin, Figs. 23 and 24.

43. The calculated thrust-moment combinations at crown and springing, Figs. 25 and 26, again showed much more strength than was indicated by the strength interaction curves. Fig. 27 displays the crack pattern for Specimen 5-1.

Specimen 6-2

44. Specimen 6-2 was modeled for finite-element analysis as shown in Fig. 28, with 64 nine-node isoparametric concrete elements and 32 three-node steel bar elements.

45. Deflections and strains correlated reasonably well between analysis and testing, Figs. 29, 30, and 31, but the ring strength was underestimated by analysis by about 15 percent.

46. Thrusts and moments at critical sections, Figs. 32 and 33, again indicated more strength than was shown by the interaction envelope. Fig. 34 displays the crack pattern for Specimen 6-2.

Specimen 8-1

47. The remarkable feature of this analysis is the tremendous overestimation of the actual strength of the ring in Specimen 8-1, Fig. 35. This was a thin ring, $R/H = 4.0$, and failure was ductile, involving yielding of the steel, Figs. 36 and 37.

48. Why the analysis results in such unduly high strength is not understood. Further study of the data is necessary to explore the sequence of cracking and crushing of the ring.

49. Again, the moment-thrust curves indicated that the strength envelopes were extremely conservative, Figs. 38 and 39. Fig. 40 displays crack patterns for Specimen 8-1.

Analysis of the Effect of EM Load Distribution

50. Considerable insight into the relation between the effects of the radial test loading and the uniform EM loading that it is intended to represent can be gained by a study of the equilibrium of applied and internal forces.

Equilibrium

51. The EM loading consists of uniform vertical pressure w and uniform lateral pressure kw as shown in Fig. 41. The radial or normal pressure is

$$p_N = \frac{w}{2}[(1 + k) - (1 - k) - (1 - k)\cos 2\theta] \qquad (1)$$

The tangential, or shear traction, on the ring is

$$p_T = \frac{w}{2} (1 - k) \text{Sin}2\theta \qquad (2)$$

52. The vertical and horizontal resultants of the radial pressure p_N on the quarter ring, and therefore the axial forces N_{sp} and N_{cr} on the springing and crown sections due to the radial pressure only (the test loading), are by integration of the Y- and X-components of p_N

$$N^N_{sp} = \frac{wR}{3} (2 + k) = \frac{8}{3\pi} P_{cr} (2 + k) \qquad (3)$$

$$N^N_{cr} = \frac{wR}{3} (2k + 1) = \frac{8}{3\pi} P_{cr} (2k + 1)$$

In Equation 3, the concentrated crown load P_{cr} for the 16-point test loading is calculated by multiplying the distributed load w by the tributary length $2\pi R/16$.

53. The vertical and horizontal resultants of the tangential tractions p_T on the quarter ring, and therefore the axial springing and crown forces due to these shears, are

$$N^T_{sp} = \frac{wR}{3} (1 - k) \qquad (4)$$

$$N^T_{cr} = \frac{wR}{3} (k - 1)$$

The sums of Equations 3 and 4, which satisfy equilibrium with the EM loads, are

$$N_{sp}^{N} + N_{sp}^{T} = wR \tag{5}$$

$$N_{cr}^{N} + N_{cr}^{T} = k \cdot wR$$

54. If only the radial pressure is applied, as in the WES test loading, the total axial springing and crown forces due to the EM loading are underand overestimated by the ratio of the forces of Equations 3 and 5:

$$\frac{N_{sp}^{test}}{N_{sp}^{EM}} = \frac{1}{3}(2 + k); \quad \frac{N_{cr}^{test}}{N_{cr}^{EM}} = \frac{1}{3}(2 + \frac{1}{k}) \tag{6}$$

The radial and tangential pressures, as given by Equations 1 and 2, are shown in Fig. 42. The neglect of the latter, as in the WES tests, is equivalent to the change of the uniform EM loads w and kw to the variable loads marked w_{Test} in Fig. 42. The ratios of the areas underneath the two stress distributions that represent the resultant loads are given by Equation 6.

55. Referring to the freebody of Fig. 43 of the quarter ring under EM loads, moment equilibrium requires the

$$M_{cr} + M_{sp} = \frac{wR^2}{2}(1-k) \tag{7}$$

For radial components only, applied in the test loading, moment equilibrium of the freebody of Fig. 43 (moment center at "0" for convenience) and use of Equation 3, require that

$$M_{cr} + M_{sp} = \frac{wR^2}{3}(1 - k) \tag{8}$$

56. The sum of the moments under EM loading is always greater by 50 percent than that under test loading.

57. Any solution, elastic or inelastic, must satisfy Equations 3 and 8 for the test loading, and Equations 5 and 7 for the EM loading.

Hypothesis Regarding Strength Under EM and Under Test Loadings

58. Combining Equations 3 and 8 for test loading, and Equations 5 and 7 for EM loading, the following is obtained:

$$N_{sp}^{Test} = \frac{2 + k}{1 - k} \cdot \frac{1}{R} (M_{sp} + M_{cr})$$

$$N_{sp}^{EM} = \frac{2}{1 - k} \cdot \frac{1}{R} (M_{sp} + M_{cr})$$

Assuming now that for a given ring at failure, the sum of moments $(M_{cr} + M_{sp})$ is a constant for any loading, then the ratio of the springing loads, which is equal to the ratio of the total applied vertical loads, is

$$\frac{N_{sp}^{Test}}{N_{sp}^{EM}} = 1 + \frac{k}{2} \qquad (9)$$

Since this is always greater than unity, it is concluded that the total test loading at failure will always exceed the total EM loading at failure.

59. Unfortunately, the computer results that follow do not bear this conclusion. Further analysis of the finite-element results should be carried out to explore the actual moments and thrusts at the critical sections at failure.

Comparison of Ring Behavior and Strength Under Test and EM Loadings

60. Figs. 44 through 49 show total vertical load versus crown deflection curves for the six specimens that were analyzed. Two different loading conditions were considered for each specimen: the testing load (also called 16-Point Loading) and the EM loading. The curves for the two loading conditions are superimposed in each plot for easy comparison.

61. Contrary to Equation 9, which predicted greater total load at failure under test than under EM loading, all of these plots indicate greater capacity under EM loading, ranging from a few to well over 70 percent. Obviously, the hypothesis that the sum of the crown and springing moments at failure might be constant (on which Equation 9 was based) must be incorrect.

62. A detailed study of the combinations of thrust and moment at crown and springing under which failure occurred is required to shed light on the actual conditions that controlled failure under both loading conditions. The cited strength increase of over 70 percent in the case of Specimen 8-1 seems quite implausible. Further analytical studies and possibly some testing might be useful to understand these predictions and their validity. Unfortunately, these are notwithin the scope of the project, but DCEAE strongly suggests that these be done at an appropriate time.

Analysis of the Effect of Load Confinement

Effect of In-Plane Confinement

63. Specimen 2-1, R/H = 1.5, R = 7.5 in., was analyzed by the finite-element method for the following loadings: 2-point, 4-point, 8-point, and the previously considered 16-point test loading. The finite-element grid and the material properties were identical to those used earlier.

64. Figs. 50 and 51 show the load-deflection curves resulting from these analyses. In this plot, the total vertical load resultant, equal to twice the thrust at springing line, was used as a common load indicator, rather than the previously used crown load, which would be meaningless in this case.

65. These curves clearly show the beneficial effect of confinement on the ring strength. They also indicate the transition from a ductile, bending-type behavior for the two-point load, to a brittle, compression-type failure under increasing confinement.

Effect of Out-of-Plane Confinement

66. In simulating a long culvert pipe by means of a short ring, as was done in the WES tests, the situation is converted from a plane-strain to a plane-stress problem. This raises the question of the relation of the stiffness and strength of the former to the latter.

67. In classical linear elasticity, the stiffness in plane strain is increased by the ratio $1/(1 - \nu^2)$ over that in plane stress. The actual stresses remain the same. Under inelastic behavior, the situation is more complex, but it might be expected that for specimens in which failure is due to spalling of the concrete under in-plane compression, the strength increase might be considerable. This is borne out by the plane-strain analysis of Specimen 2-1, which was selected for this analysis because it failed basically by crushing of the compression concrete. Fig. 52 shows a great strength increase due to the assumption of plane strain for this specimen. The experimental curve indicated that the actual specimen was closer to the plane-stress condition.

68. On the other hand, in predominant bending, when failure is initiated by yielding of the steel, the increase of strength due to plane strain might be minor. Fig. 53, which shows the load-deflection curve for Specimen 8-1, verifies this condition. Fig. 52 provides food for thought regarding the relationship of plane-stress test results and the actual plane-strain condition prevailing in long pipes in the ground.

Design Recommendations

69. Specific design recommendations need much more study, but as a possible approach, DCEAE suggests a simplified approach that may have possibilities, pending further comparison with experimental and finite-element results.

Simplified Strength Analysis

70. Rings tested at WES collapsed in general by discrete failure at critical sections. Plastic analysis assuming discrete hinge formation at the crown and springing sections appears to be a useful approach to the determination of collapse loads on these rings. Such an analysis presumes ductile failure. If the assumption of perfect ductility is not satisfied, the plastic collapse load provides an upper bound, or overestimation, of the actual strength of the rings. Furthermore, because of the simplicity of the method, the influence of various factors, such as the distribution of the applied loads, can be explored easily and systematically.

Approach

71. Plastic or collapse analysis must satisfy two conditions:

a. Equilibrium, or static admissibility. At no point on the structure may the section or member strength be exceeded--if the structure can stand up, it will.

b. Collapse, mechanism condition, or kinematic admissibility. The member strength must be reached at sufficient points to permit the structure to collapse--if the structure can collapse, it will. The member strength will be obtained from the axial force-moment strength interaction curves provided in Wright and Chiarito.*

72. Equilibrium conditions for these rings under test and EM loadings have been discussed, and Equations 1 through 8 will be used in the current section. Using the relations, the ring strengths under these two loading conditions will be determined and applied to several of the test specimens.

Strength of Sections

73. Personnel at DCEAE visualize ring collapse as shown in Fig. 17. To satisfy the condtions of static and kinematic admissibility, they set the moments at the crown and springing sections equal to their strengths. The member strengths under axial load N_o and moment M_o are given by the strength interaction curves of Wright and Chiarito,* which have the shape shown in Fig. 54. To simplify the analysis, the curved portions representing tension and compression failure are replaced by straight lines that can be represented by the equation

$$N_o = a + b \cdot M_o \tag{10}$$

where a and b are determined from the curve fitting procedure shown in Fig. 55.

74. In addition to pure tension or compression failure, DCEAE could also visualize ring collapse by attainment of plastic hinges near the balance point. In this case, the moment is equal to the value indicated by the

---

* Wright and Chiarito, op. cit.

vertical cutoff and inserted into Equation 7 or 8. A check for the proper regime is the cost of the discontinuities inherent in the linearizations. An alternate method would be to express the strength envelope as a continuous function, but the nonlinearity of this expression would require a trial-and-error solution.

Ring Strength Under EM Loading

75. From Equation 7, and letting the uniform collapse load be called w_p

$$M_{o\,cr} + M_{o\,sp} = \frac{W_p R^2}{2}(1 - k) \tag{11}$$

76. From Equation 5,

$$N_{o\,cr} = k \cdot W_p R: \; N_{o\,sp} = W_p R \tag{12}$$

77. Solving Equation 10 for M_o, substituting Equation 12, and into Equation 11, the following is obtained:

$$w_p = \frac{\frac{a_{cr}}{b_{cr}} + \frac{a_{sp}}{b_{sp}}}{R\left[\left(\frac{k}{b_{cr}} + \frac{1}{b_{sp}}\right) - \frac{R}{2}(1 - k)\right]} \tag{13}$$

When the crown and springing sections are equal and both fail in either tension or compression, then $a_{cr} = a_{sp} \equiv a$, and $b_{cr} = b_{sp} \equiv b$, and Equation 13 simplifies to

$$w_p = \frac{4a}{R} \frac{1}{2(1 + k) - b(1 - k)R} \tag{14}$$

Ring Strength Under Test Loading

78. From Equation 8,

$$M_{o\,cr} + M_{o\,sp} = \frac{w_p R^2}{3}(1 - k) \tag{15}$$

79. From Equation 3,

$$N_{o\,cr} = \frac{w_p R}{3}(2k + 1);\ N_{o\,sp} = \frac{w_p R}{3}(2 + k) \tag{16}$$

80. Solving Equation 10 for M_o, substituting Equation 16, and substituting into Equation 15, the following is obtained:

$$w_p = \frac{\frac{a_{cr}}{b_{cr}} + \frac{a_{sp}}{b_{sp}}}{\frac{R}{3}\left[\left(\frac{2k + 1}{b_{cr}} + \frac{2 + k}{b_{sp}}\right) - R(1 - k)\right]} \tag{17}$$

For $a_{cr} = a_{sp} \equiv a$, $b_{cr} = b_{sp} \equiv b$, Equation 17 simplifies to

$$w_p = \frac{6a}{R} \cdot \frac{1}{3(1 + k) - b(1 - k)R} \tag{18}$$

In terms of the concentrated applied crown load $P_{cr} = \frac{\pi R}{8} \cdot w_p$,

Equation 18 becomes

$$P_{p\,cr} = \frac{3\pi a}{4} \cdot \frac{1}{3(1 + k) - b(1 - k)R} \tag{19}$$

Ring Strength - Examples

81. In this section, the method is demonstrated by applying it to two different rings, a thin one failing in tension and a thick one failing in compression. The calculations are simplified by making several assumptions:

a. Springing and crown sections have identical strength envelopes. This is considered appropriate for two reasons. The moment-thrust paths presented earlier indicate much greater strength than shown by the envelopes

within the compression and balanced regions, and there is considerable uncertainty about the actual steel strength in the thin rings failing in tension,

b. Tensile and compressive regimes of the strength envelope are represented by straight lines, as already suggested in Fig. 53. In addition, the balanced region has been represented by a vertical cutoff indicating constant yield moment over a range of thrusts.

82. These assumptions are not of a basic nature but were made to save time. DCEAE believes that the results are valid within the accuracy of the specified information in this case. Given more time, the stated assumptions can easily be transcended, but were considered outside the scope of this task.

83. Records of loads actually applied to these thin rings indicated load ratios far from those specified. Actual load ratio on Specimen 8-1 was 2.2:1, and that on Specimen 8-2 was 2.7.1. The ring strength under these load ratios is computed, for comparison with test results.

84. Section strength was taken from the linearized crown strength envelope, as shown in Fig. 56. For tension failure, the strength constants were $a = -8.1$ kips; $b = 1.25$ 1/in. for $N_o \leq 14$ kips. Ring radius $R = 9.0$ in. Substituting these values into Equation 19 for the test loading, the failure strength for different load ratios k is obtained:

$$p_{pcr} = \frac{1}{.432 - .745k} \text{ kips} \qquad (20)$$

85. For thrusts $N_o \geq 14$ kips, both crown and springing moments are assumed at their failure value of $M_o = 17.64$ kip-in., and obtain the ring strength from Equation 8.

86. Fig. 57 shows the results of the plastic analysis for different load ratios k, along with failure strengths from test. The actual strengths in the tensile zone are below the predicted plastic strengths. This may possibly be due to an overestimation of the steel strength in these specimens. Specimen 8-3, at a load ratio of 2:1, failed near the balance point, and the underestimation of the actual strength may have been due to the conservative strength envelope mentioned earlier.

Compression Failure - Specimens 2-1 through 2-3

87. Section strength was taken from the linearized crown strength envelope, as shown in Fig. 58. For compression failure, the strength constants were: $a = 123$ kips , $b = -1.025$ 1/in. , for $N_o \geq 50$ kips . For balanced failure at 30 kips, $< N_o < 50$ kips , $M_o = 70$ kip-in. Ring radius $R = 7.50$ in.

88. For compression failure, Equation 20 gives these values:

$$p_{pcr} = \frac{1}{.0369 - .0162k} \text{ kips}$$

Fig. 59 shows the results of the plastic analysis for different load ratios k compared with test results where available. The test strengths follow the same trend as predictions by plastic analysis, but are consistently on the high side, presumably because of the conservative strength envelope mentioned earlier.

Effect of Load Ratio

89. It may be observed from Figs. 57 and 59 that rings failing in tension are much more sensitive to the load ratio k than those failing in compression. That this is generally so can be deduced by recasting Equation 20 in the following form:

$$p_{pcr} = \frac{3\pi}{4} a \cdot \frac{1}{(3 - bR) + (3 + bR)k} \text{ kips}$$

90. For tension failure, b is positive, and the coefficient of the load ratio k in the second denominator term will be large. Conversely, for compression failure, b is negative, and this coefficient will be small, thus minimizing the effect of the load ratio on the ring strength.

Plastic Analysis of Load Confinement

91. Lastly, the effects of load confinement on the strength of ring Specimen 2-1 are predicted using plastic theory. Fig. 60 shows the results superimposed on the load-deflection curves shown earlier in Fig. 51. The

plastic failure loads are shown in horizontal lines matched by number to the load case.

92. Close correlation is obtained for the 2-, 4-, and 8-point loadings; the 16-point test loading is underestimated considerably by the plastic analysis. In general, plastic theory appears to be able to catch the trend quite well.

Conclusions and Recommendations

93. From the analyses by DCEAE, the following conclusions and recommendations are made:

a. The test specimens tend to redistribute the applied loads in a fashion most favorable to them. Actually applied loads must be checked against those specified. The ability of these rings to redistribute applied loads during tests suggests that they may have the same ability when subjected to ground pressure. This important effect can be taken into account only by considering the in situ structure-ground interaction, considering the nonlinear behavior of the constituent materials.

b. Nonlinear finite-element analysis seems to perform well in most cases when compared with test results. In general, analysis underestimates the deflections and tends to overestimate the strength of these rings. If other nonlinear analysis results are available, these should be checked against each other; this would seem a unique opportunity to assess the reliability of different non-linear finite-element solutions. Particular attention should be paid to the effects of different material models, as well as spatial and load-step discretizations.

c. Analysis indicates cross-section strength vastly in excess of that predicted by conventional reinforced-concrete theory. A detailed study of the local finite-element results at critical sections is suggested to explore this further.

d. The diagonal tension failures apparent in some test specimens were not duplicated by analysis. Although some radical cracking was predicted by the analysis, no ring failures due to radial cracking were predicted by the finite-element analysis. These matters deserve further study.

e. Finite-element analyses indicate that more total load can be carried by these rings under EM loading conditions than under the test loading.

f. Load confinement, both within and normal to the plane of loading, tends to increase the strength of these rings considerably. Particularly for rings in which failure is due to compressive concrete crushing, the plane-strain condition leads to much greater strength than predicted for the plane-stress condition. The relation between the plane-stress test condition and the plane-strain in situ condition needs more study.

g. A design approach based on plastic analysis may have promise. This method combines the advantages of rationality and simplicity, but must be tested and developed further. A study of applicability of the plastic design method should be undertaken. The effects of radial stresses and possible shear failure could be included in formulating the section strength.

Table 1. Concrete properties.

Batch No.	Number of Cylinders Tested	Dates Tested	Age, days	Average f'_c psi	Average Initial Elastic Concrete Modulus $E_c \times 10^6$ psi	Average Poisson's Ratio	Average Tensile Strength psi
1	3	8/10/83	29	3,817	--	--	
1 (C1-1, C2-1, C2-2, C2-3, C3-1, C6-1)	12	8/24/83-9/7/83	42-56	4,213	4.19	0.152	388
2	3	8/15/83	28	4,193	--	--	
2 (C4-1, C5-1, C7-1, C8-1, C8-2, C9-1)	9	8/30/83-9/7/83	48-51	4,571	4.49	0.150	470
3	3	8/18/83	28	3,527	--	--	
3 (C4-2, C5-2, C5-3, C5-4, C6-2, C8-3	9	9/7/83-9/9/83	48-50	3,632	4.00	0.157	437

Wright and Chiarito, op. cit.

Table 2. Steel reinforcement properties.

Type	Heat Treatment	Area $in.^2$	Number of Bars Tested	Average F_y ksi	Average Modulus of Elasticity $E_s \times 10^6$ psi	Average Ultimate Stress ksi	Average Rupture Stress ksi
#2	None	0.05	5	54.2	28.1	71.7	66.1
#3	None	0.11	4	63.1	25.5	98.4	87.8
D3	4-1/2 hr to 4-2/3 hr at 1,000° F	0.031	6	68.2	27.0	74.3	64.9
D1	3-1/2 hr at 1,000° F	0.01	19	81.4	32.7	83.3	67.2

Wright and Chiarito, op. cit.

MODEL C81
LOAD DISTRIBUTION 3:1

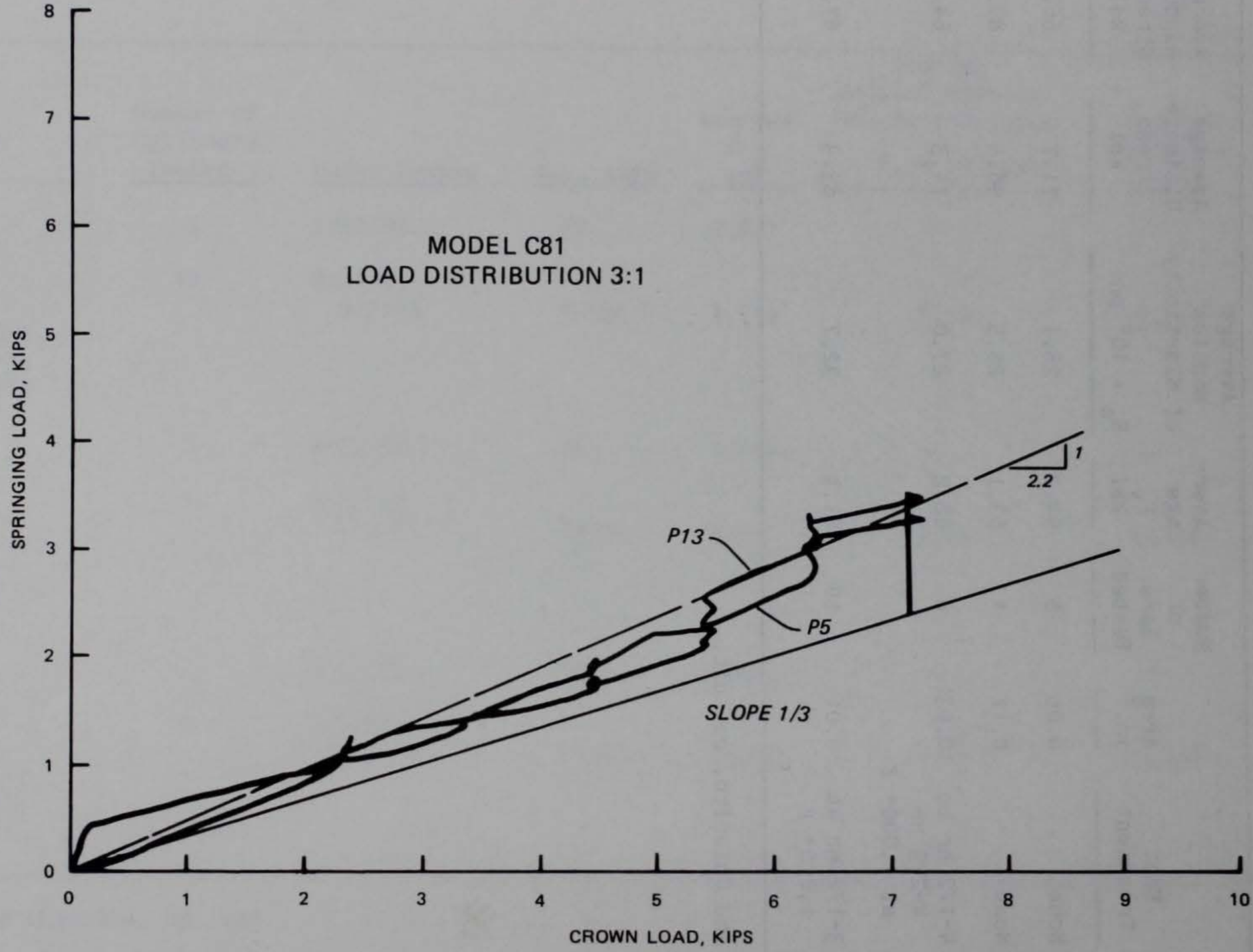

Figure 1. Load distribution for Model C81

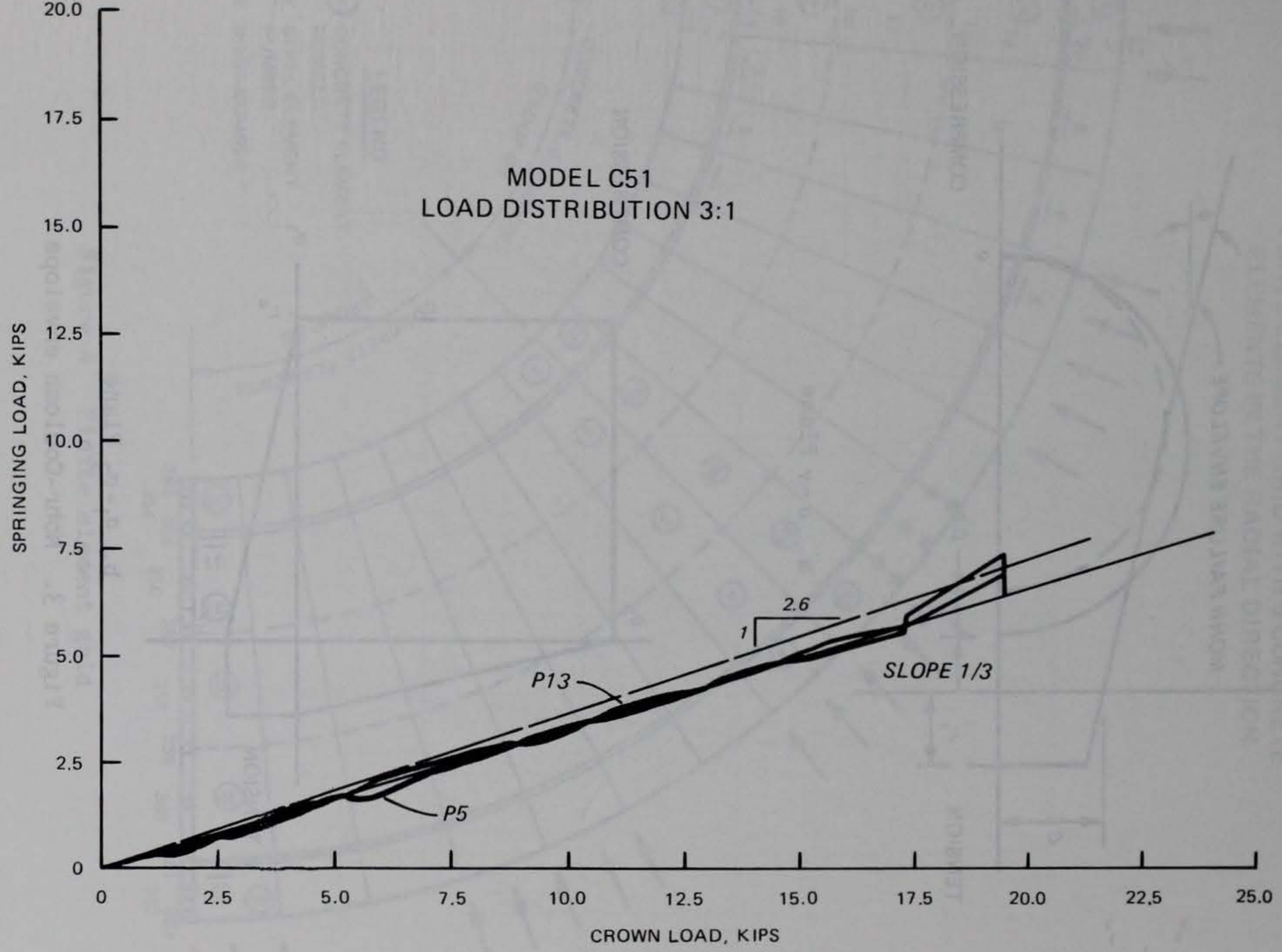

Figure 2. Load distribution for Model C51

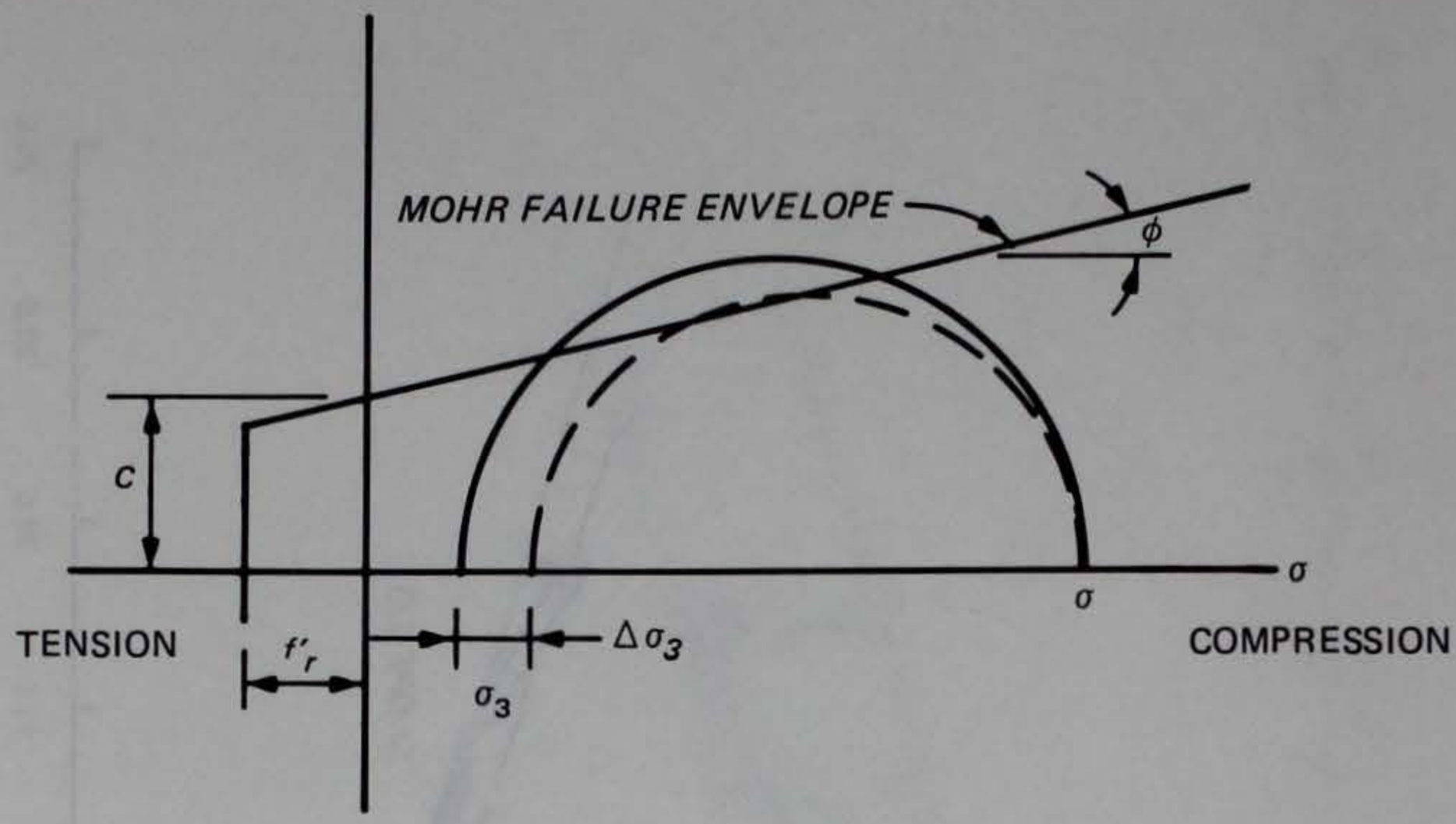

a. σ-τ Plane

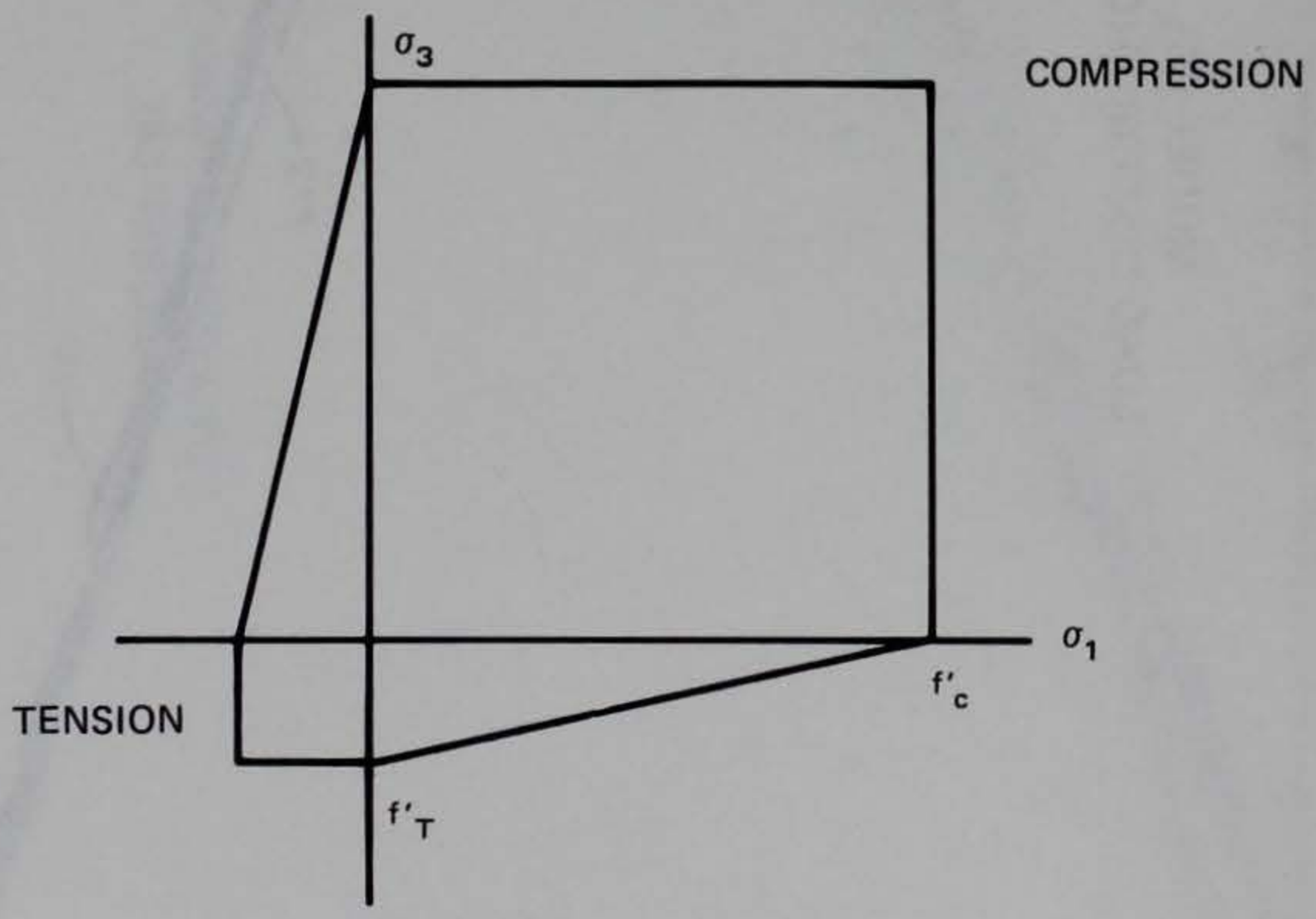

b. σ_1-σ_3 Plane

Figure 3. Mohr-Coulomb envelope

FINITE ELEMENT GRID WITH 5 CONCRETE ELEMENTS IN THE RADIAL DIRECTION

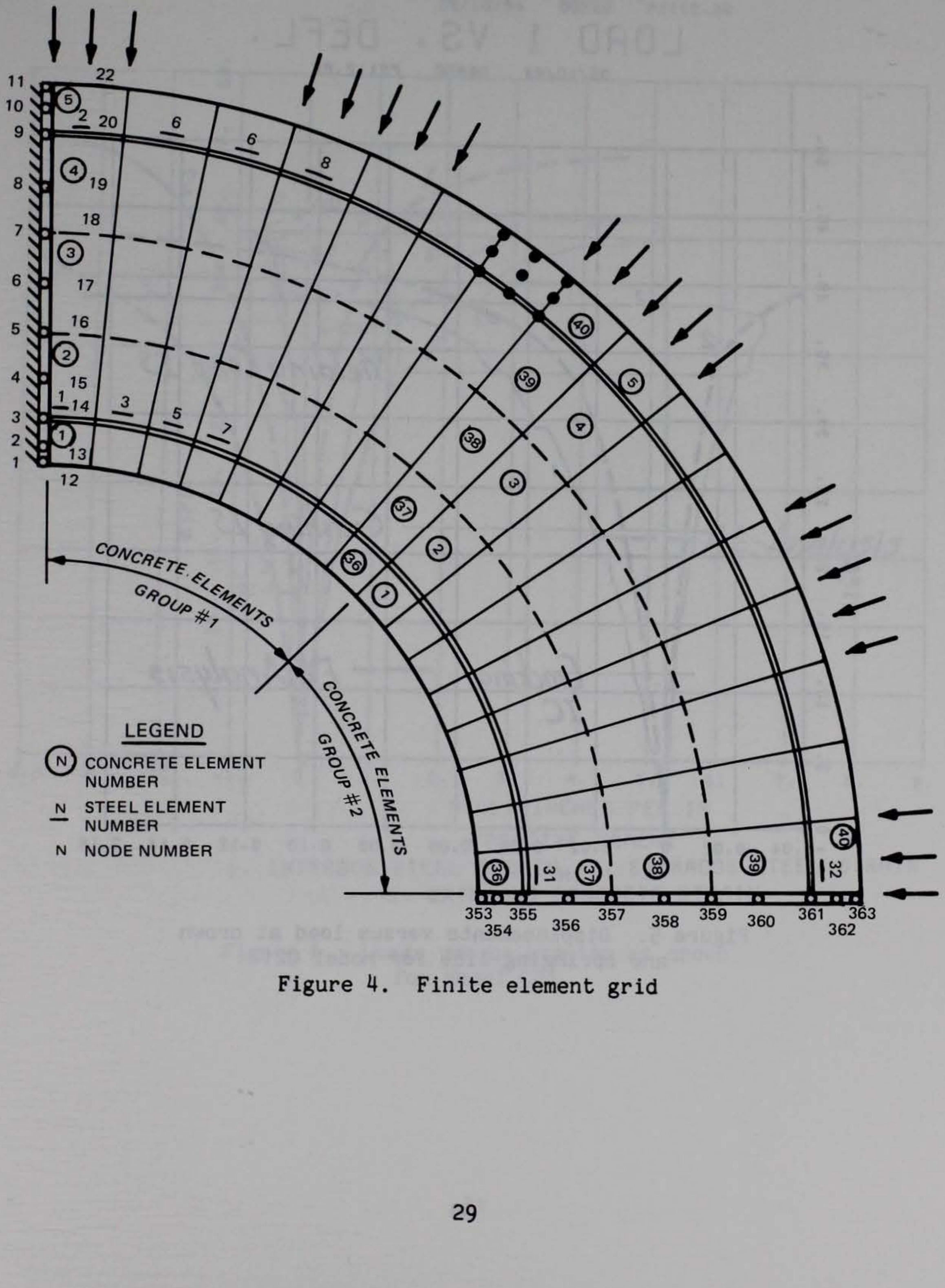

Figure 4. Finite element grid

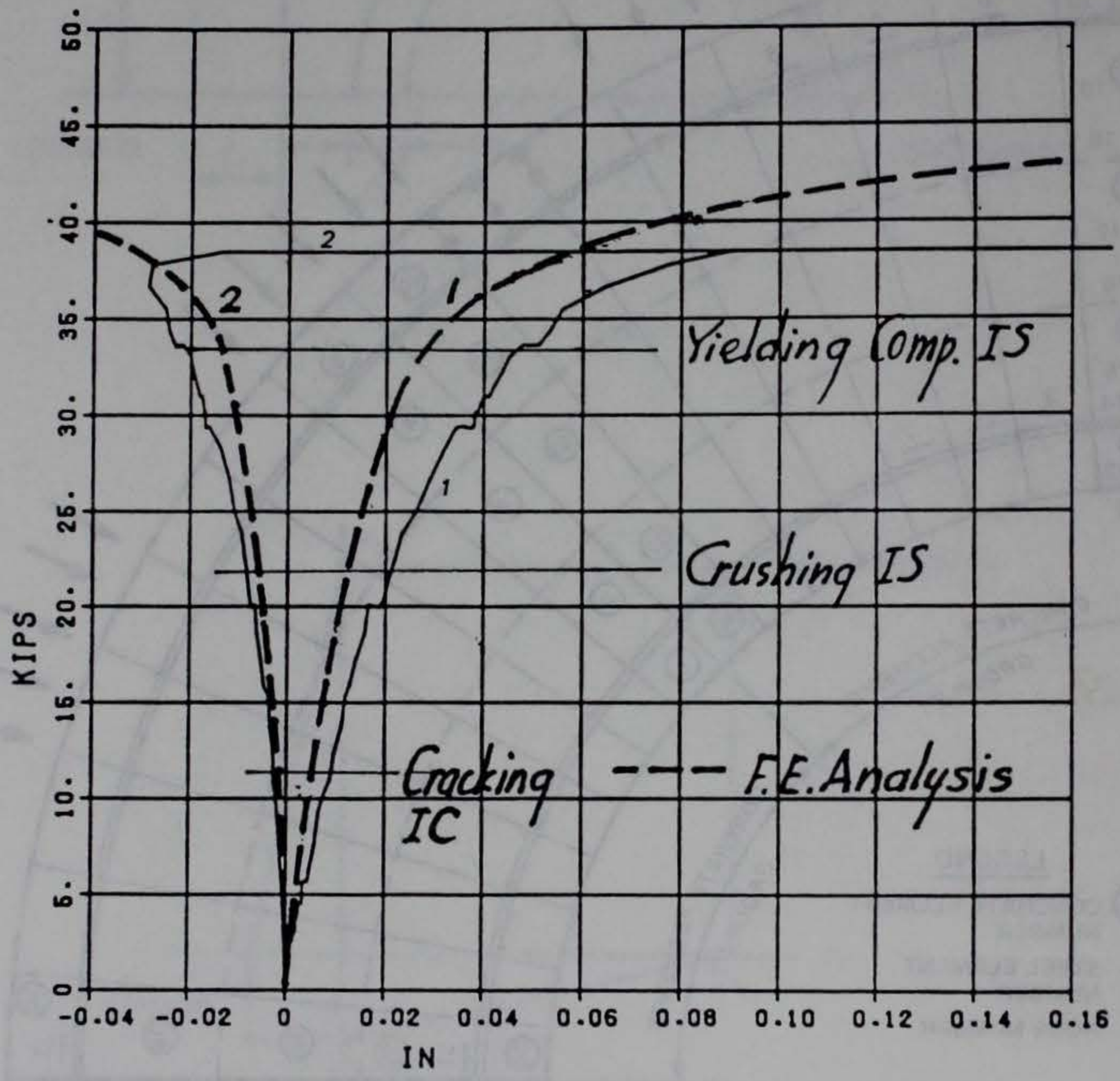

Figure 5. Displacements versus load at crown and springing line for Model C21

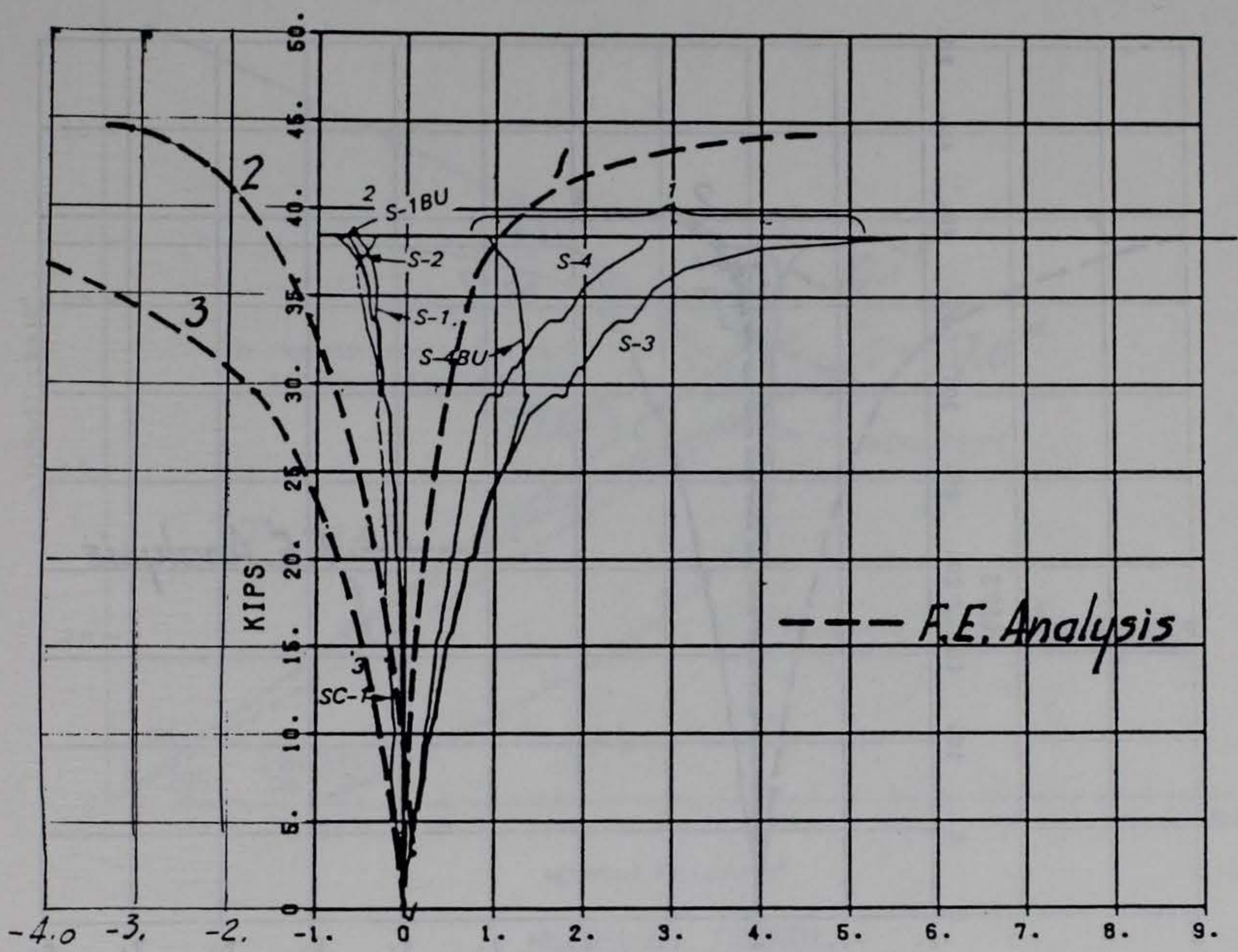

POSITIVE MOMENT

1. INTRADOS STEEL STRAIN 2. EXTRADOS STEEL STRAIN
3. EXTRADOS CONCRETE STRAIN

Figure 6. Loads versus strains at crown for Model C21

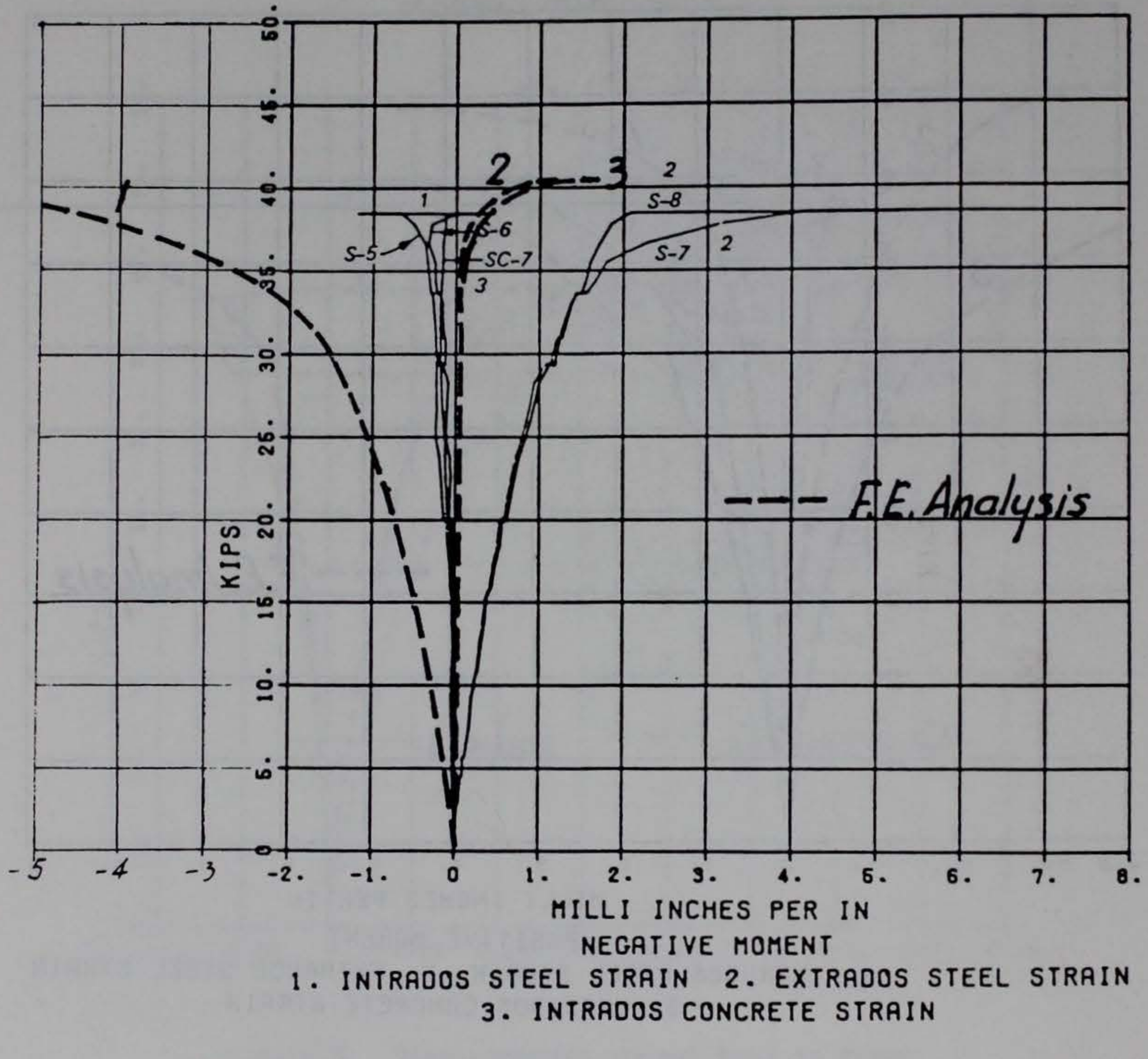

Figure 7. Load versus strains at springing line for Model C21

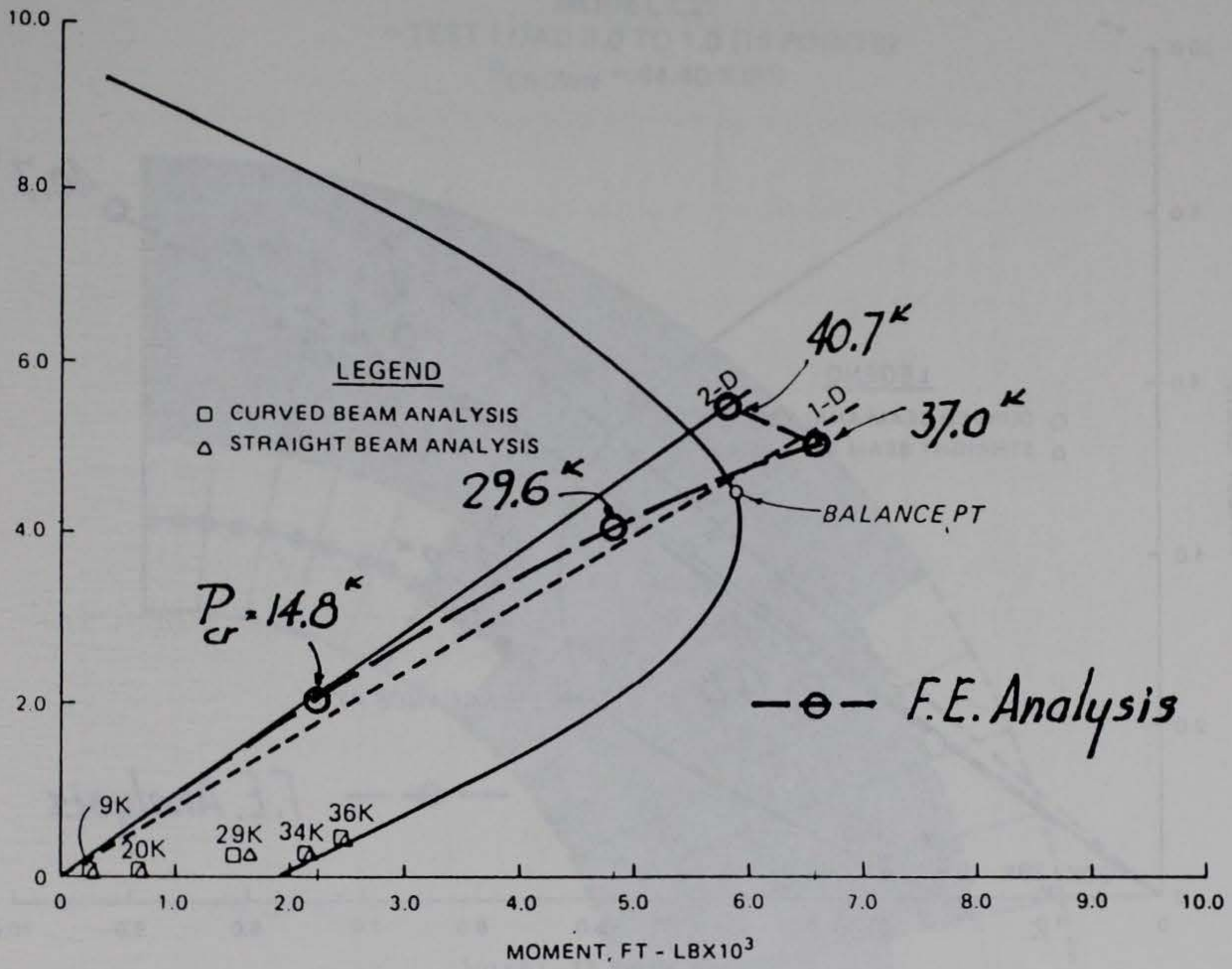

MODEL 2-1, CROWN

Figure 8. Interaction diagram at crown for Model 2-1

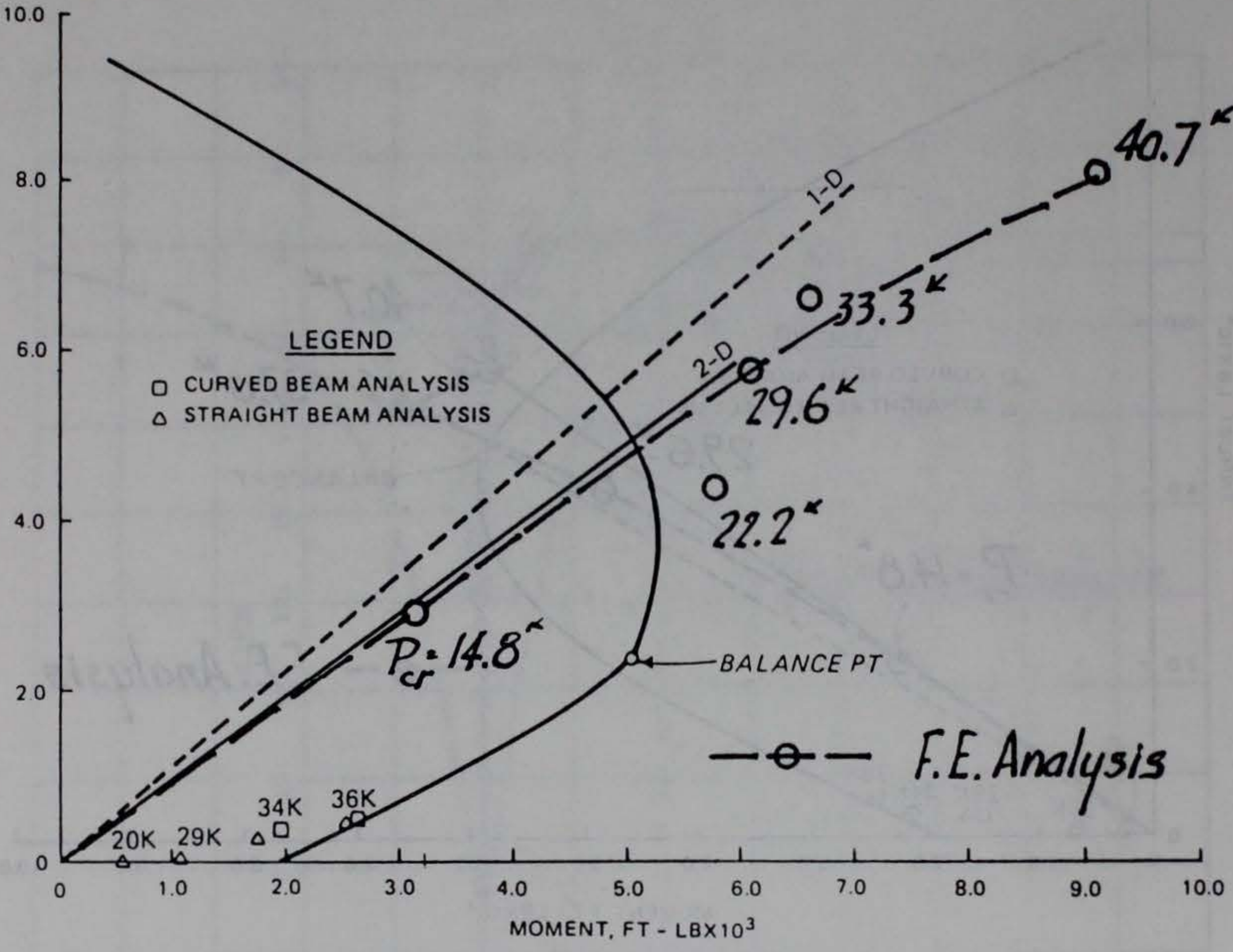

MODEL 2-1, SPRINGING LINE

Figure 9. Interaction diagram at springing line for Model 2-1

MODEL C21
~TEST LOAD 3.0 TO 1.0 (16 POINTS)
P_{CROWN} = 44.40 KIPS

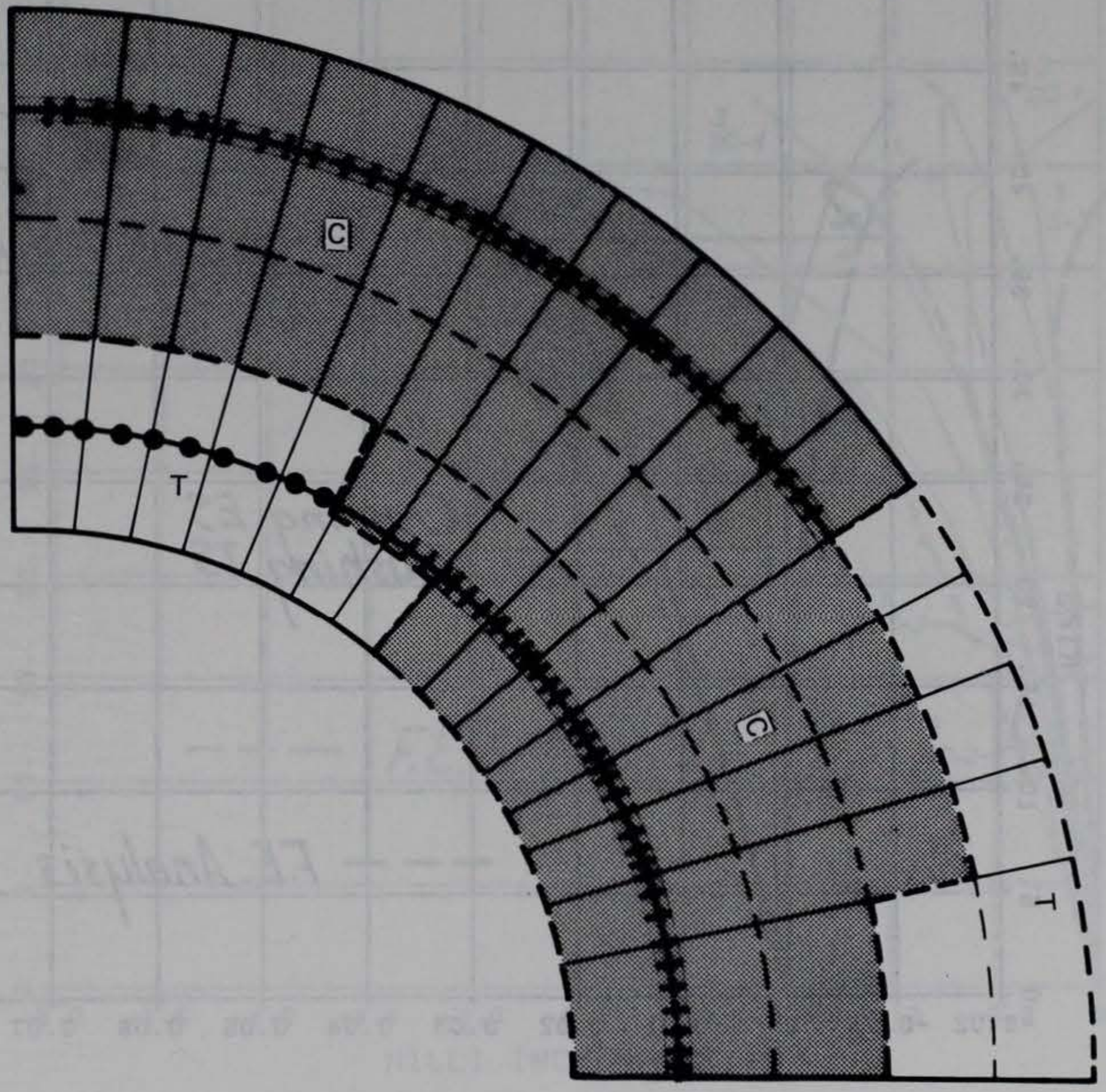

Figure 10. Crack pattern for Model C21

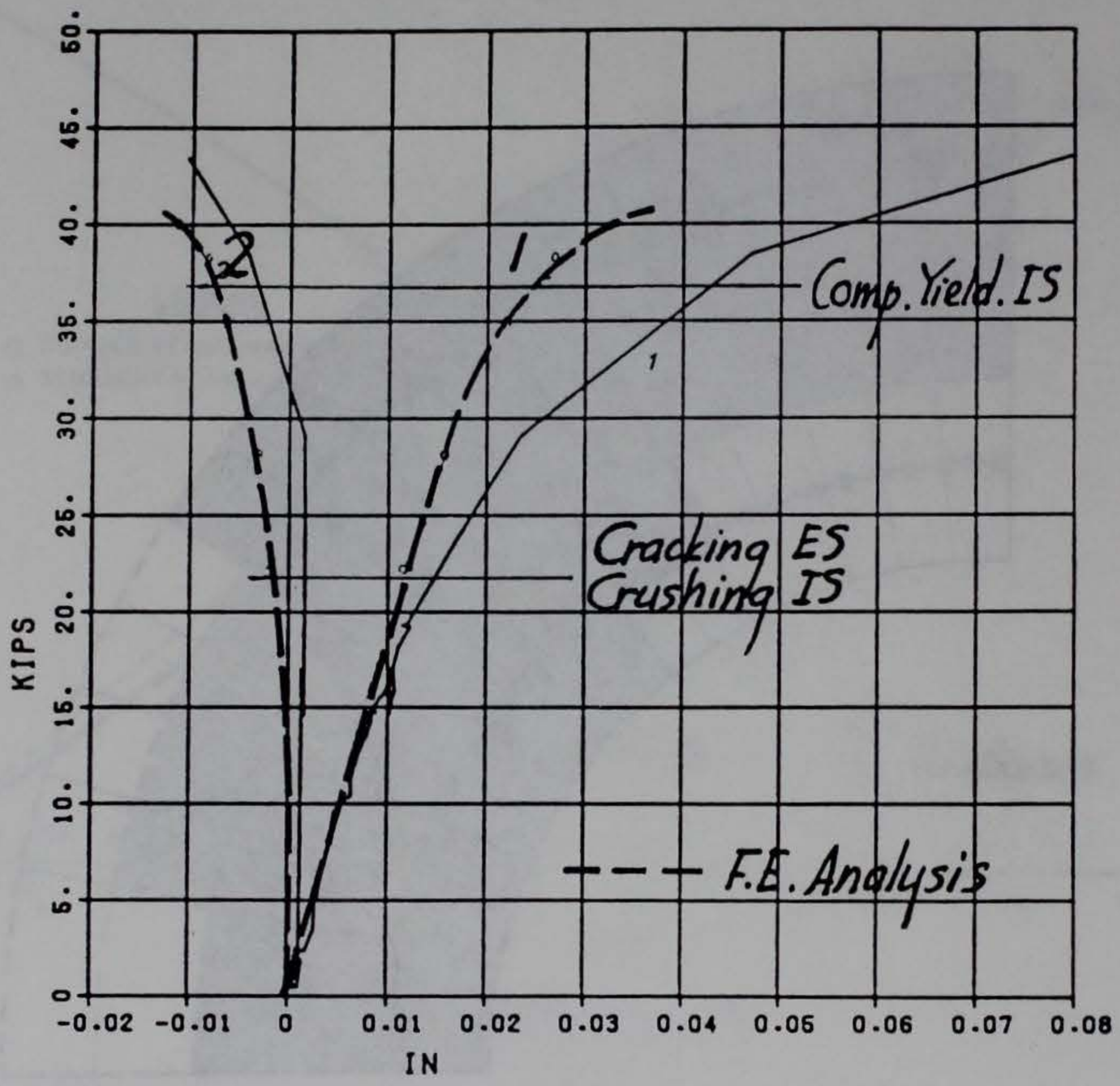

1. CROWN
2. SPRINGING LINE

Figure 11. Load versus displacements for Model C22

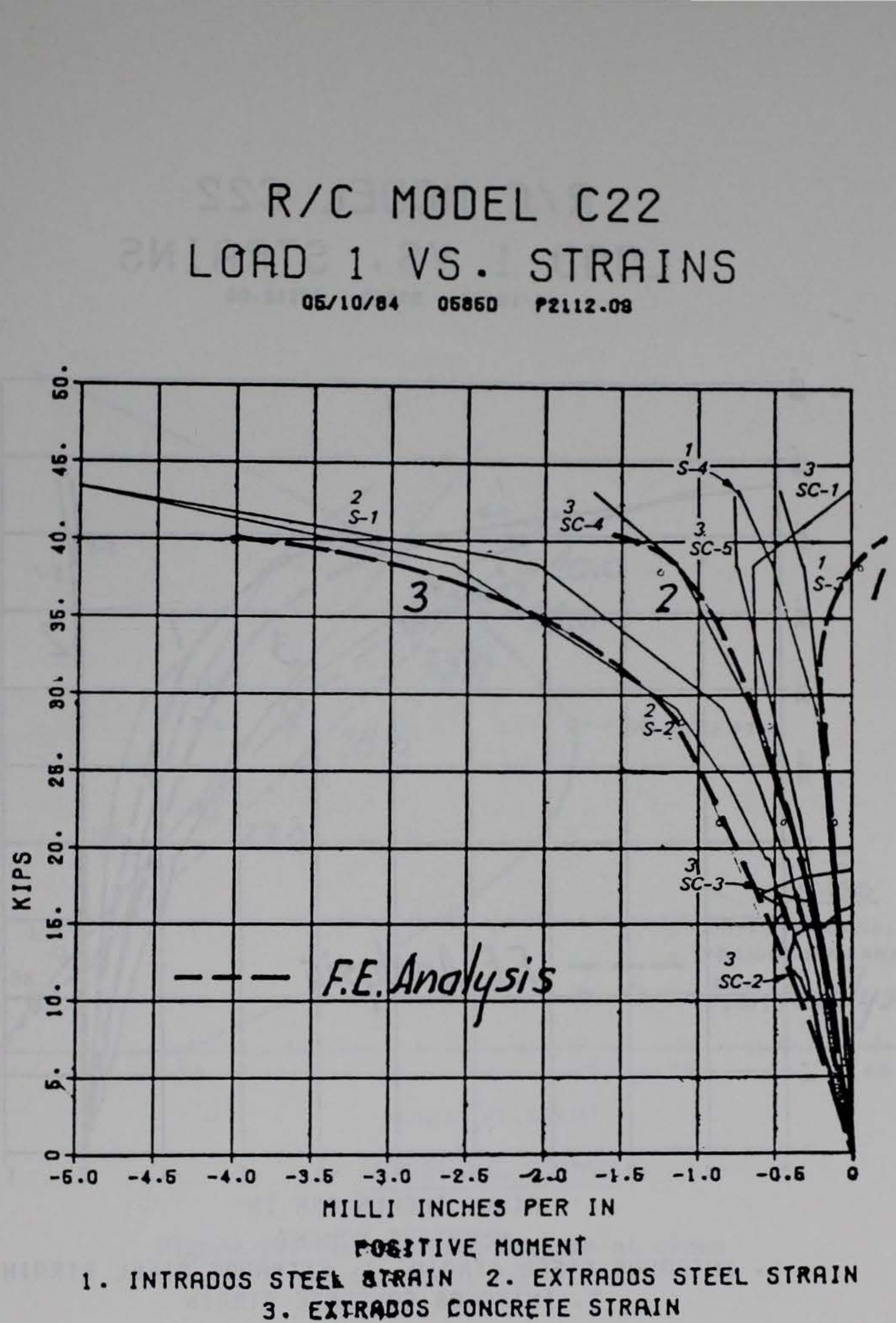

Figure 12. Load versus strain at crown for Model C22

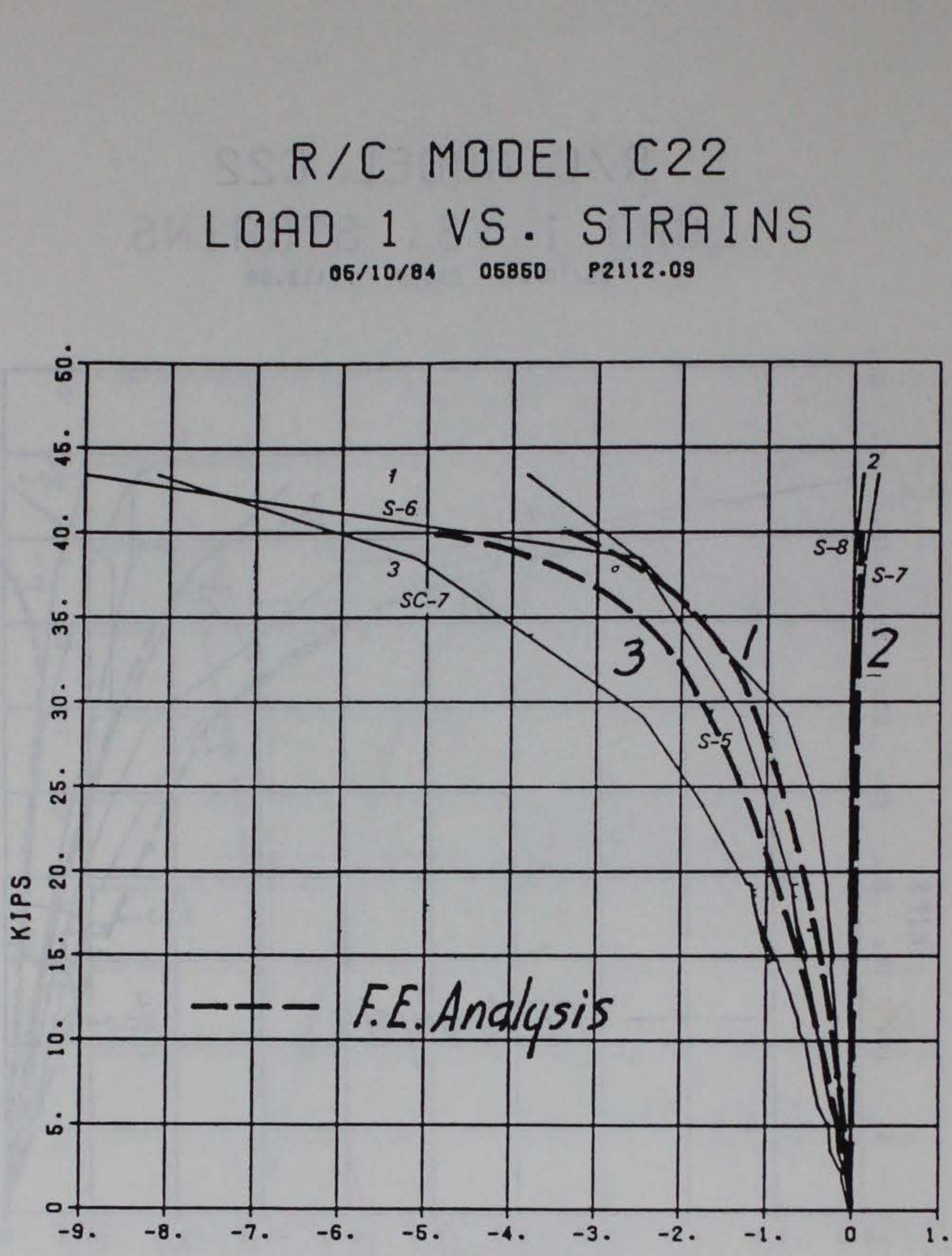

Figure 13. Load versus strains for springing line for Model C22

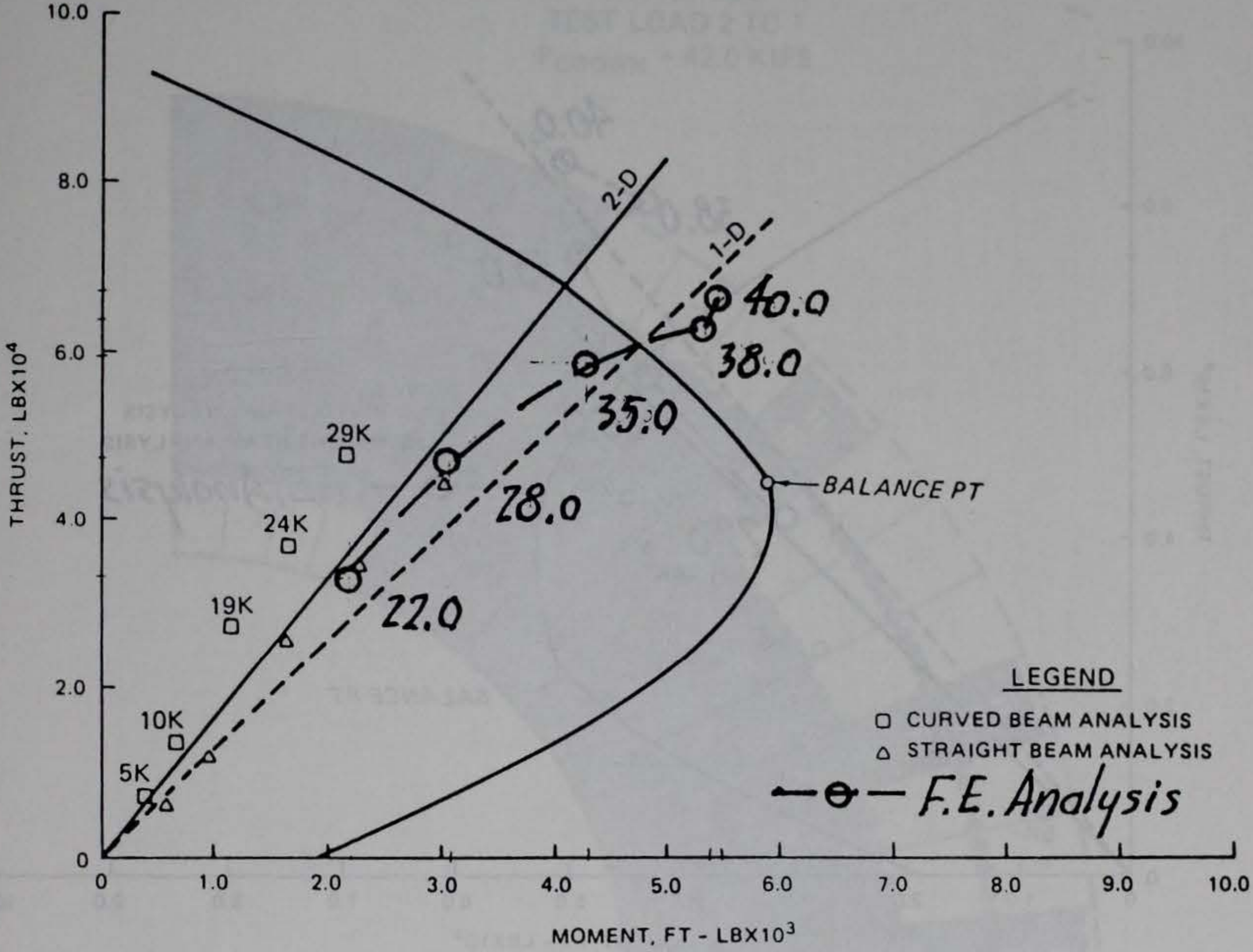

Figure 14. Interaction diagram at crown for Model 2-2

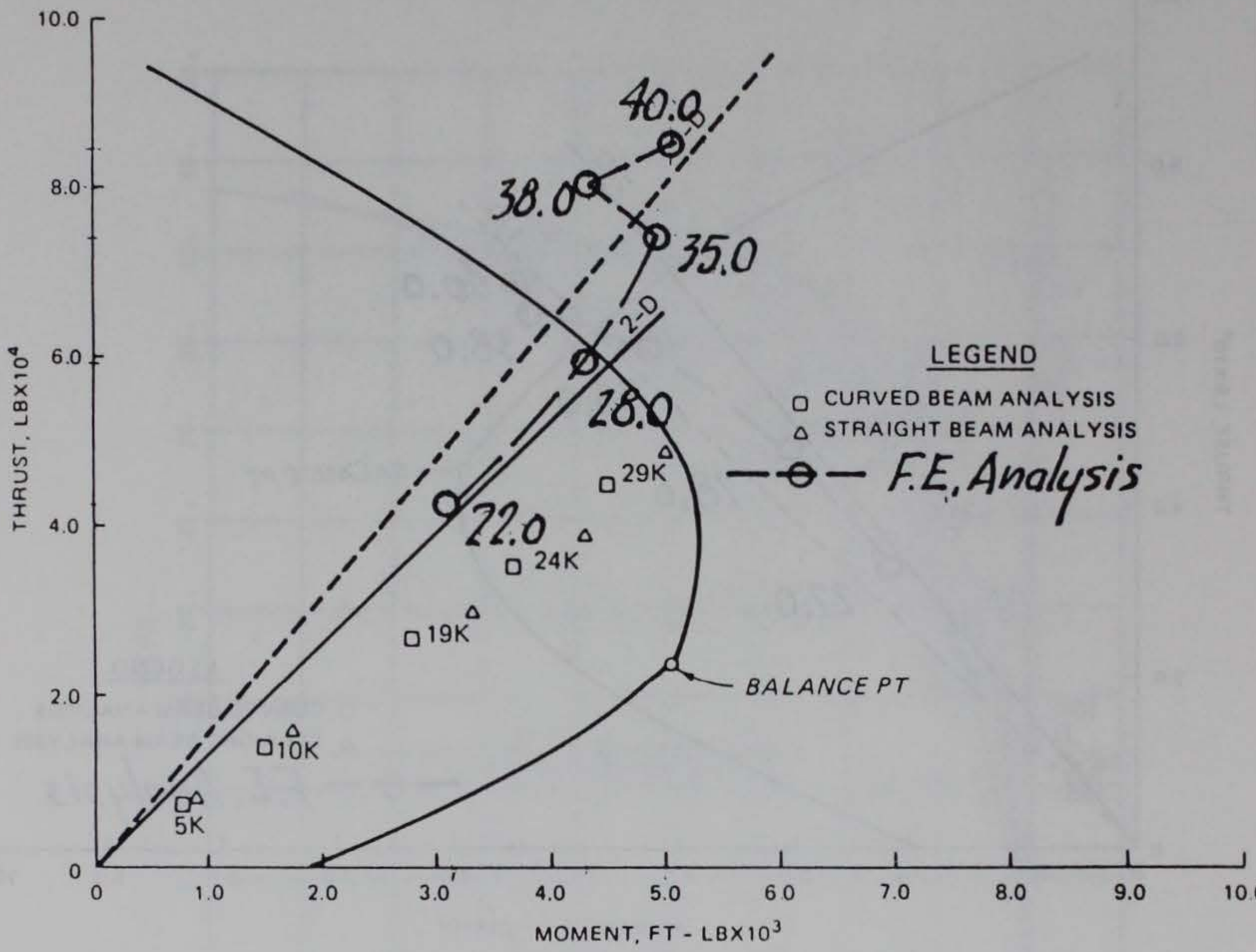

MODEL 2-2, SPRINGING LINE

Figure 15. Interaction diagram at springing line for Model 2-2

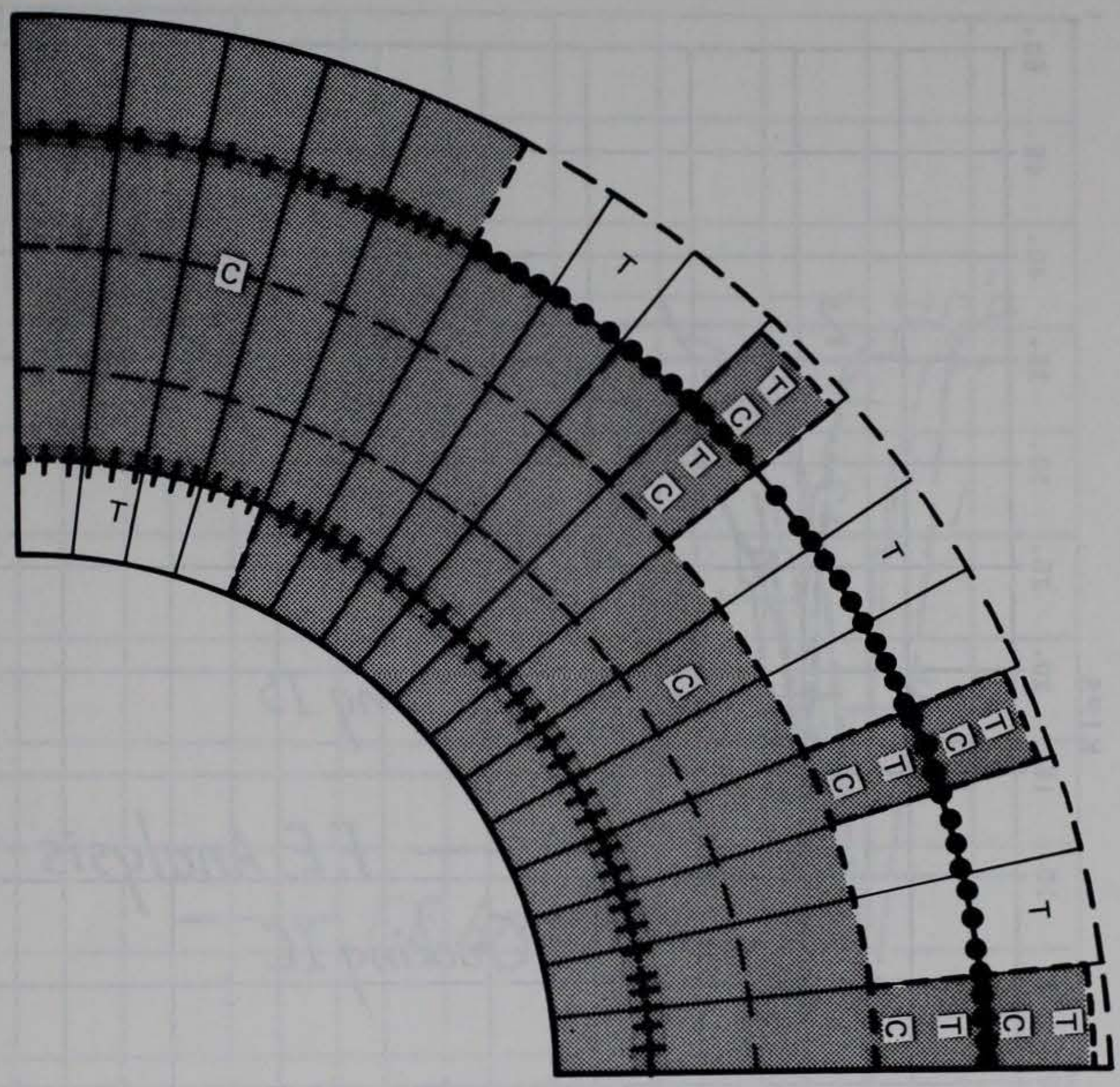

Figure 16. Crack pattern for Model C22

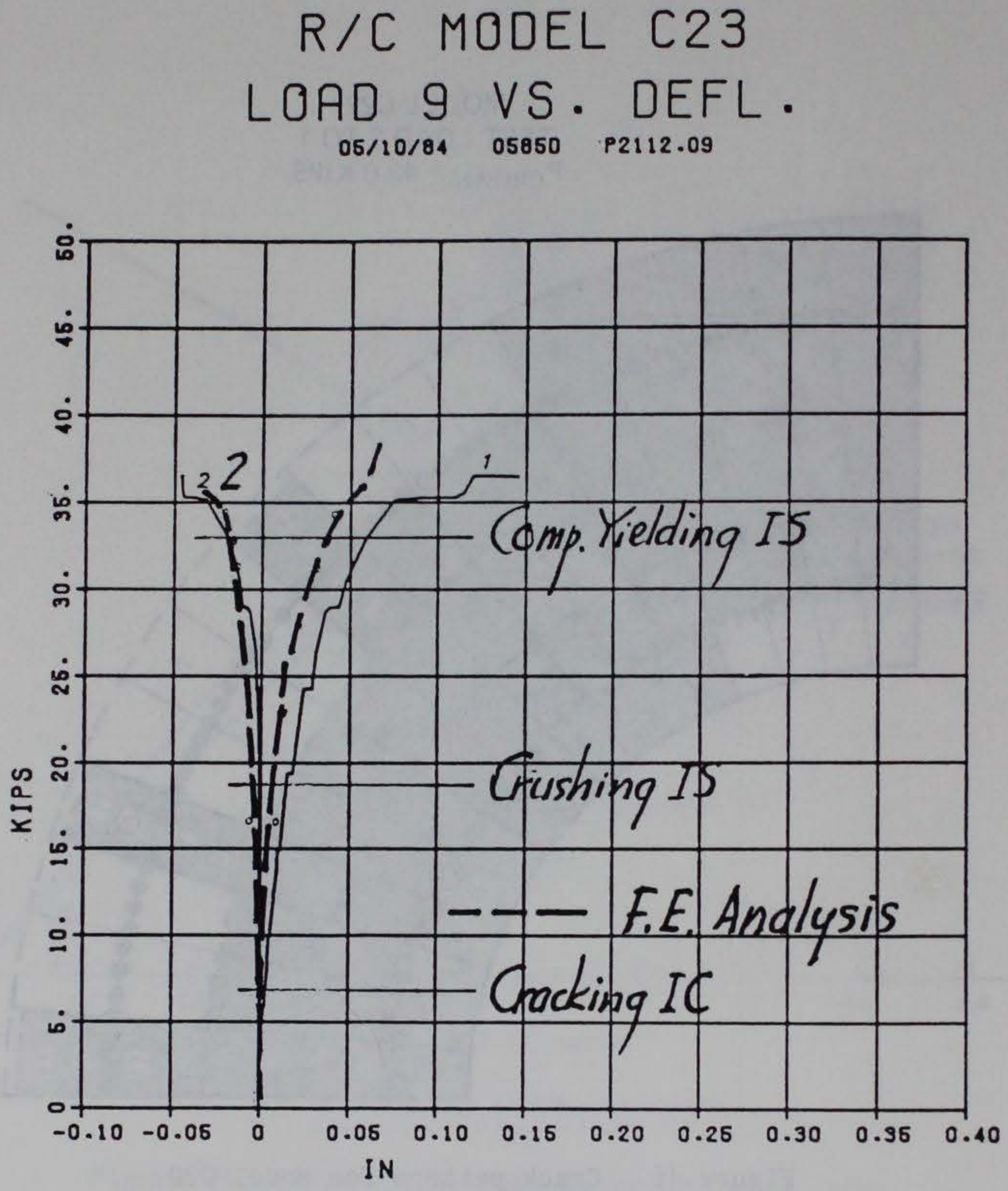

1. CROWN
2. SPRINGING LINE

Figure 17. Load versus deflections for Model C23

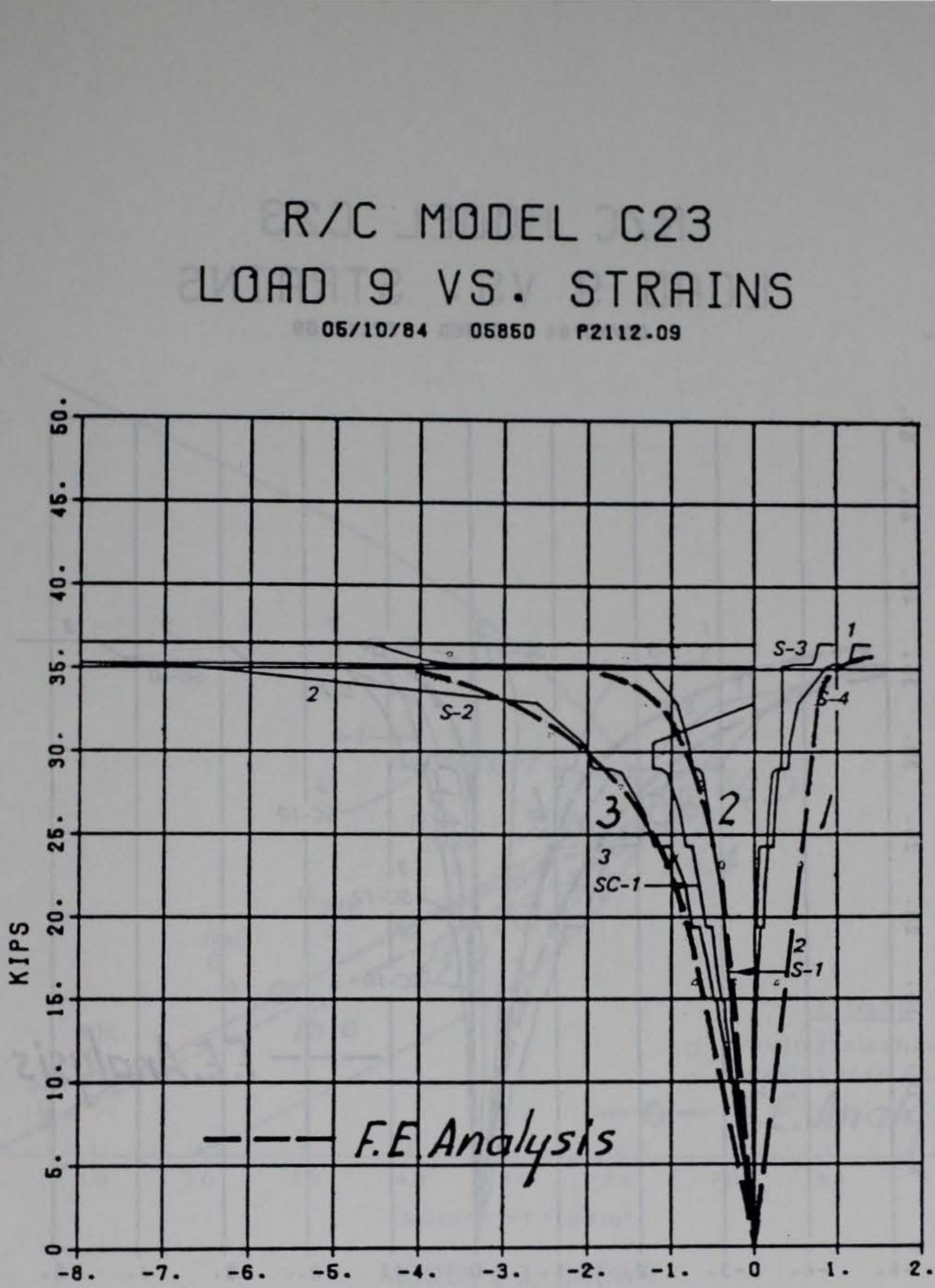

Figure 18. Load versus strains at crown for Model C23

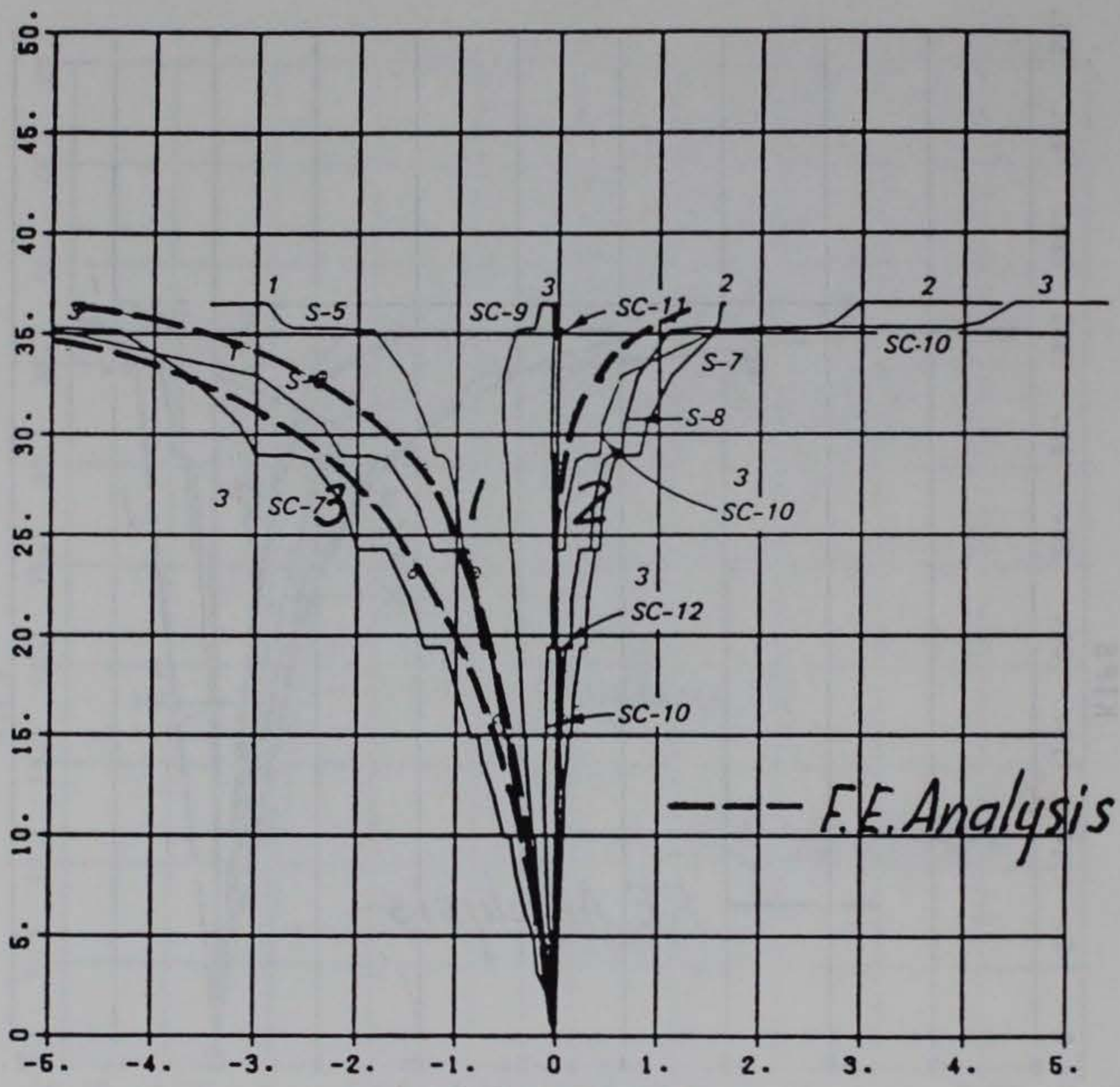

Figure 19. Load versus strains at springing line for Model C23

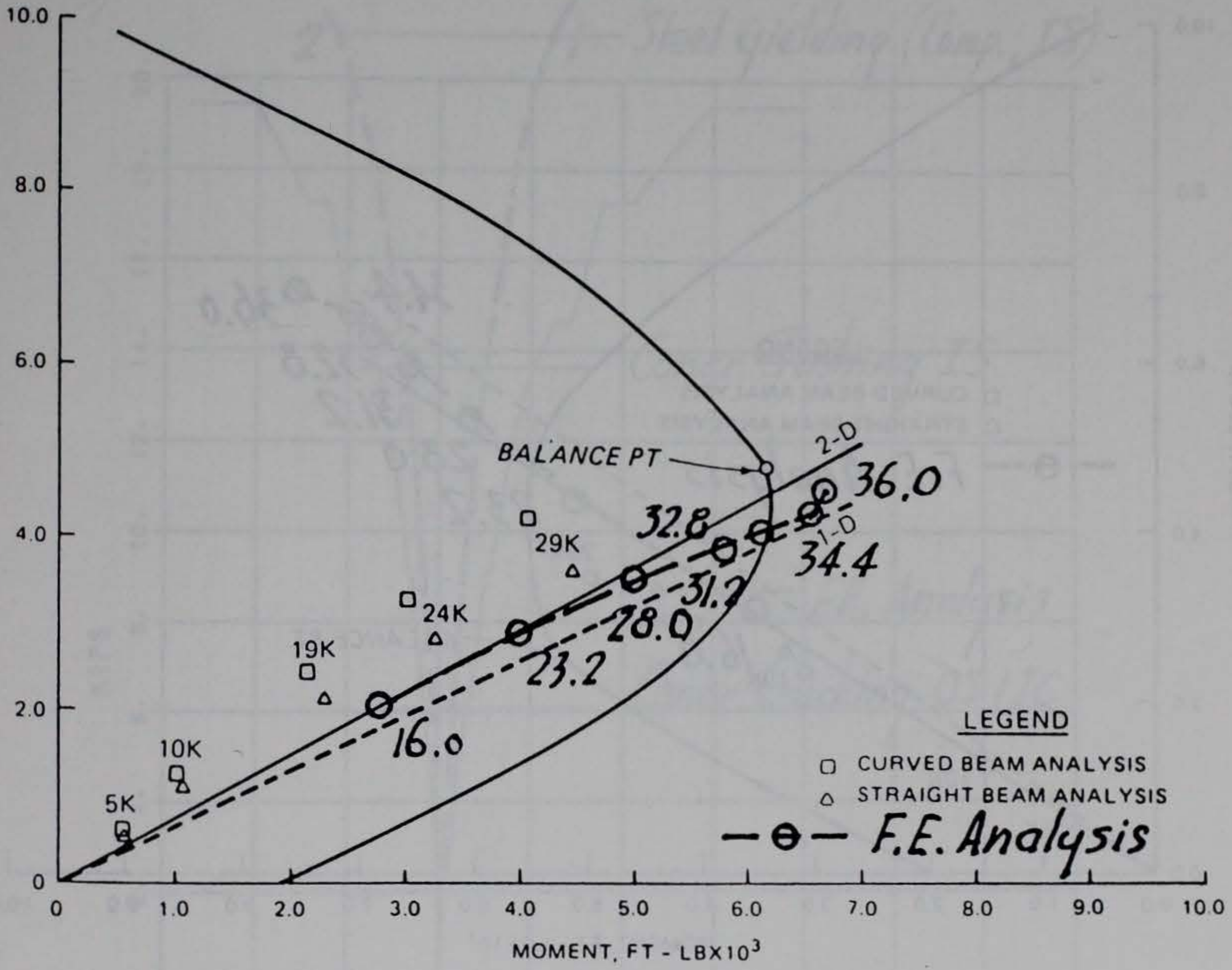

Figure 20. Interaction diagram at crown for Model 2-3

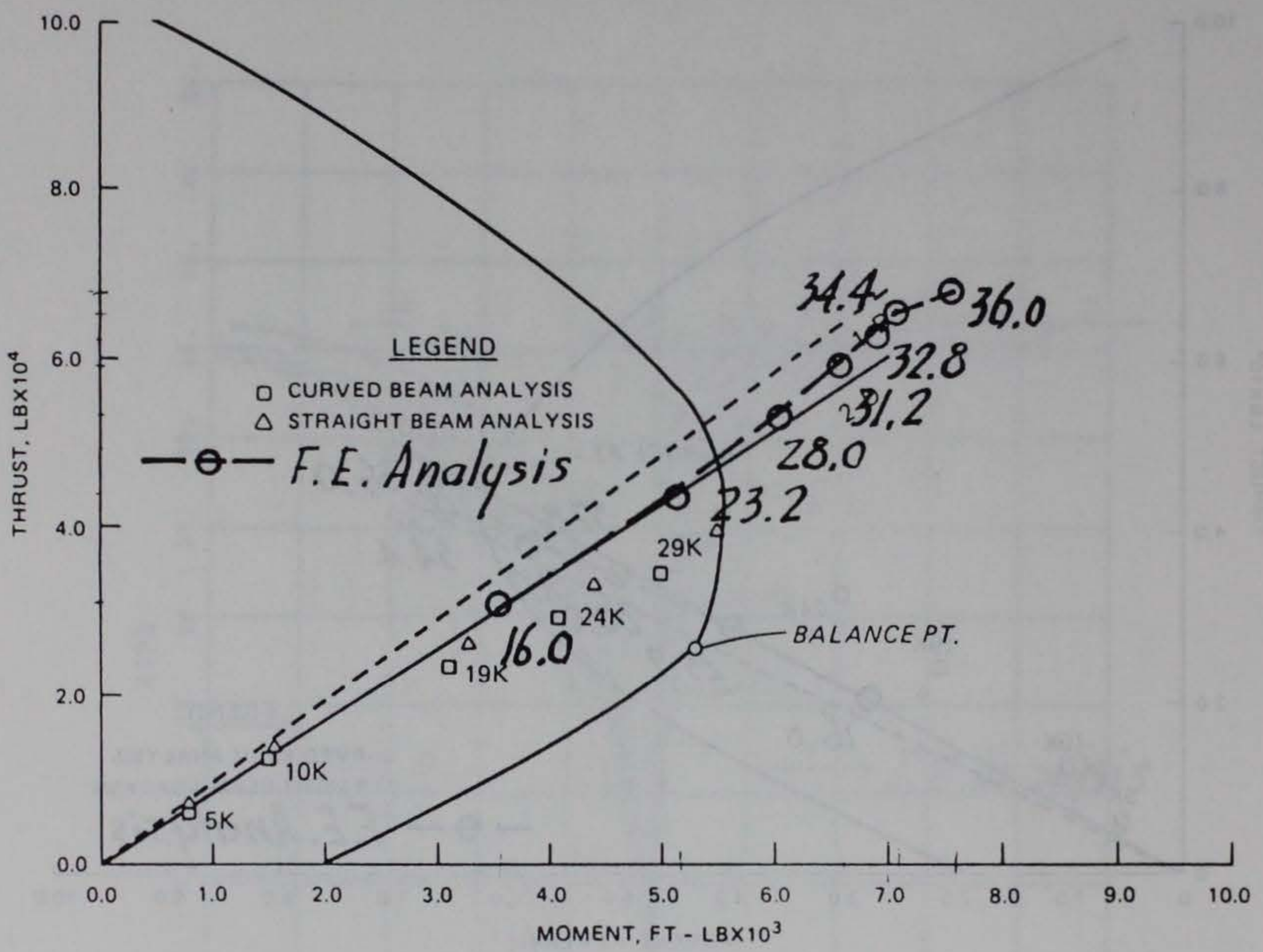

MODEL 2-3, SPRINGING LINE

Figure 21. Interaction diagram at springing line for Model 2-3

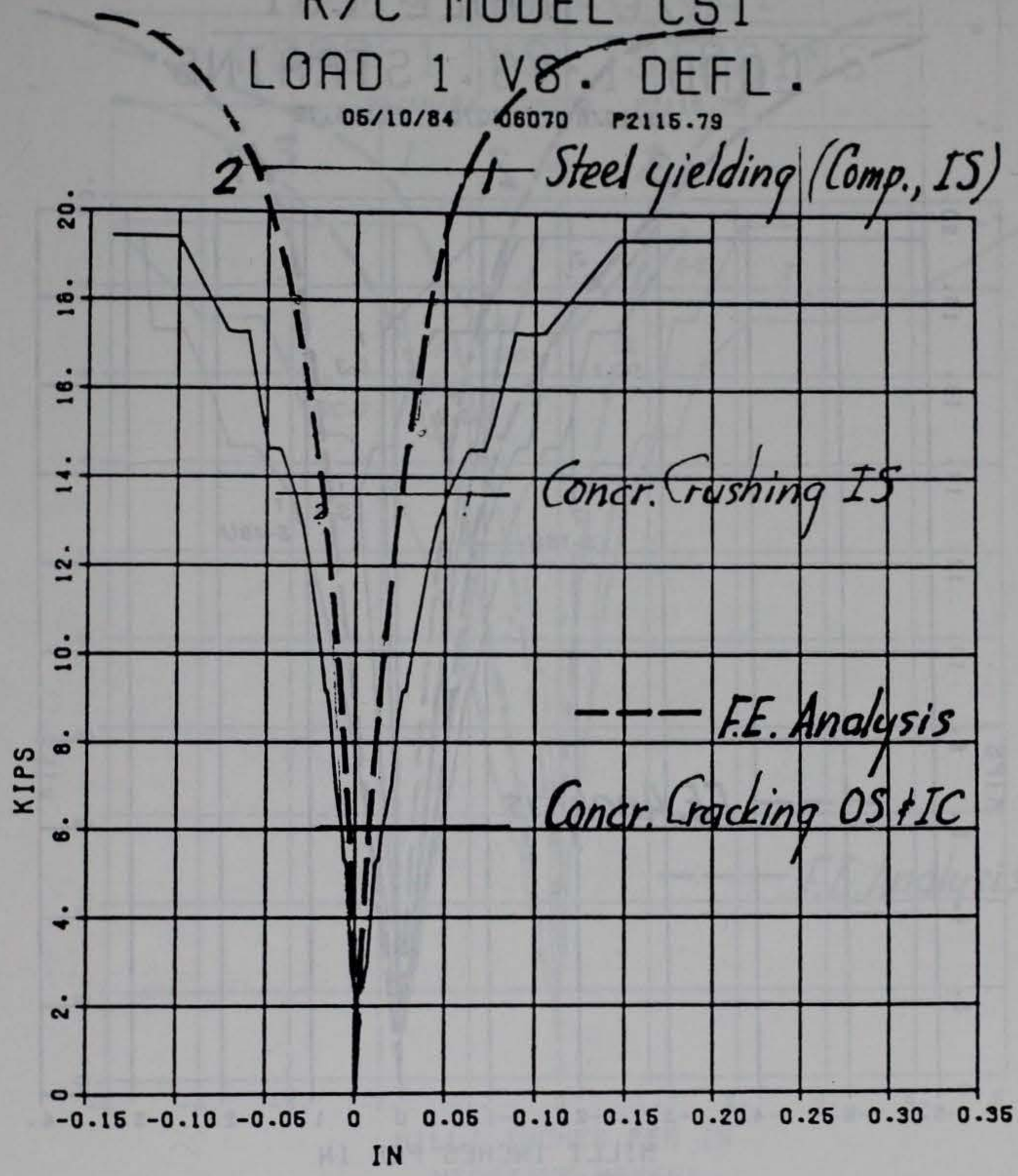

1. CROWN
2. SPRINGING LINE

Figure 22. Load versus deflections for Model C51

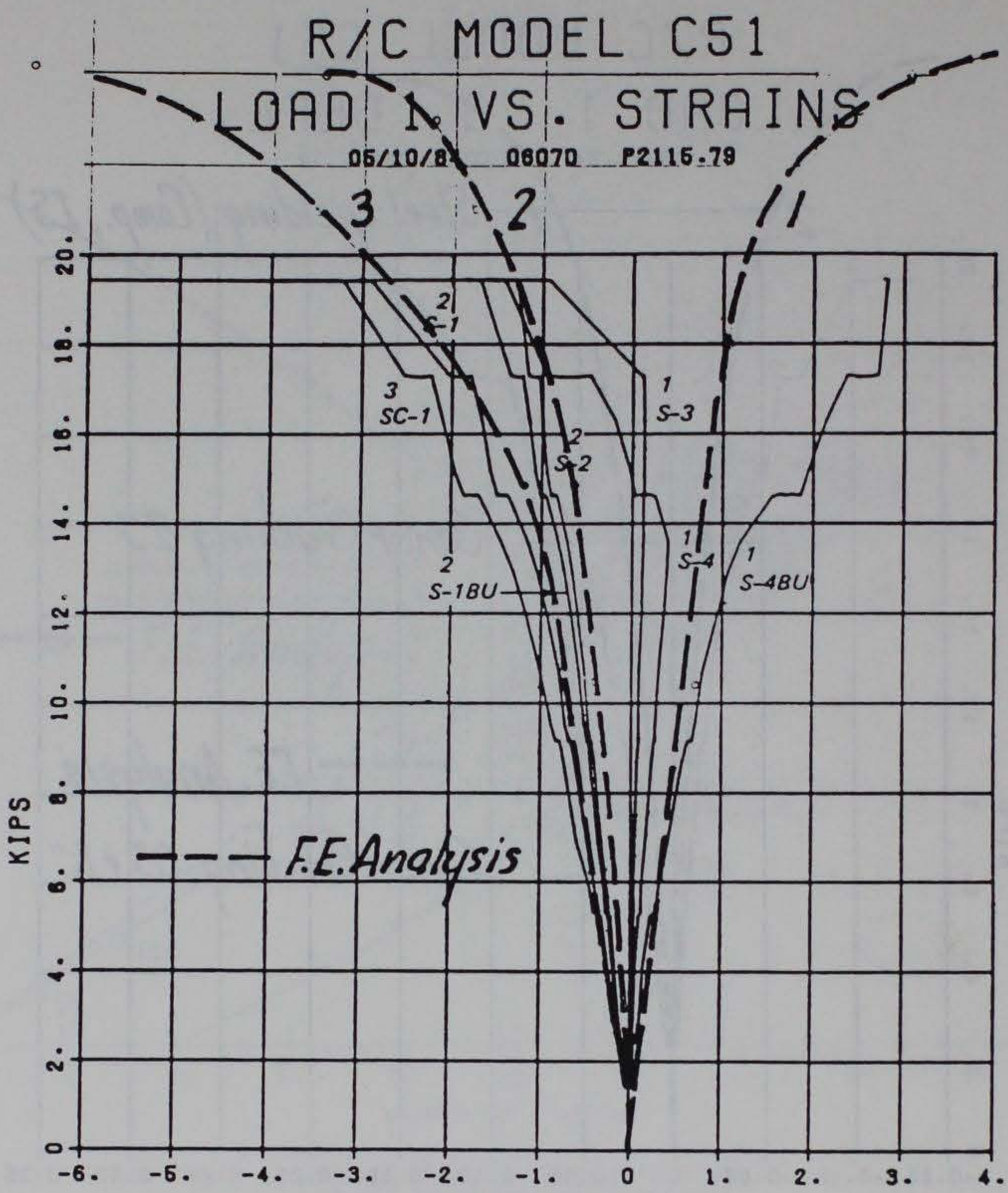

Figure 23. Load versus strains at crown for Model C51

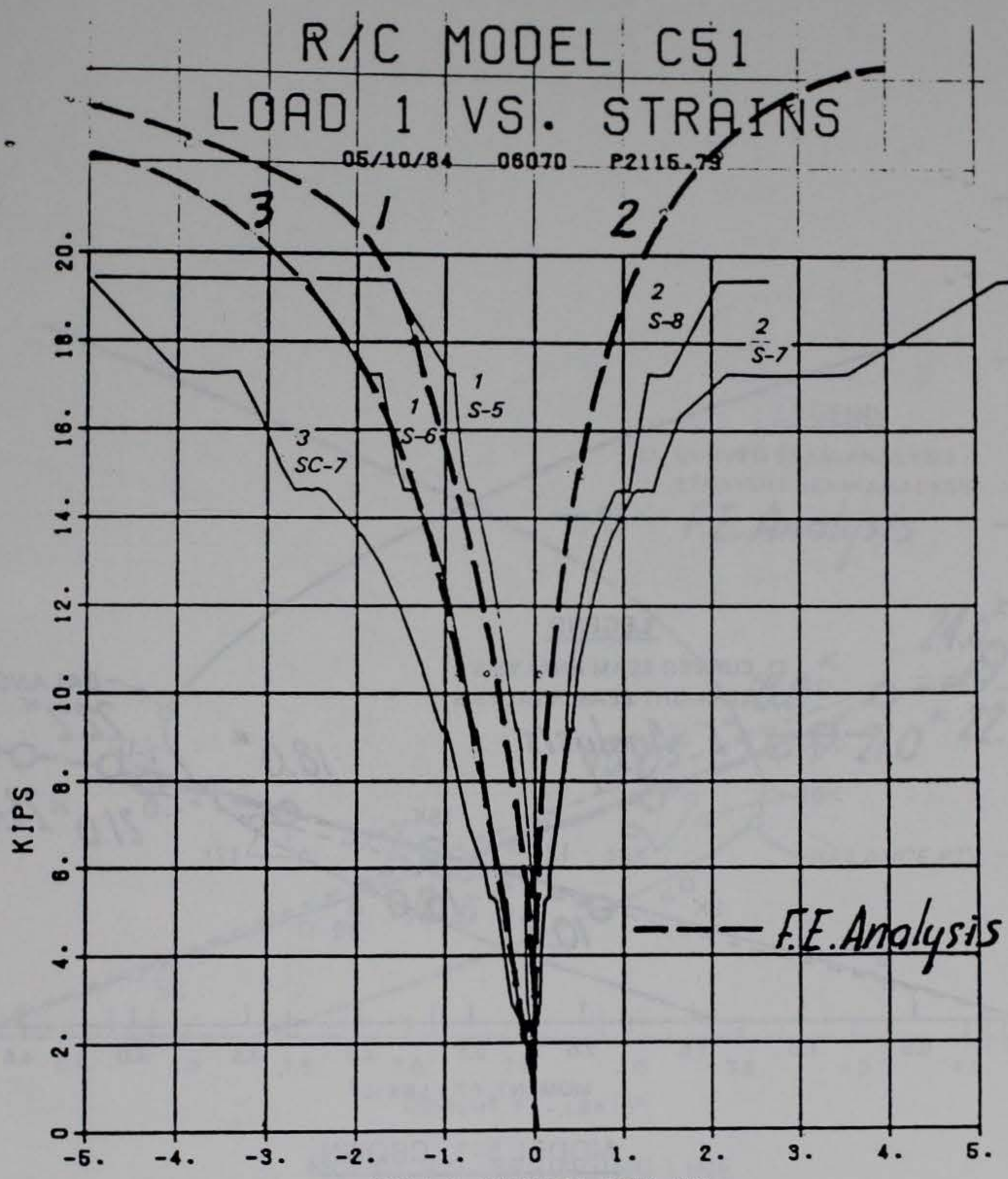

Figure 24. Load versus strains at springing lines for Model C51

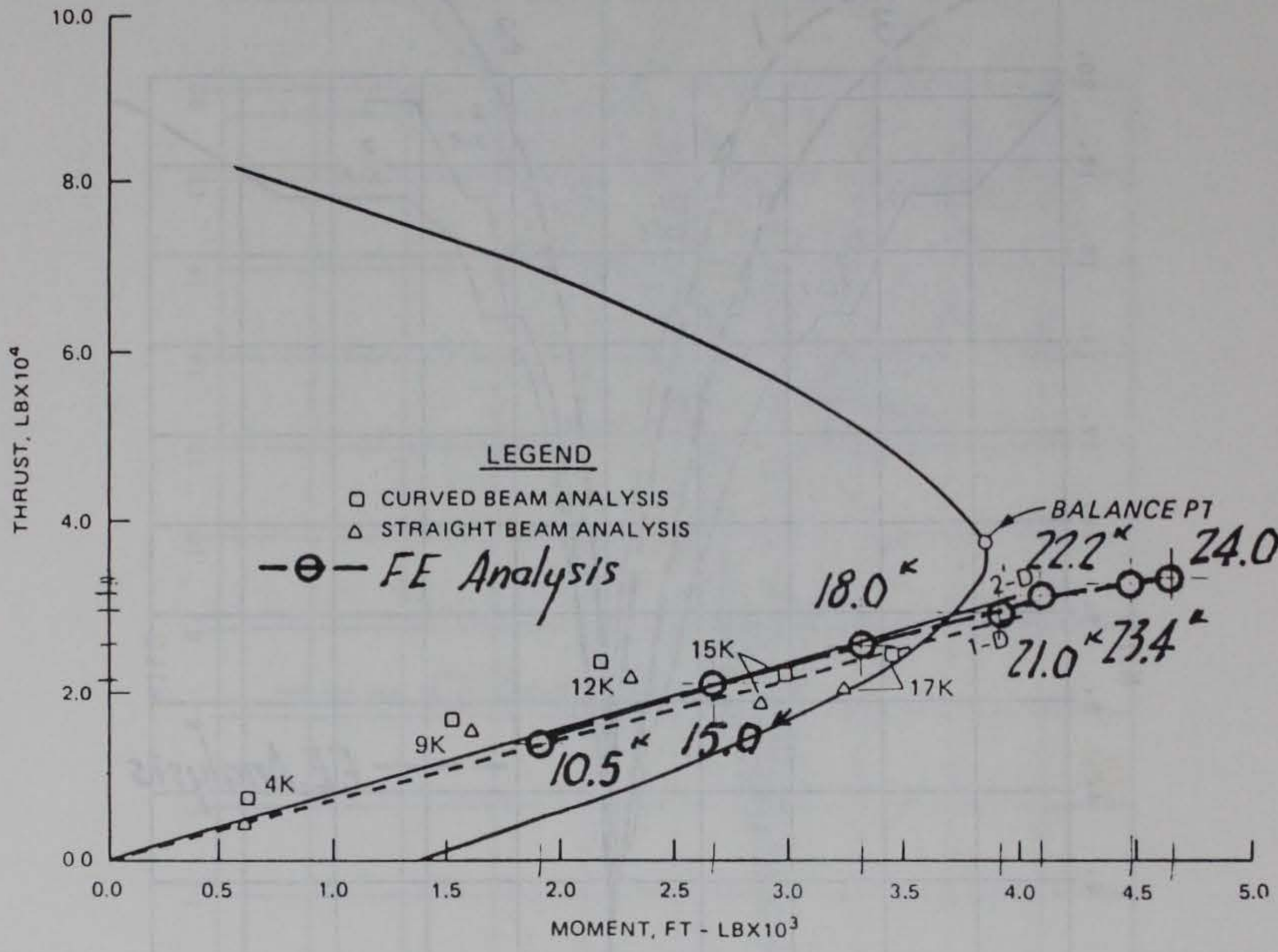

MODEL 5-1, CROWN

Figure 25. Interaction diagram at crown for Model 5-1

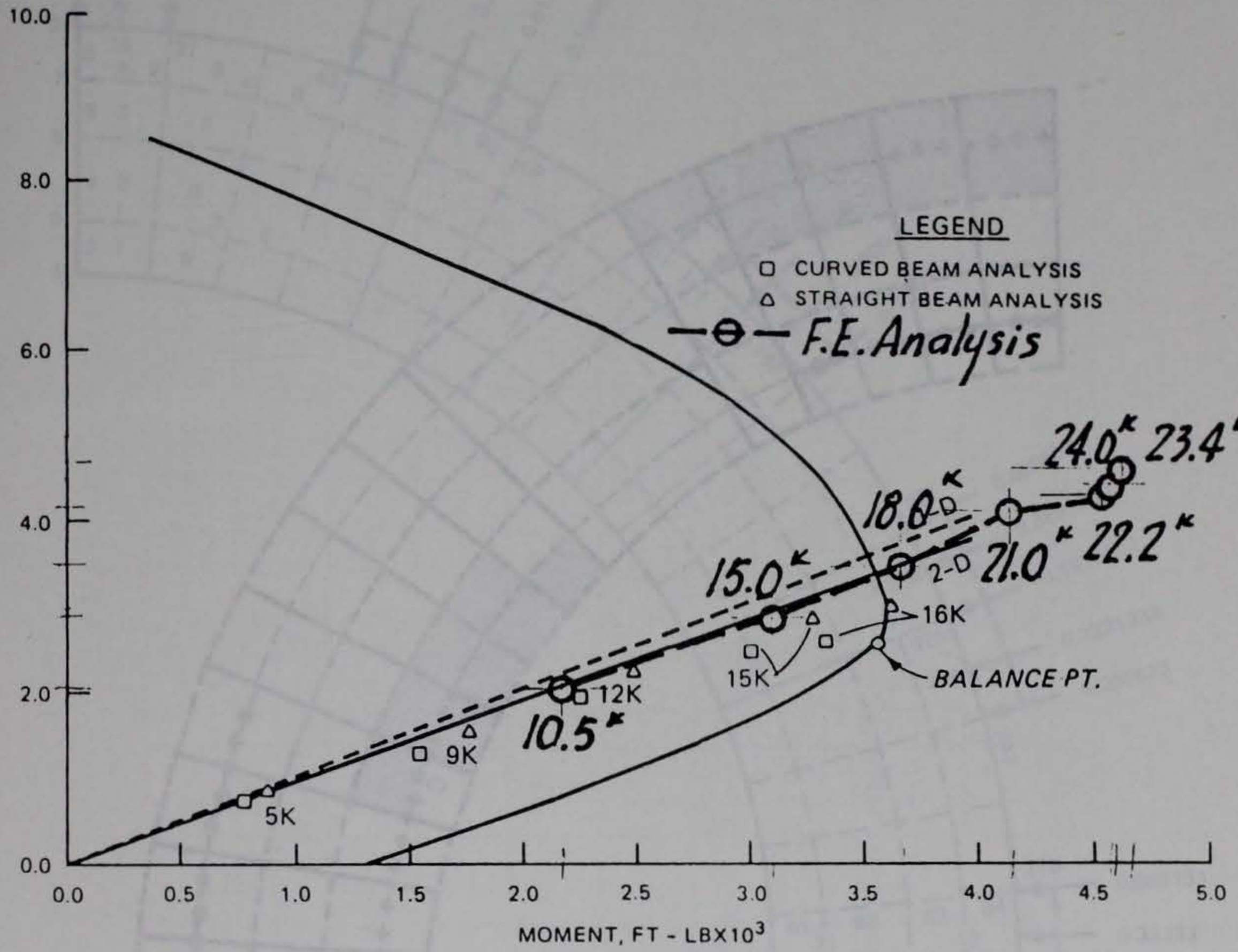

MODEL 5-1, SPRINGING LINE

Figure 26. Interaction diagram at springing line for Model 5-1

- MODEL C51
- TEST LOAD 3:1
- P_{CROWN} = 24.60 KIPS

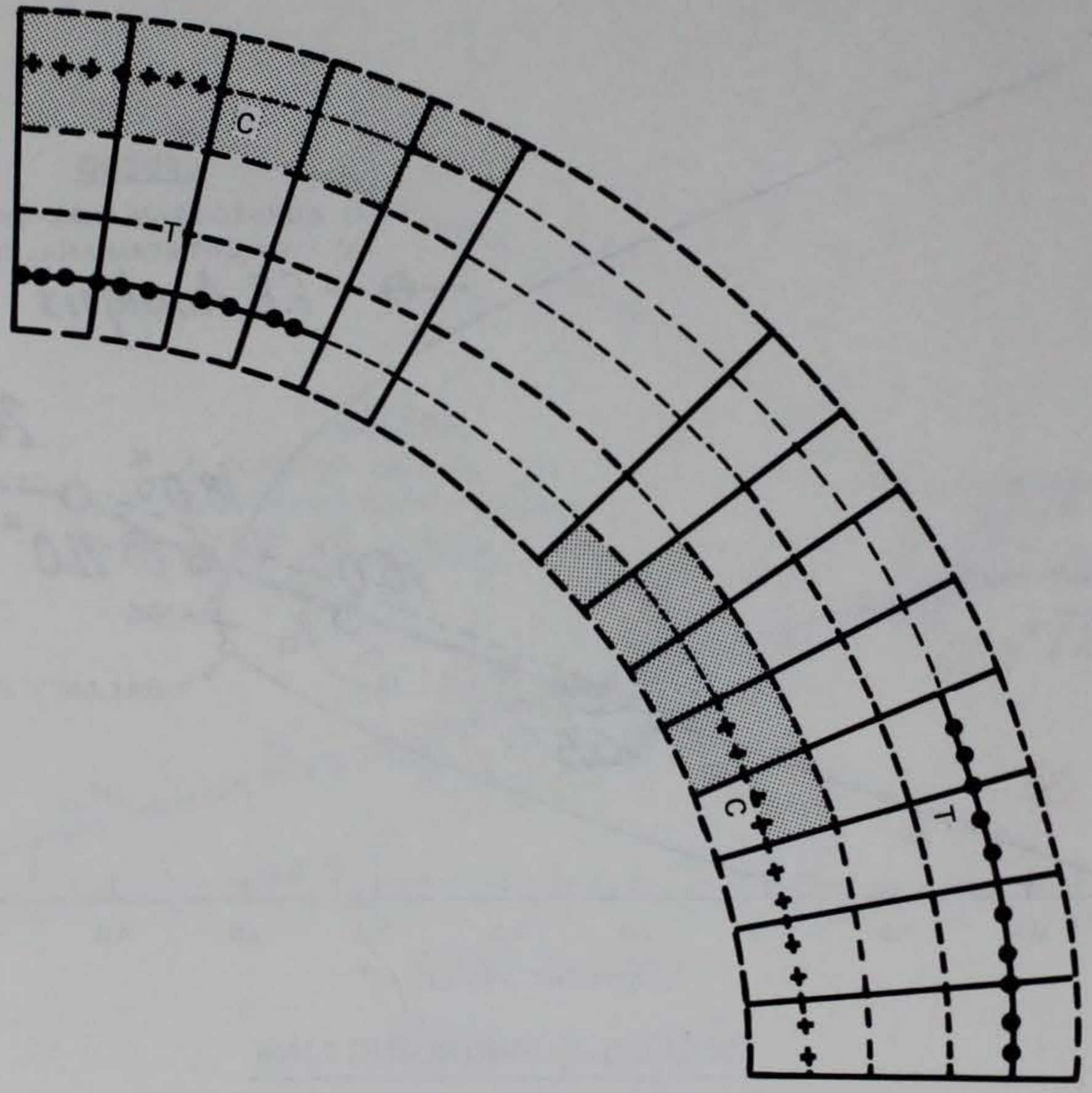

Figure 27. Crack pattern for Model C51

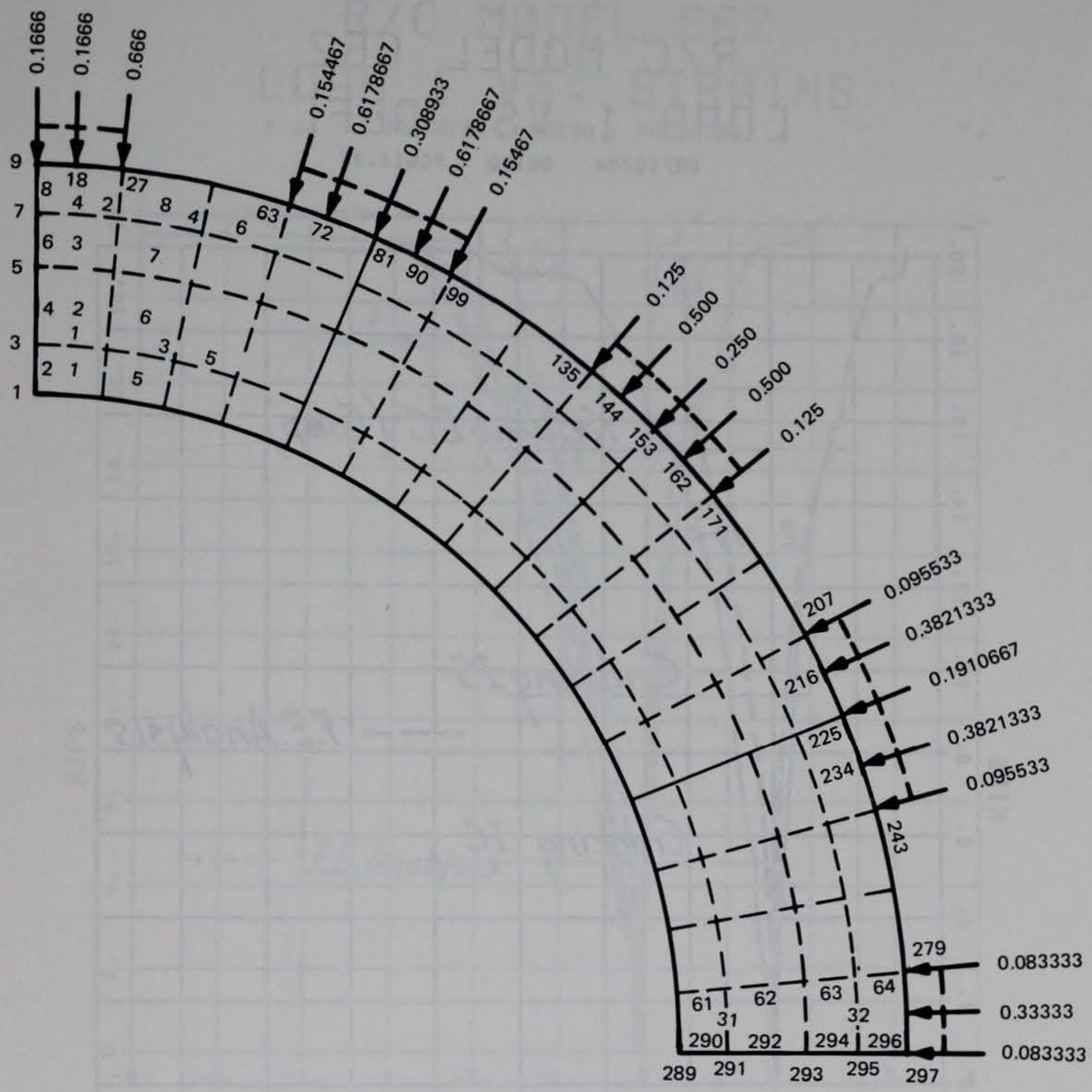

Figure 28. Finite element grid for Model C62

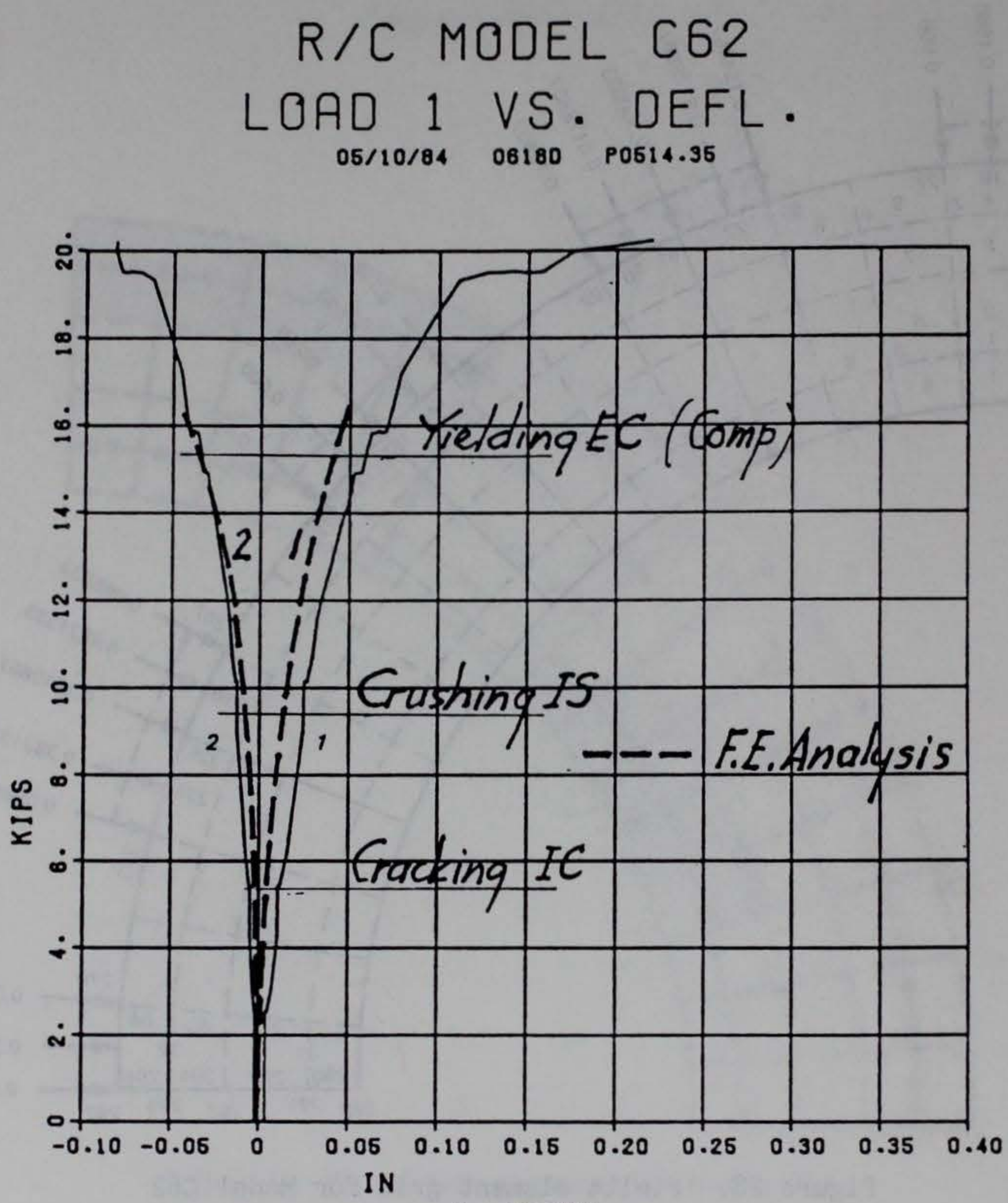

1. CROWN
2. SPRINGING LINE

Figure 29. Load versus deflections for Model C62

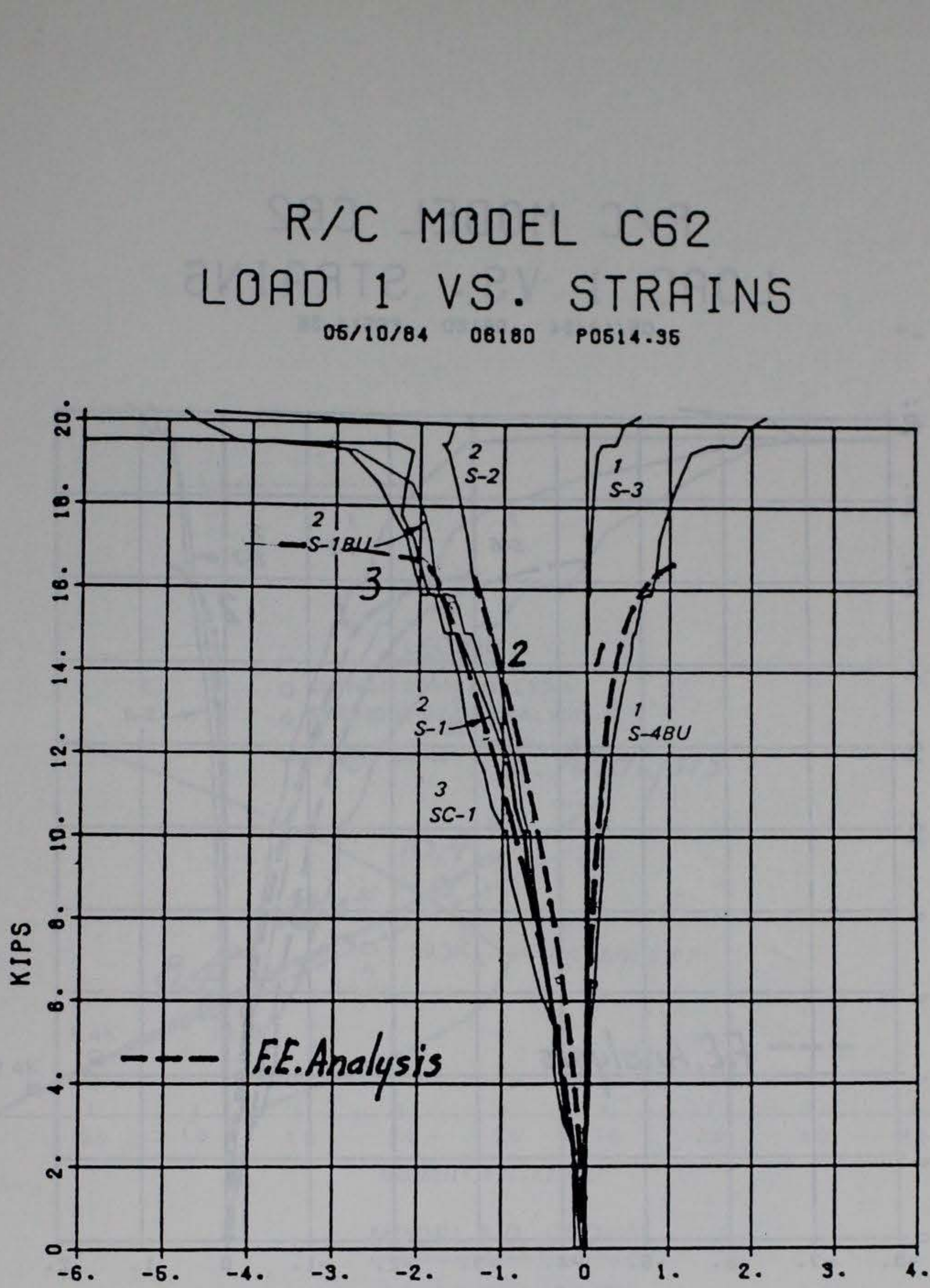

Figure 30. Load versus strain at crown for Model C62

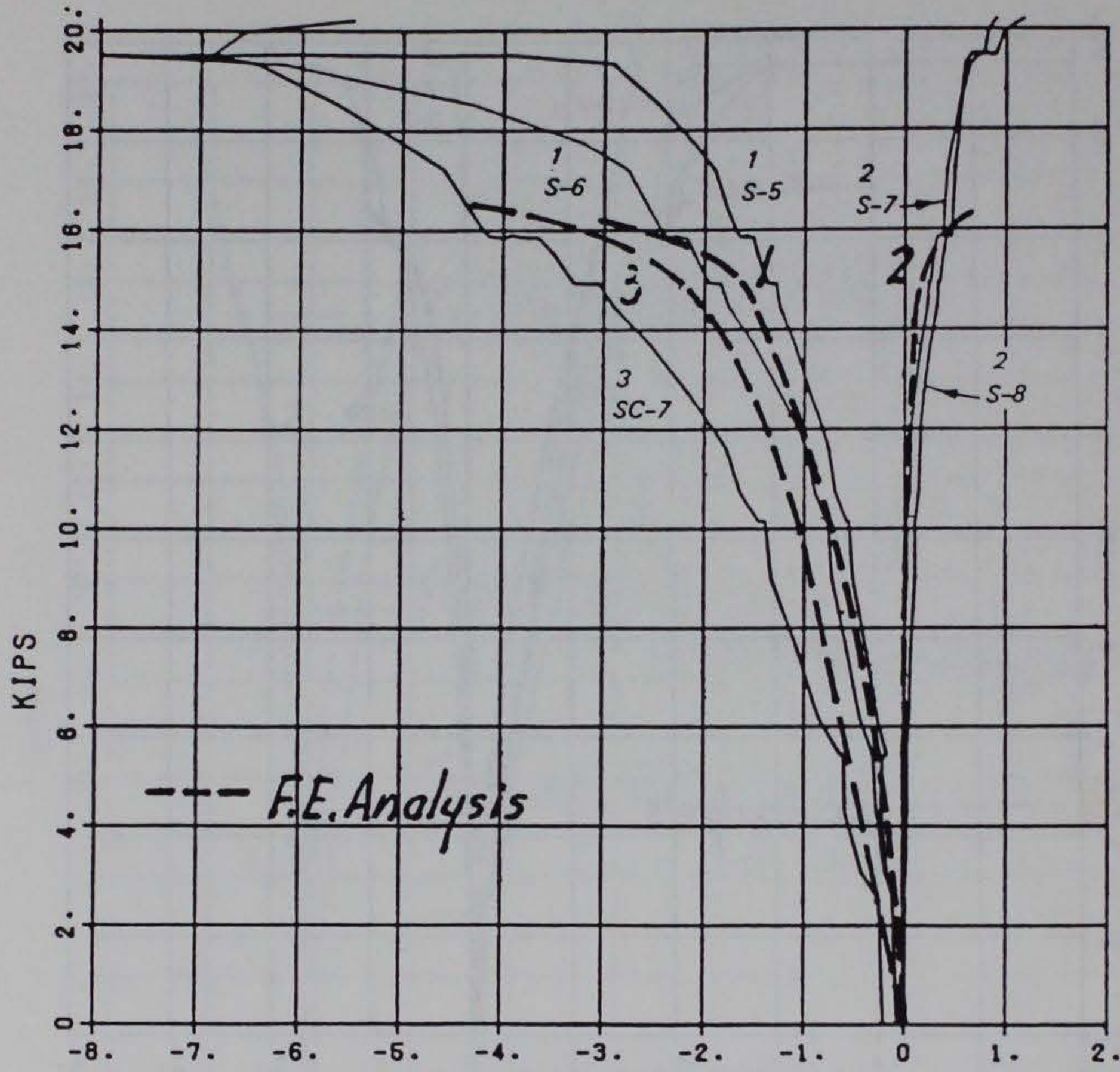

Figure 31. Load versus strain at springing line for Model C62

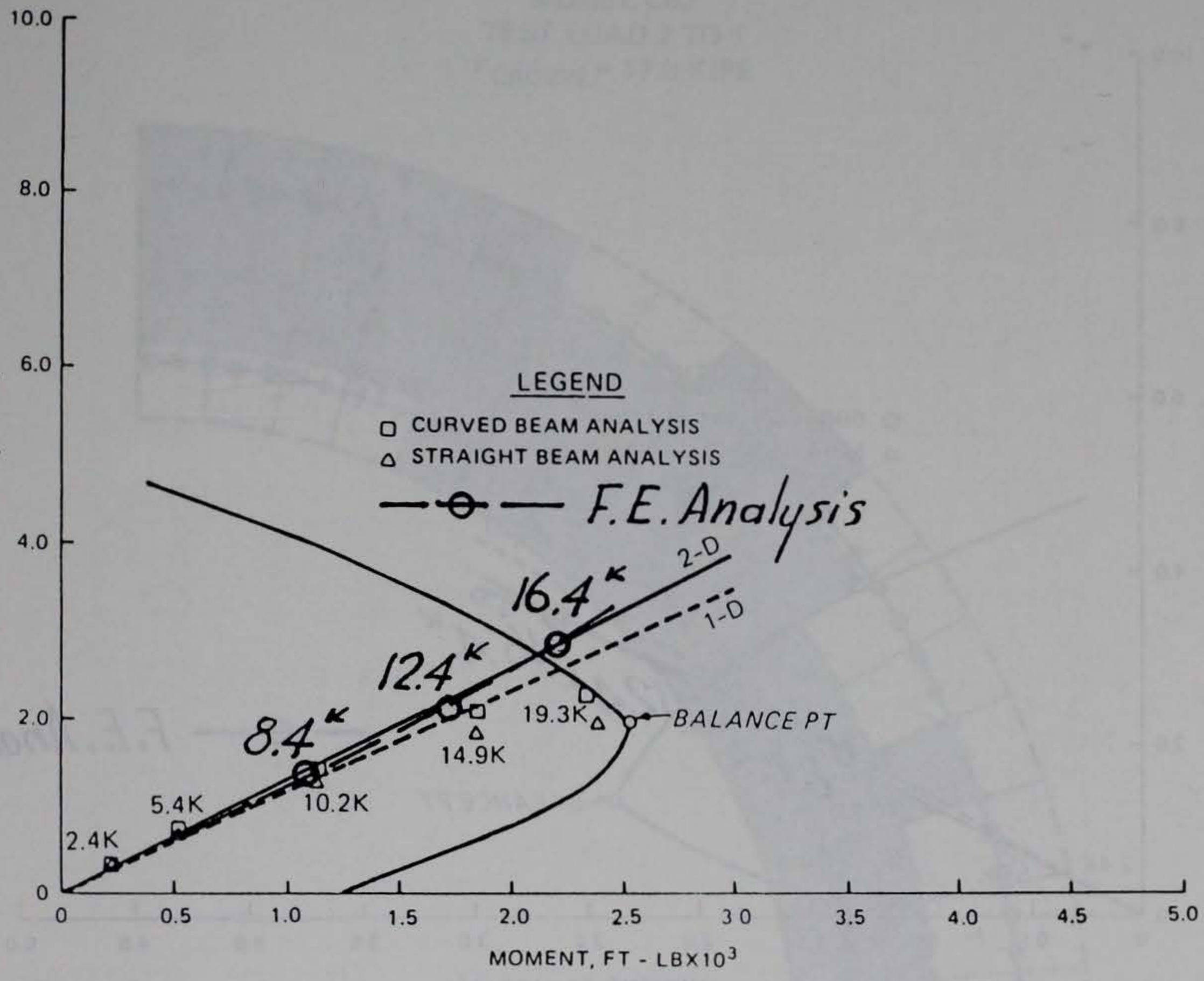

MODEL 6-2, CROWN

Figure 32. Interaction diagram at crown for Model 6-2

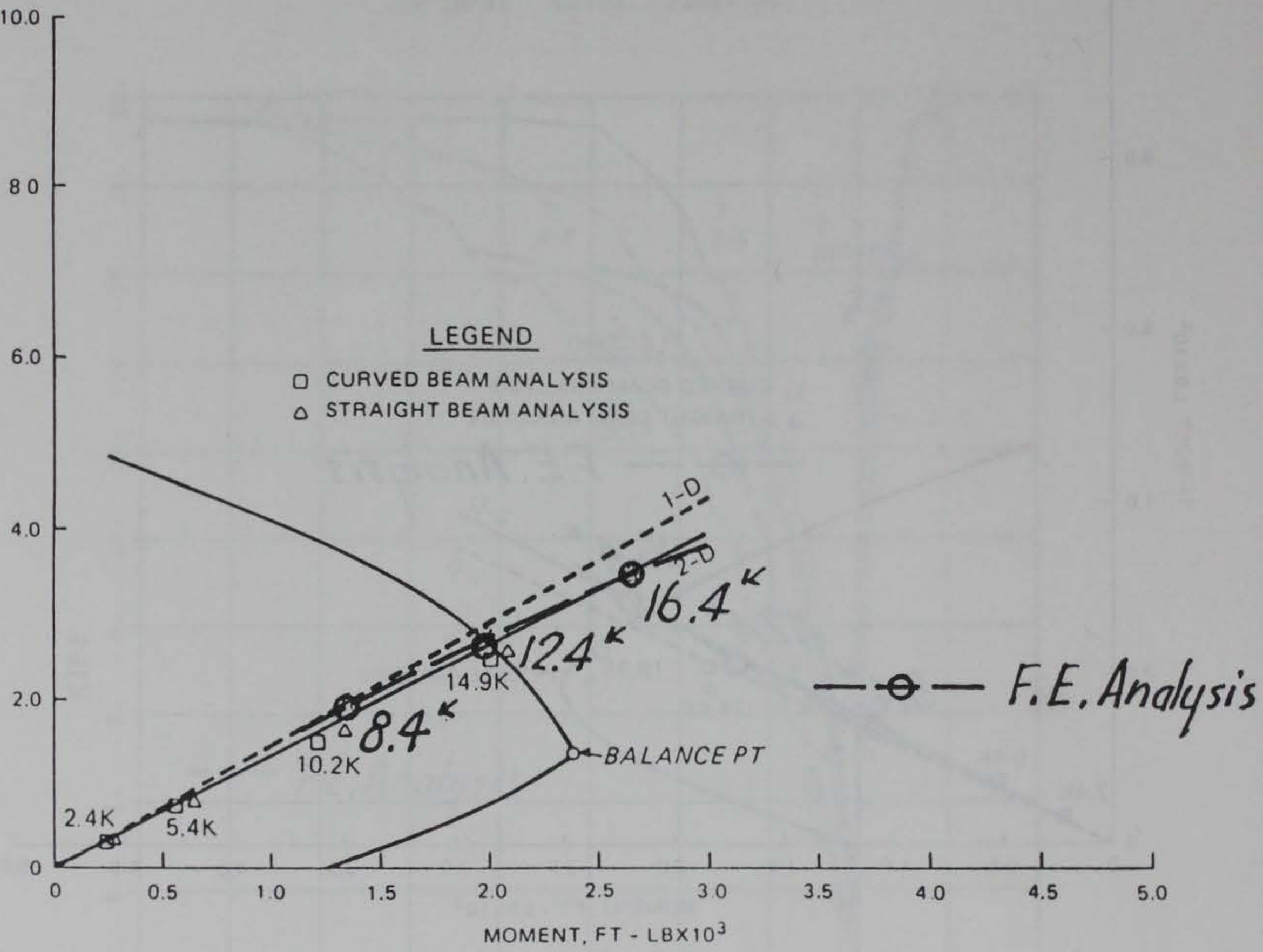

MODEL 6-2, SPRINGING LINE

Figure 33. Interaction diagram at springing line for Model 6-2

MODEL C62
TEST LOAD 2 TO 1
P_{CROWN} = 17.0 KIPS

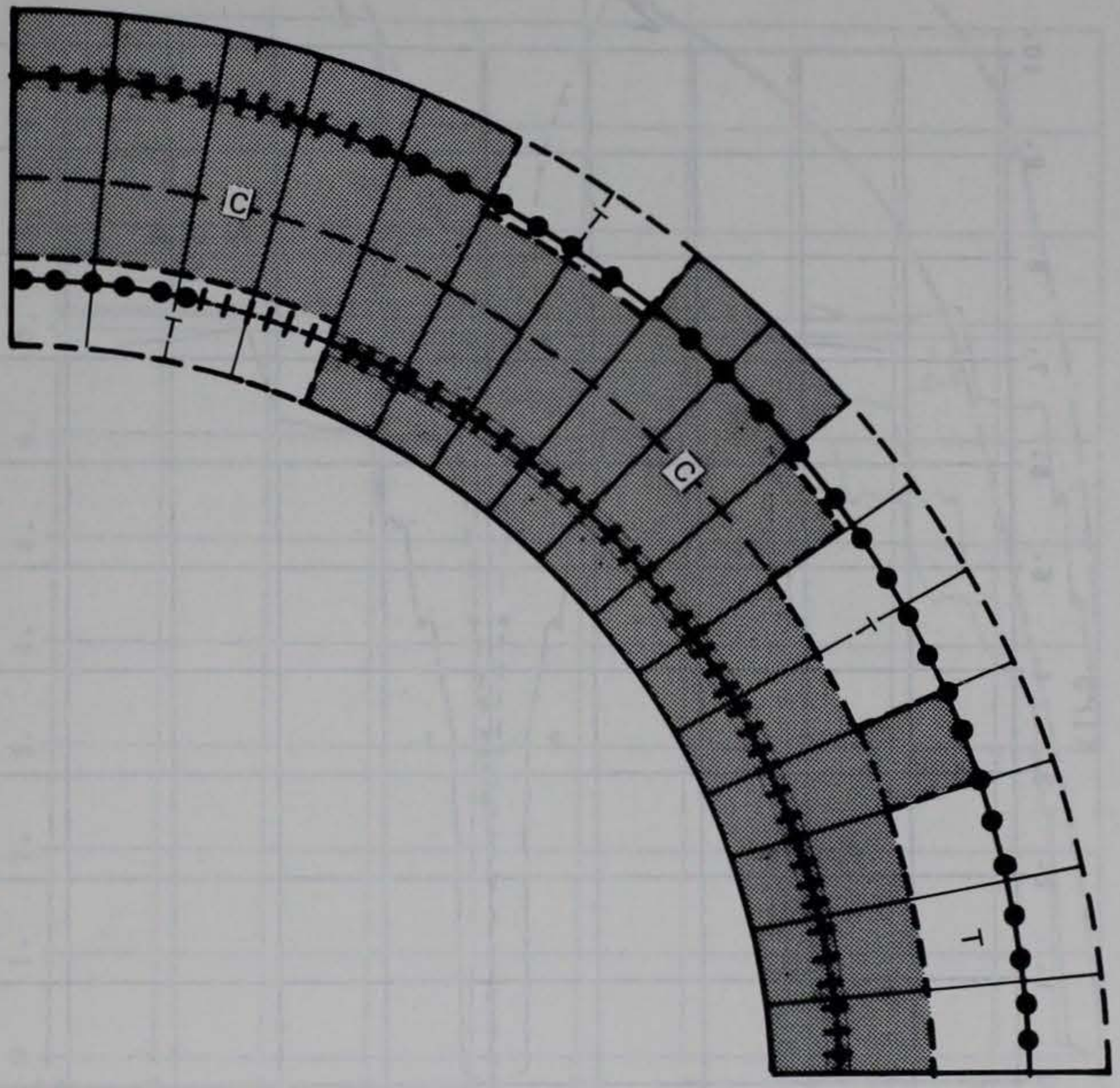

Figure 34. Crack pattern for Model C62

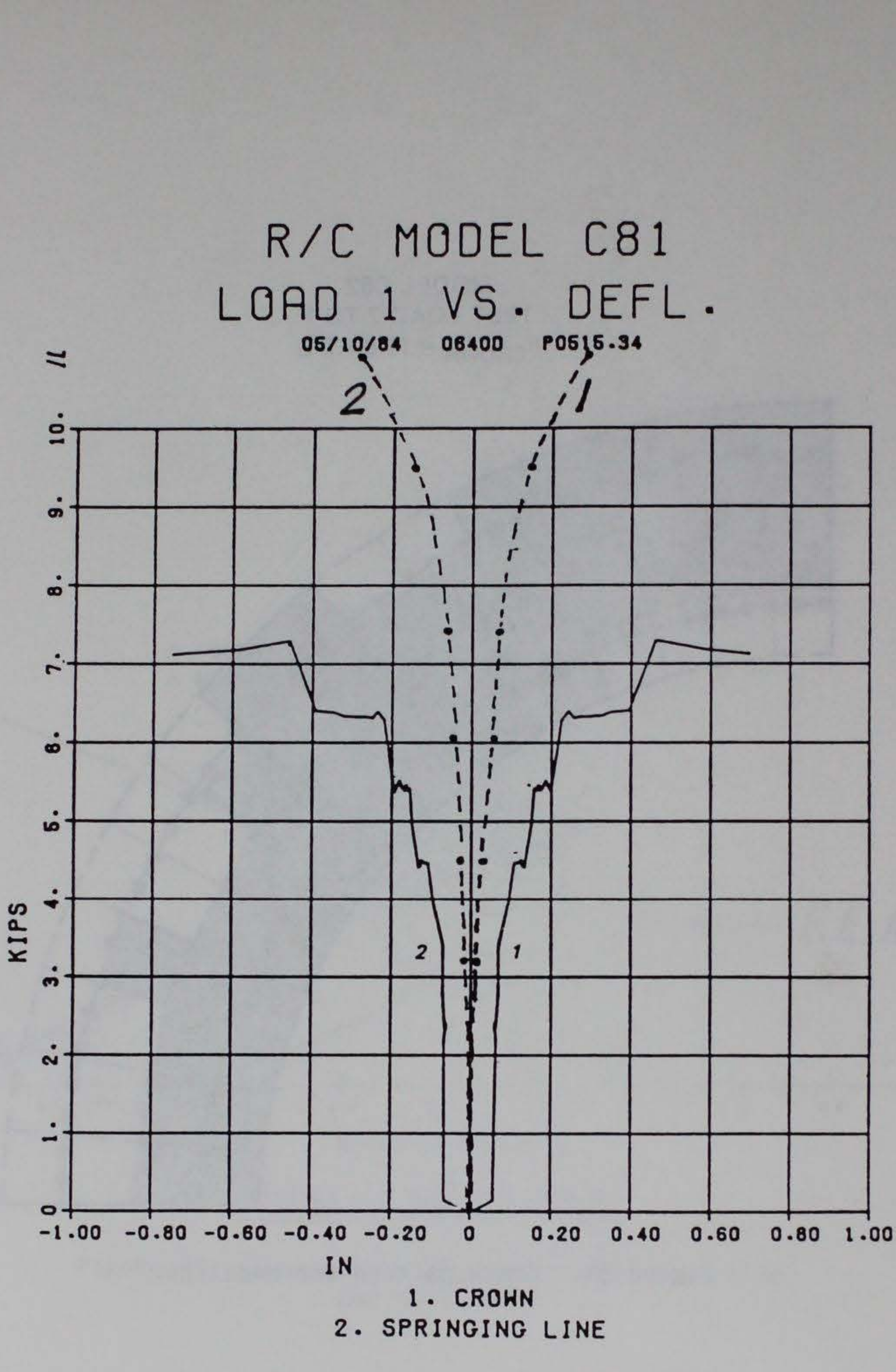

Figure 35. Load versus displacements for Model C81

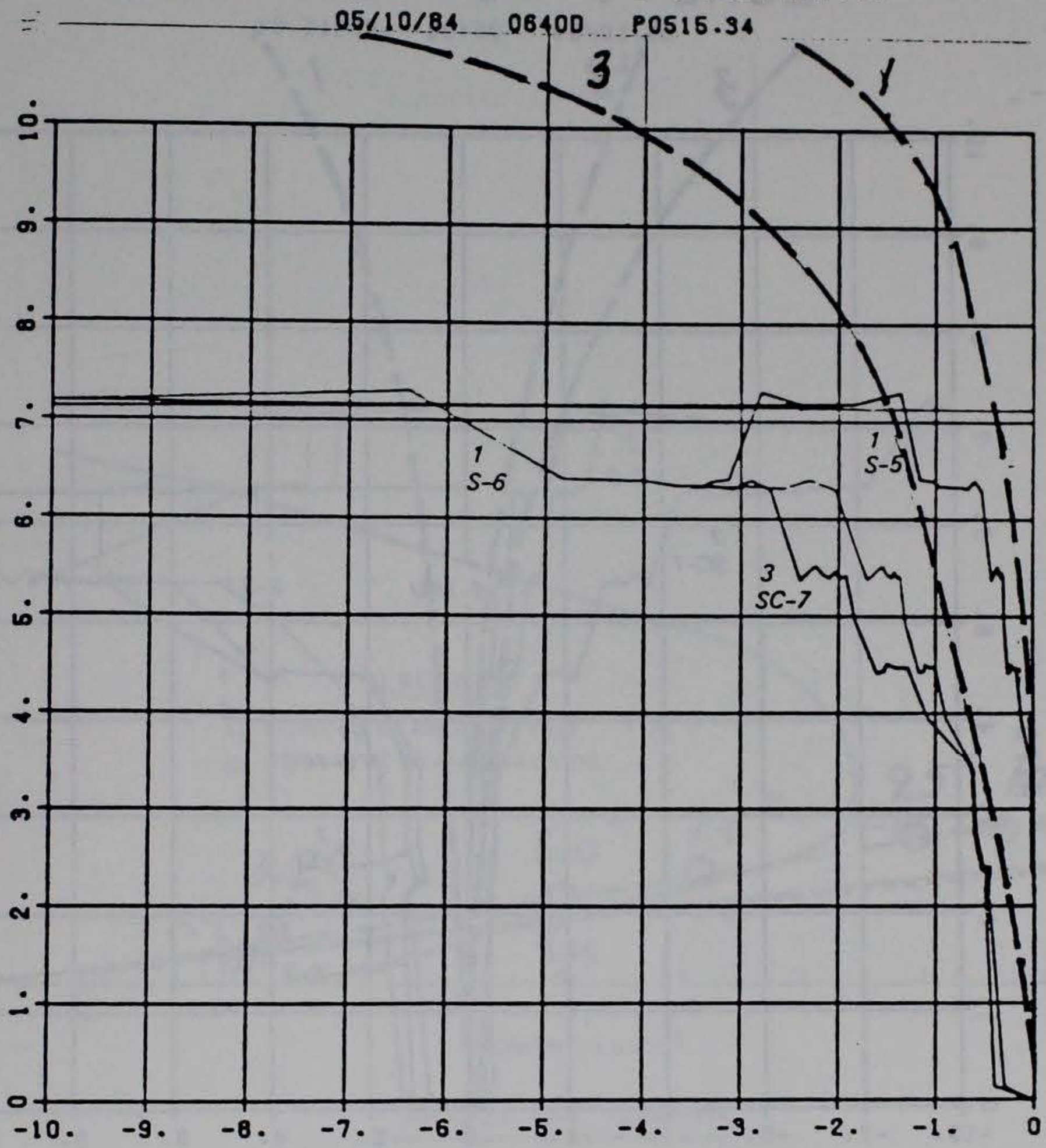

Figure 36. Load versus strain at crown for Model C81

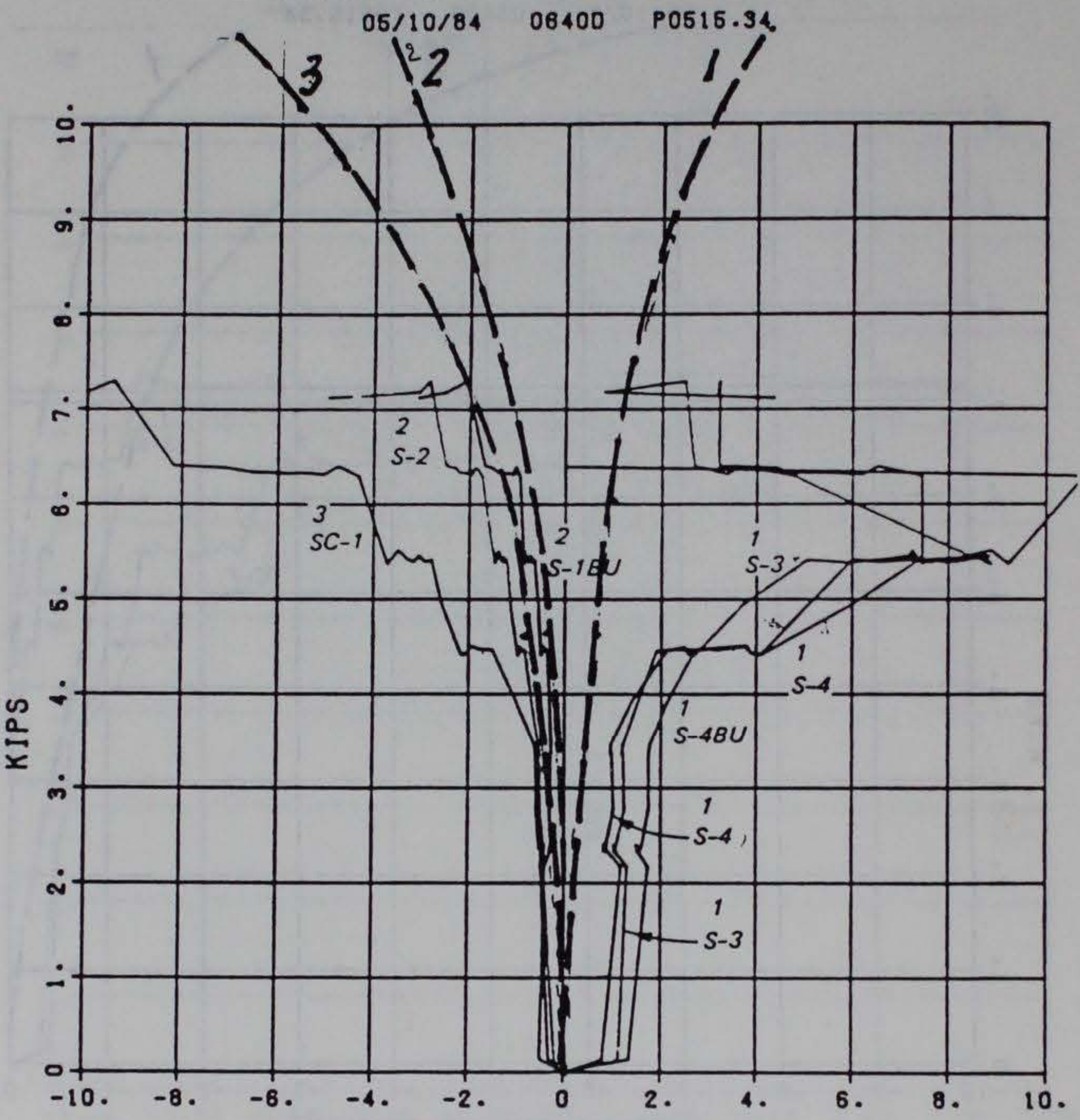

Figure 37. Load versus strains at springing line for Model C81

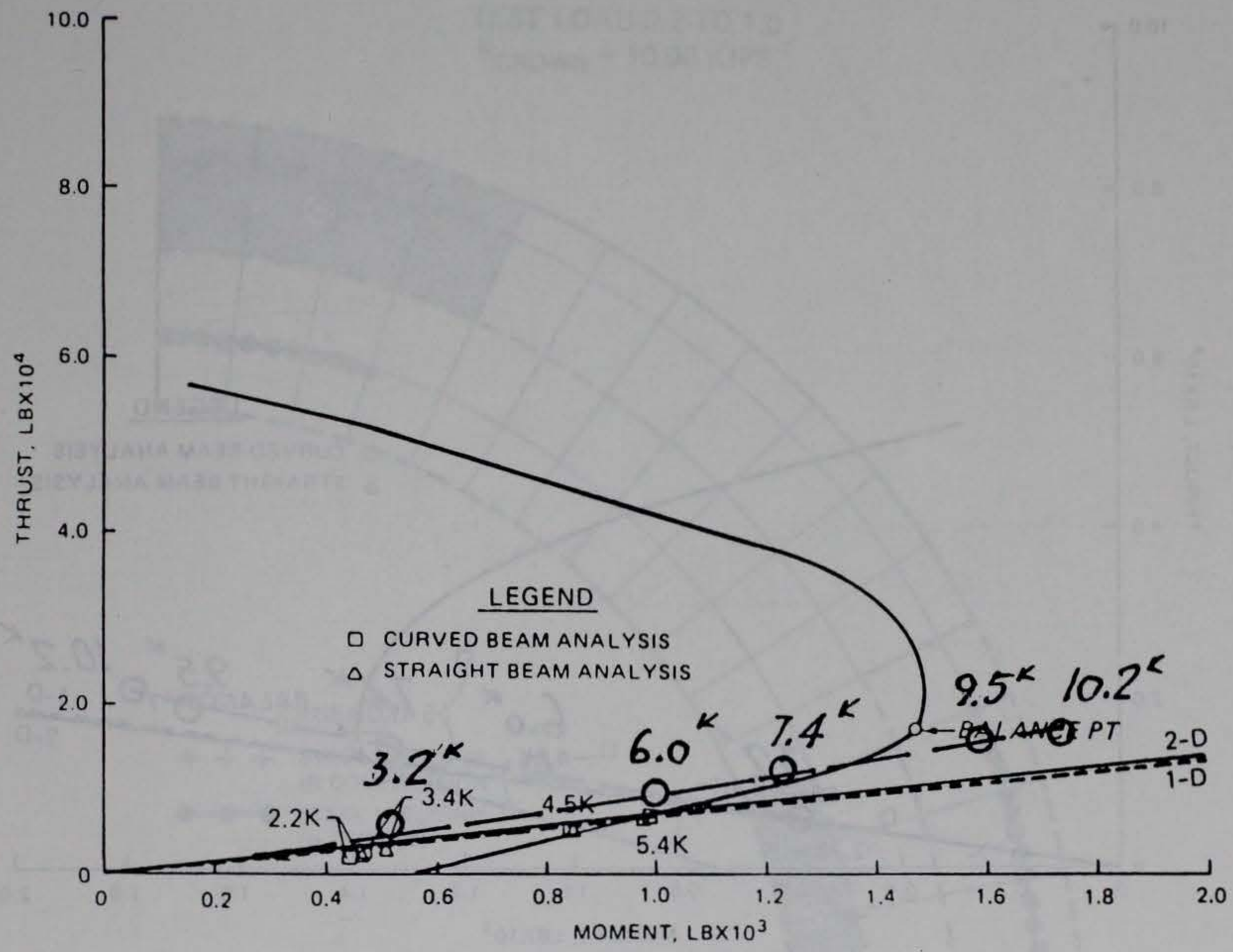

MODEL 8-1, CROWN

Figure 38. Interaction diagram at crown for Model 8-1

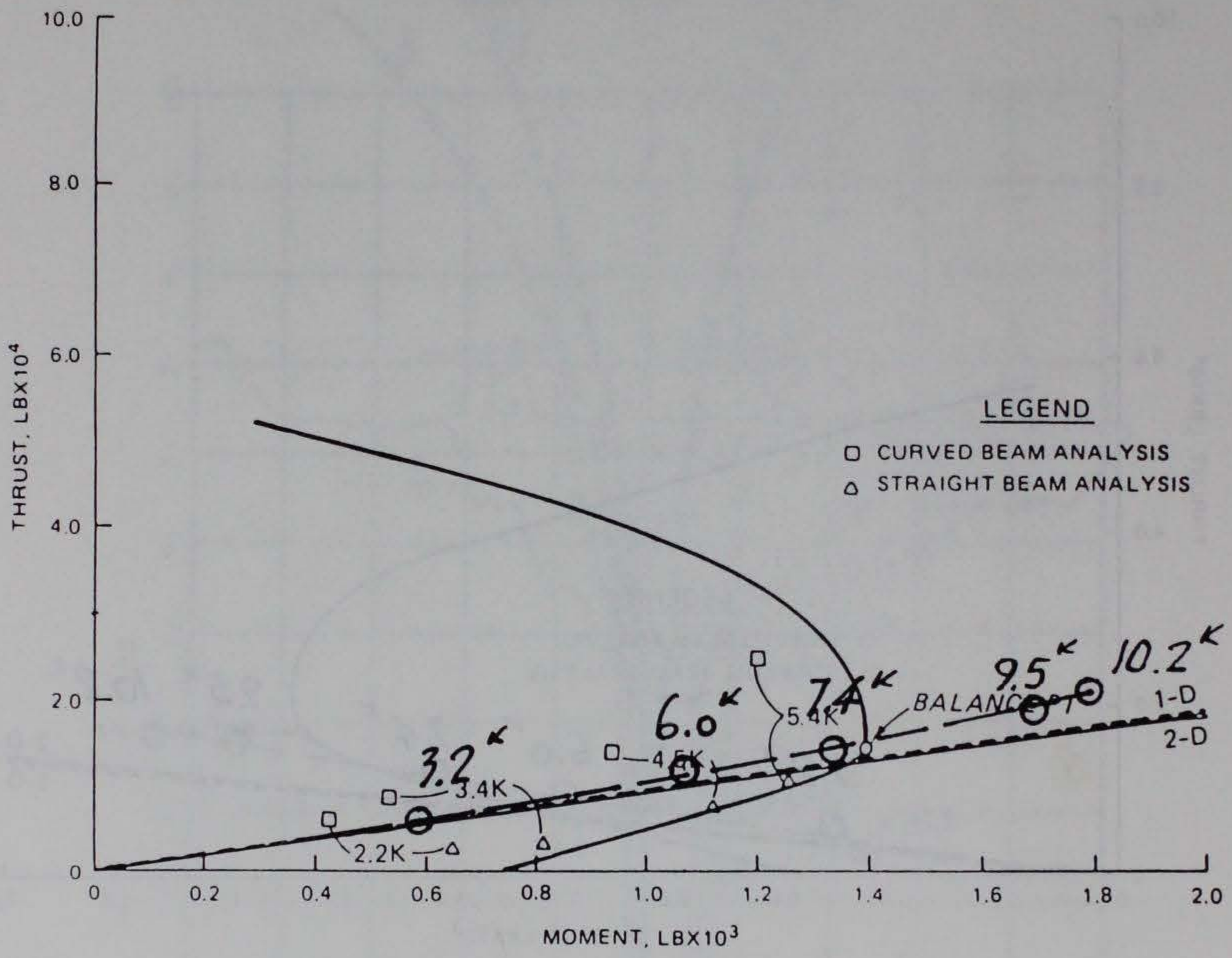

MODEL 8-1, SPRINGING LINE

Figure 39. Interaction diagram at springing line for Model 8-1

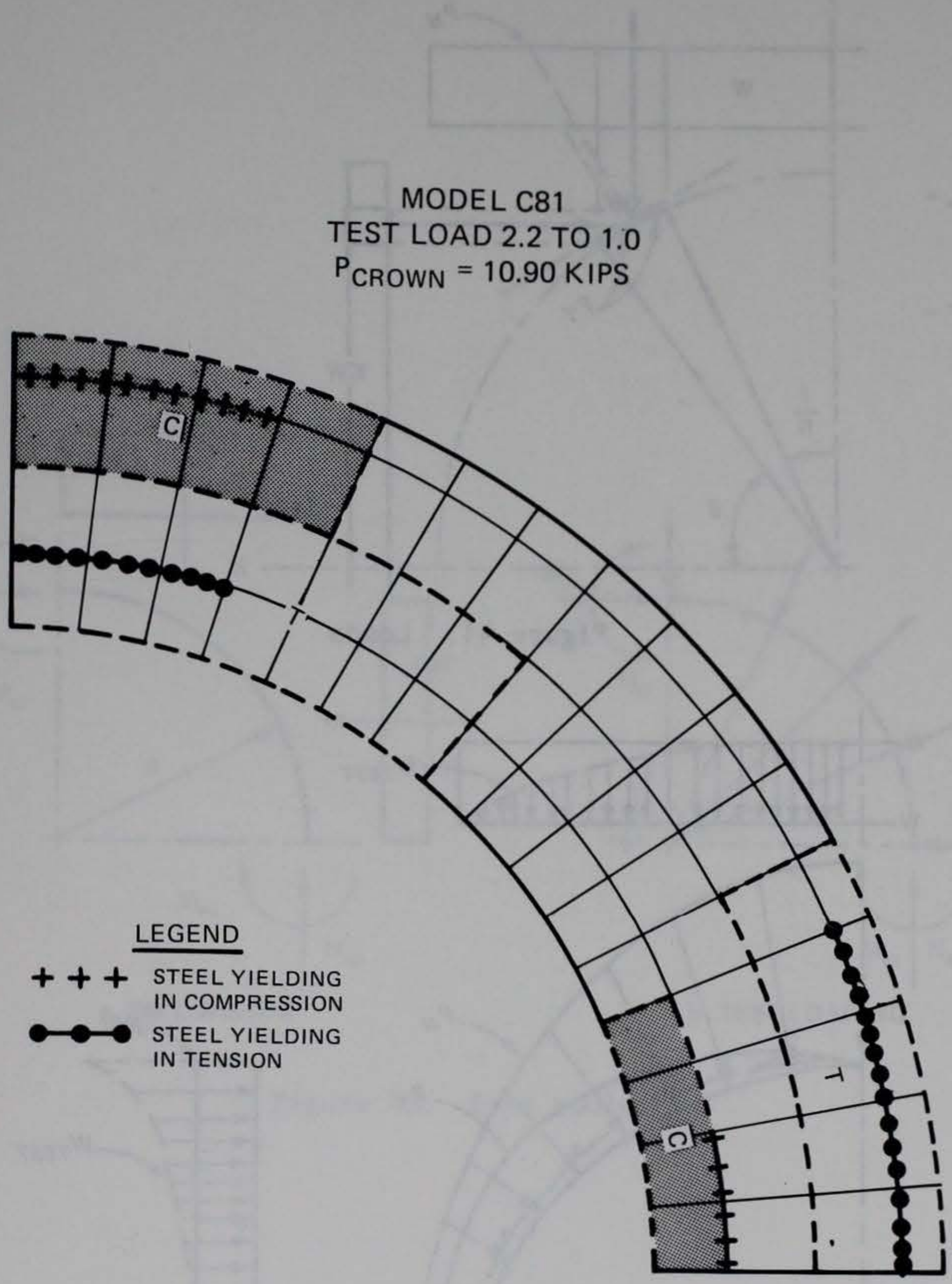

Figure 40. Crack pattern for Model C81

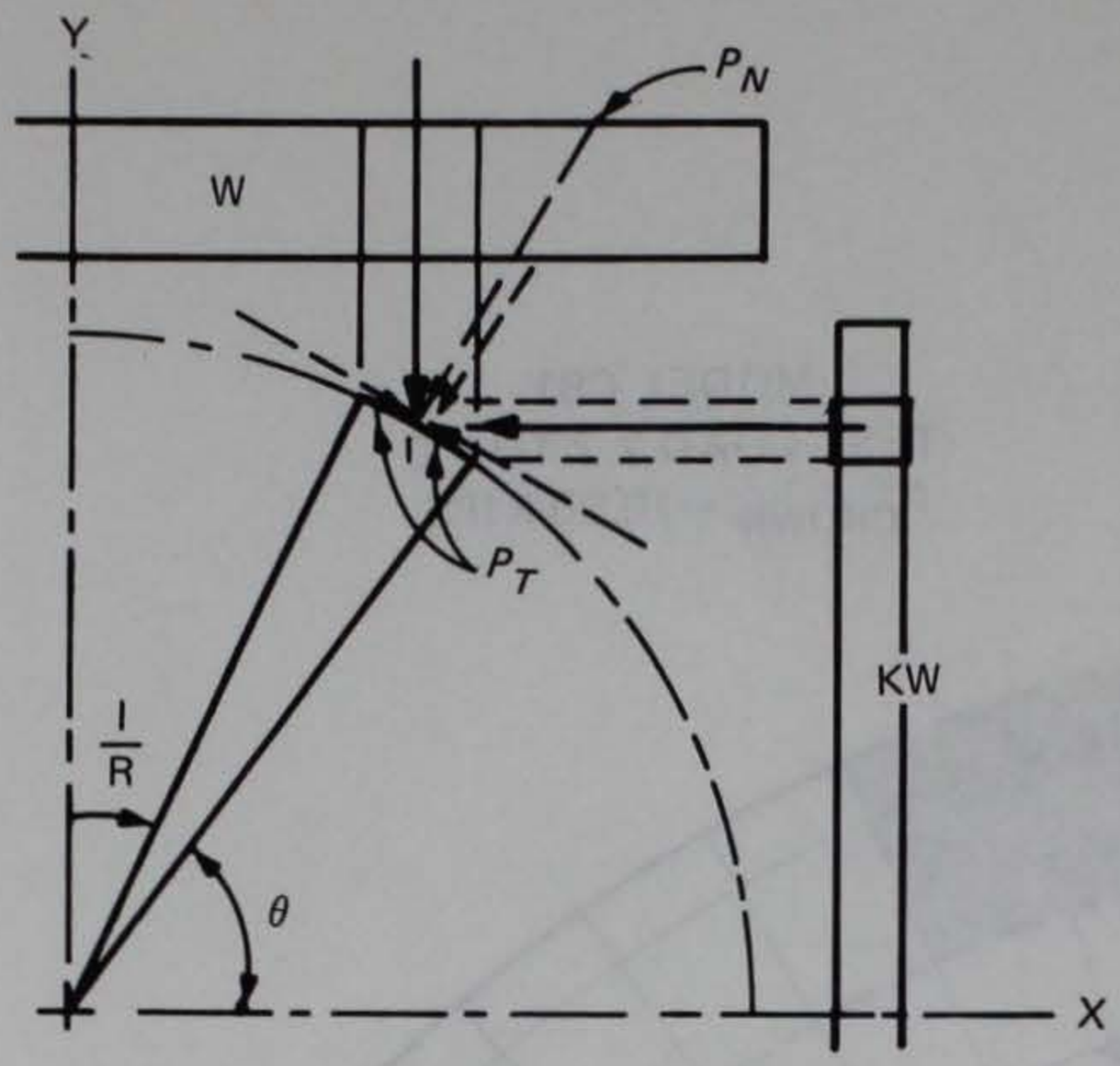

Figure 41. Loads

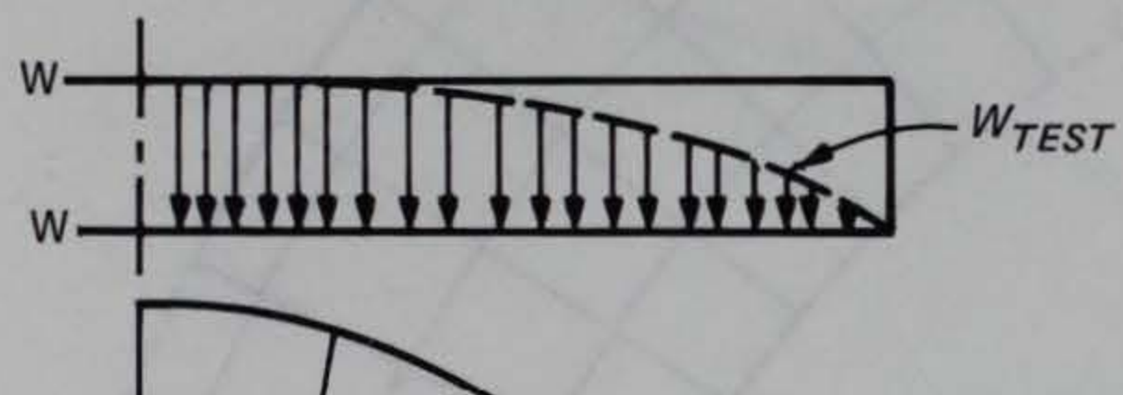

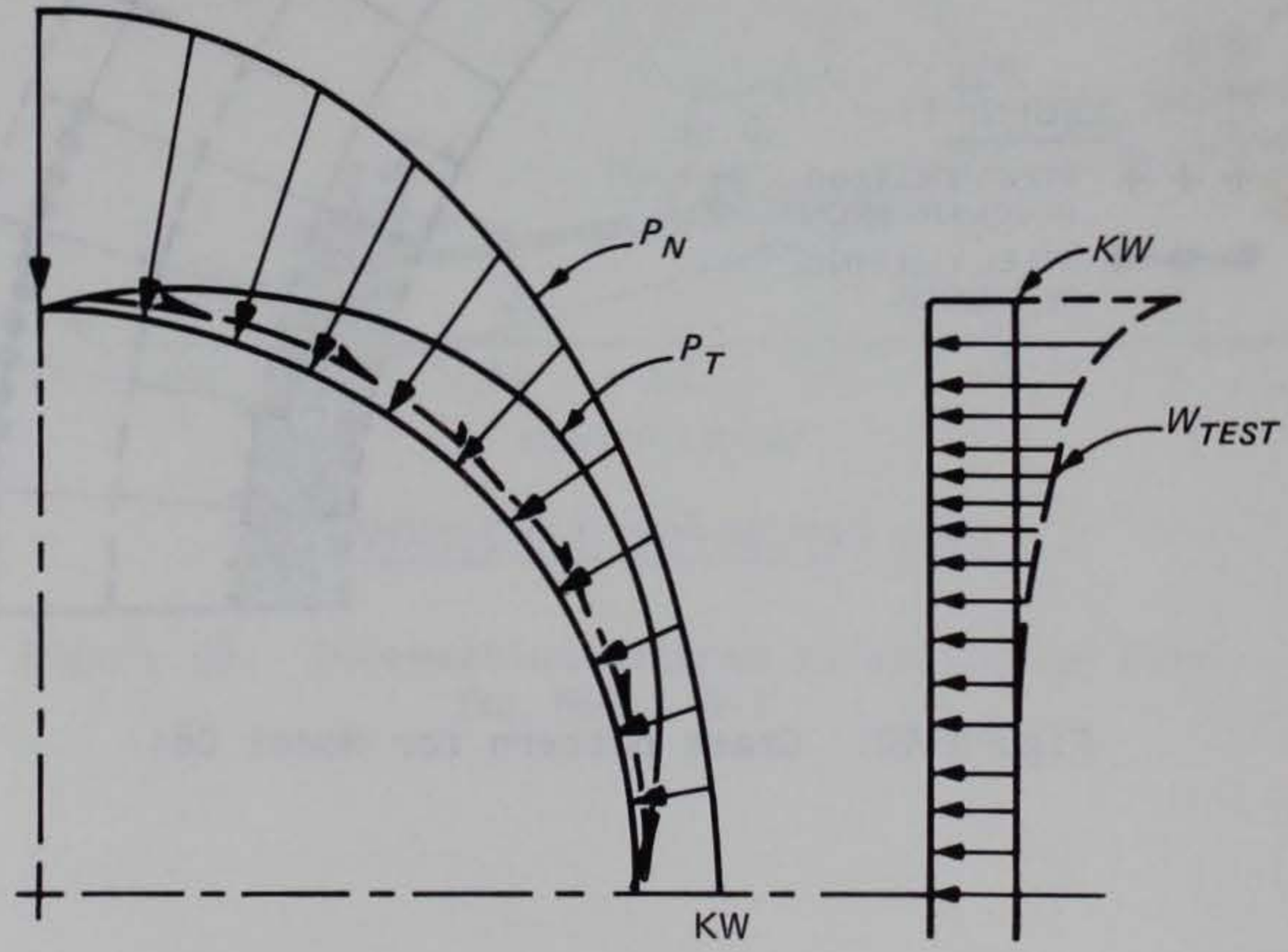

Figure 42. Surface tractions

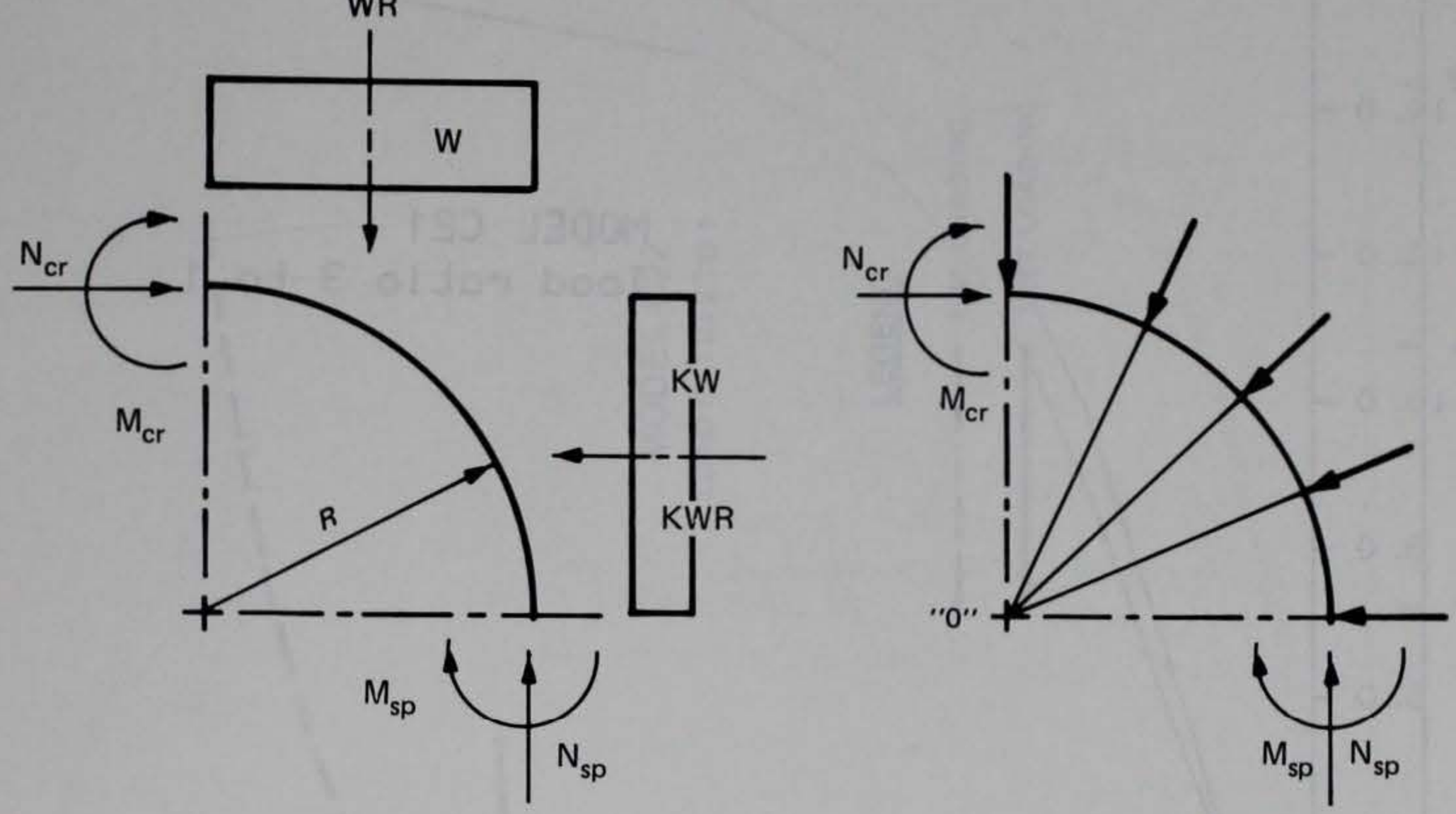

Figure 43. Free bodies

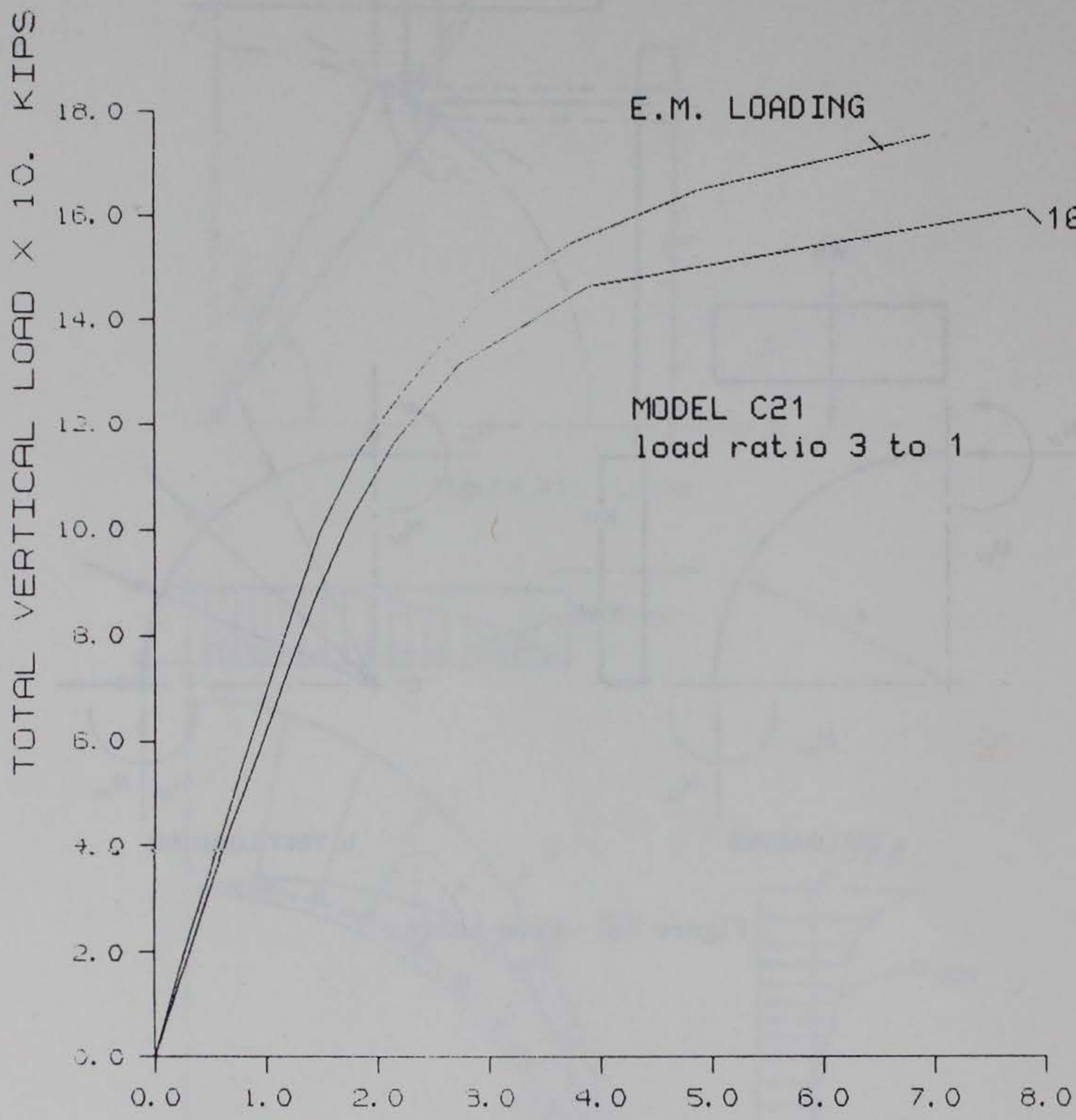

Figure 44. Load versus crown displacement for Model C21

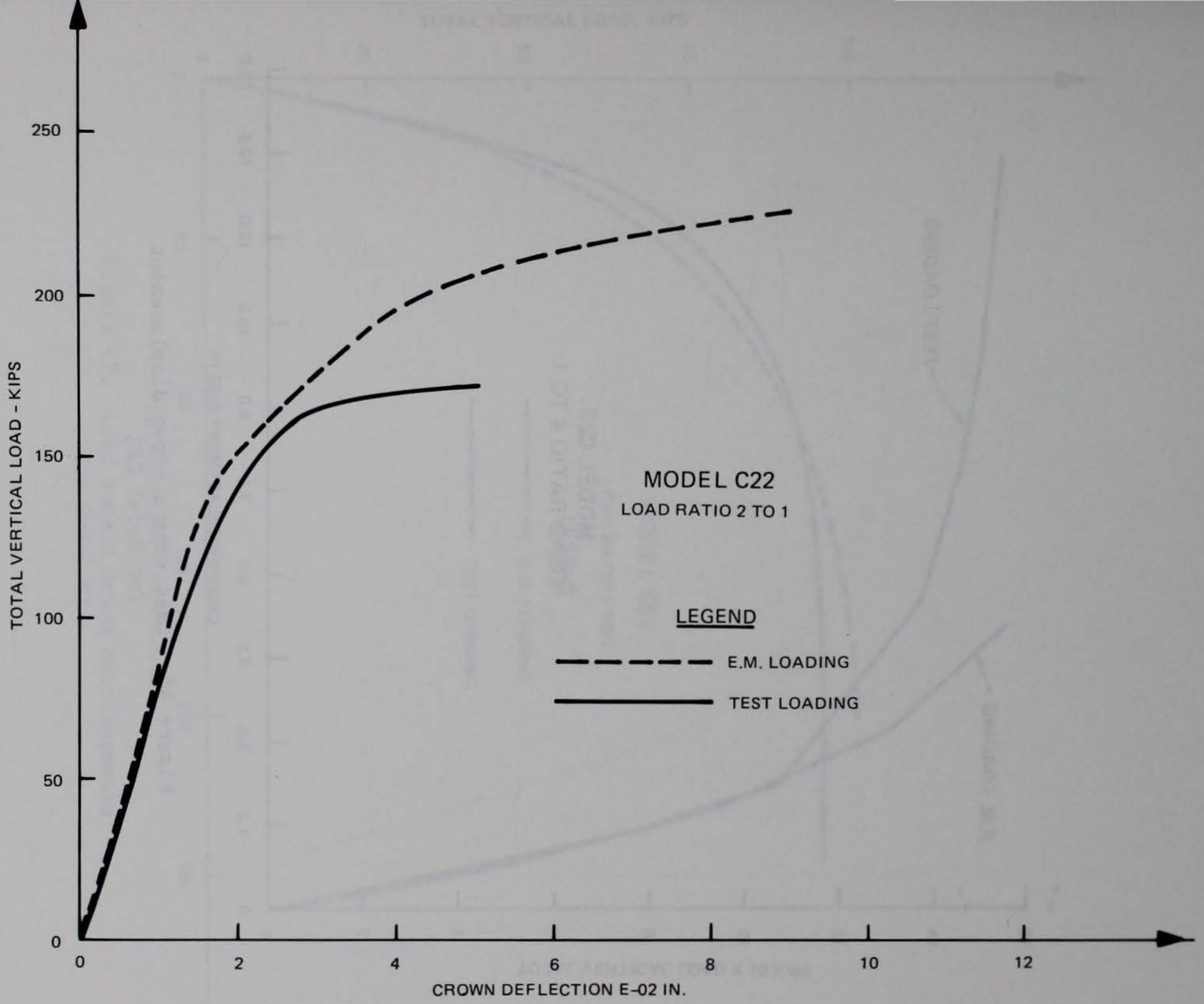

Figure 45. Load versus crown deflections for Model C22

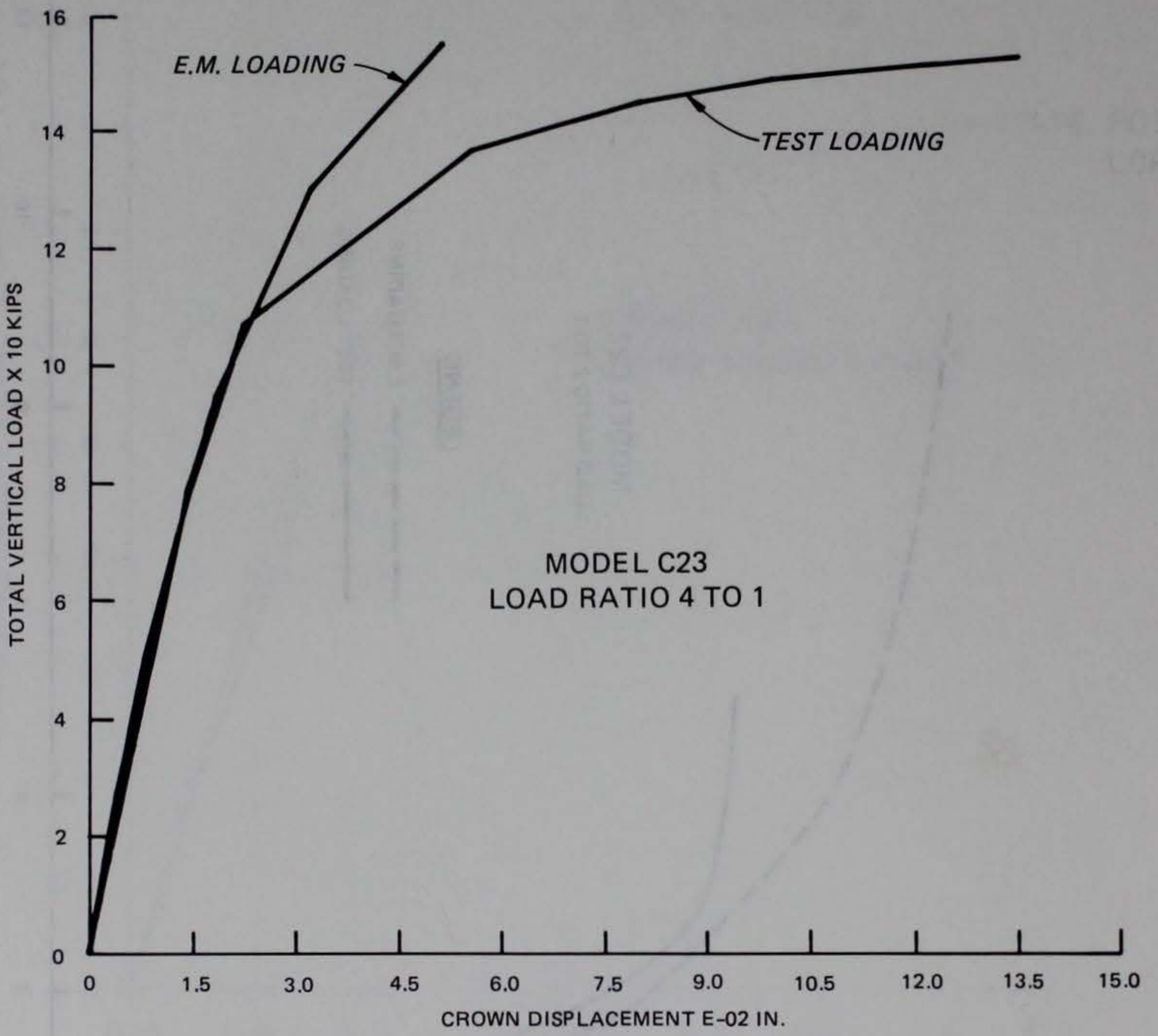

Figure 46. Load versus crown displacement for Model C23

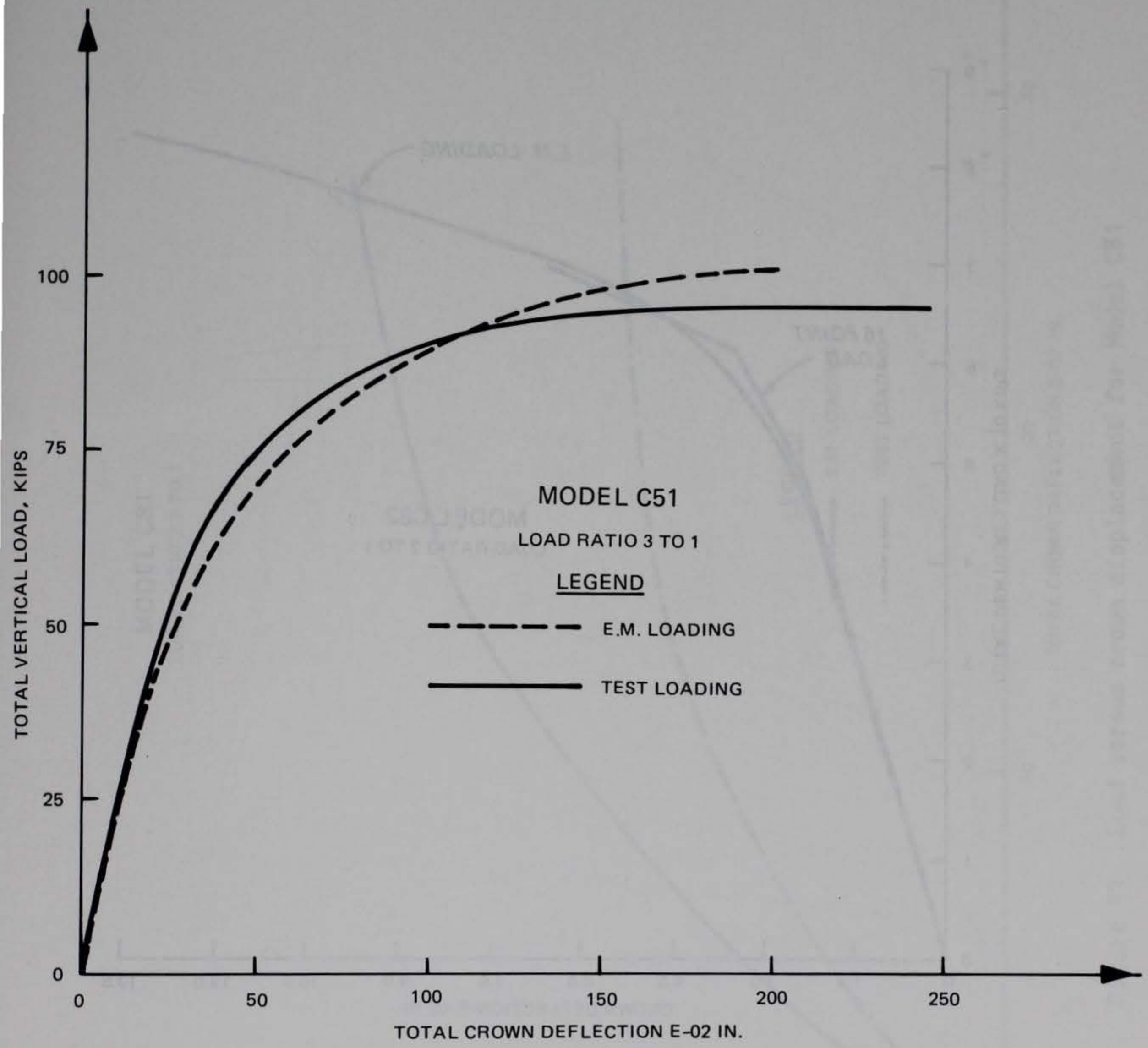

Figure 47. Load versus crown displacements for Model C51

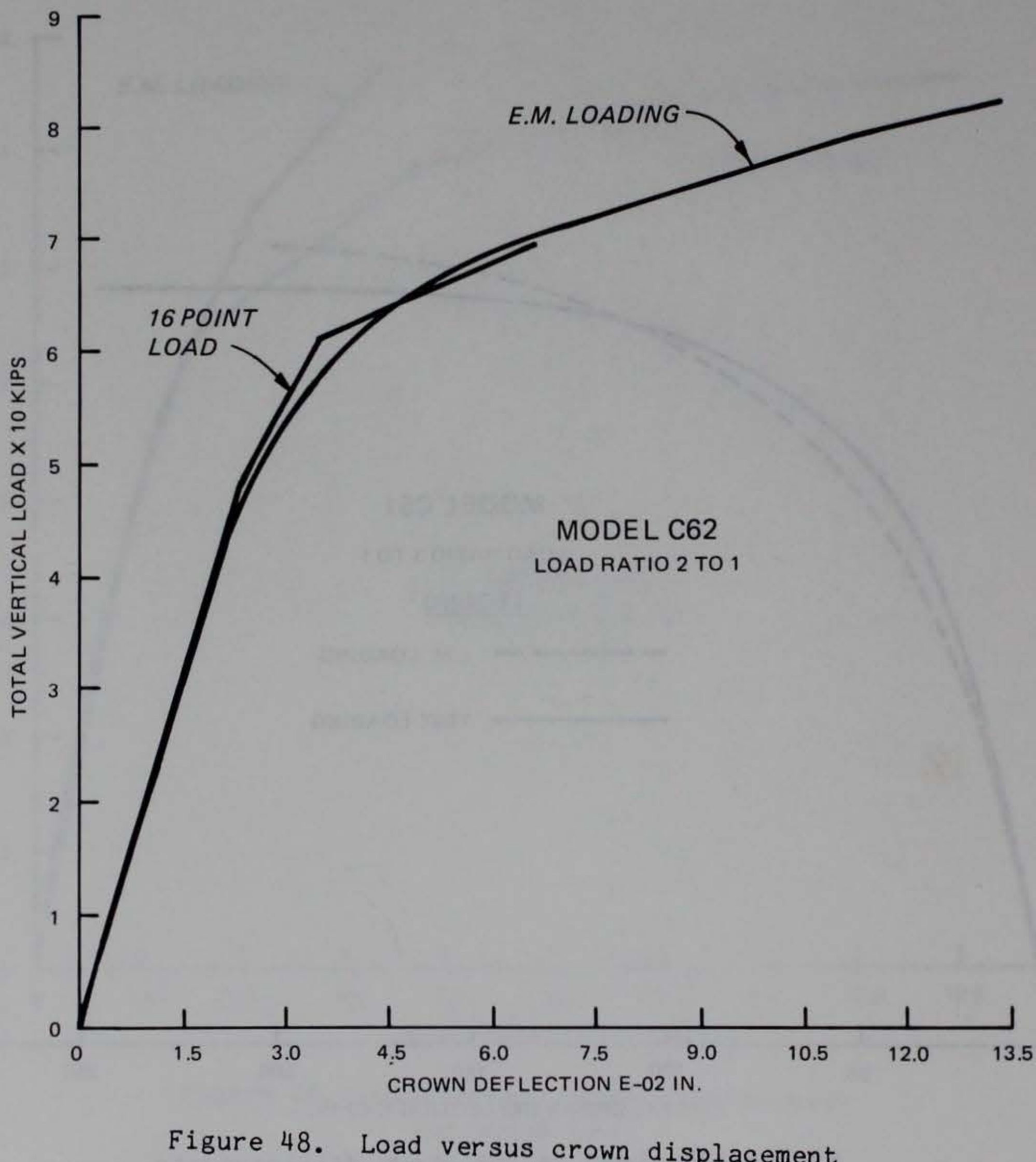

Figure 48. Load versus crown displacement for Model C62

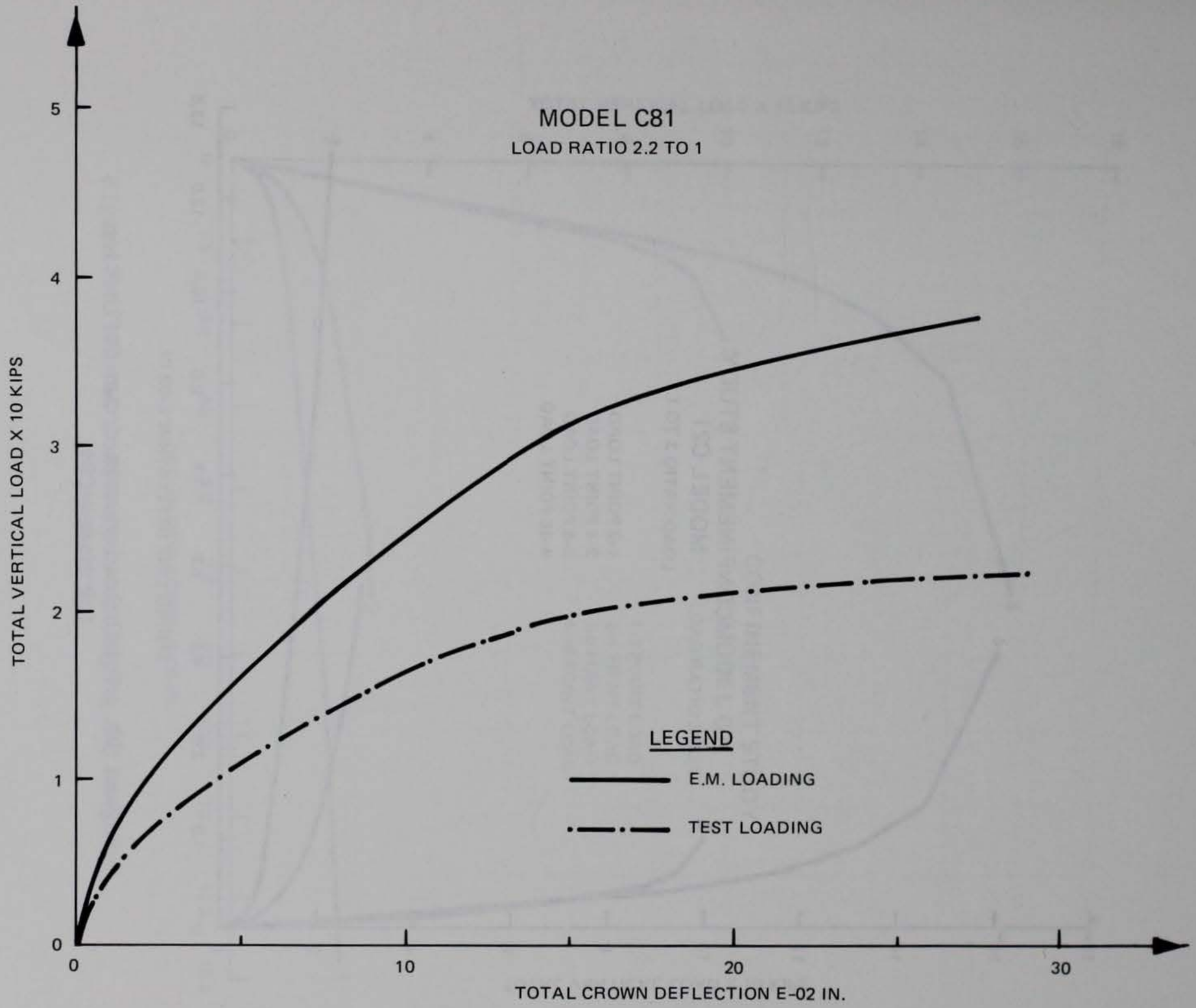

Figure 49. Load versus crown displacement for Model C81

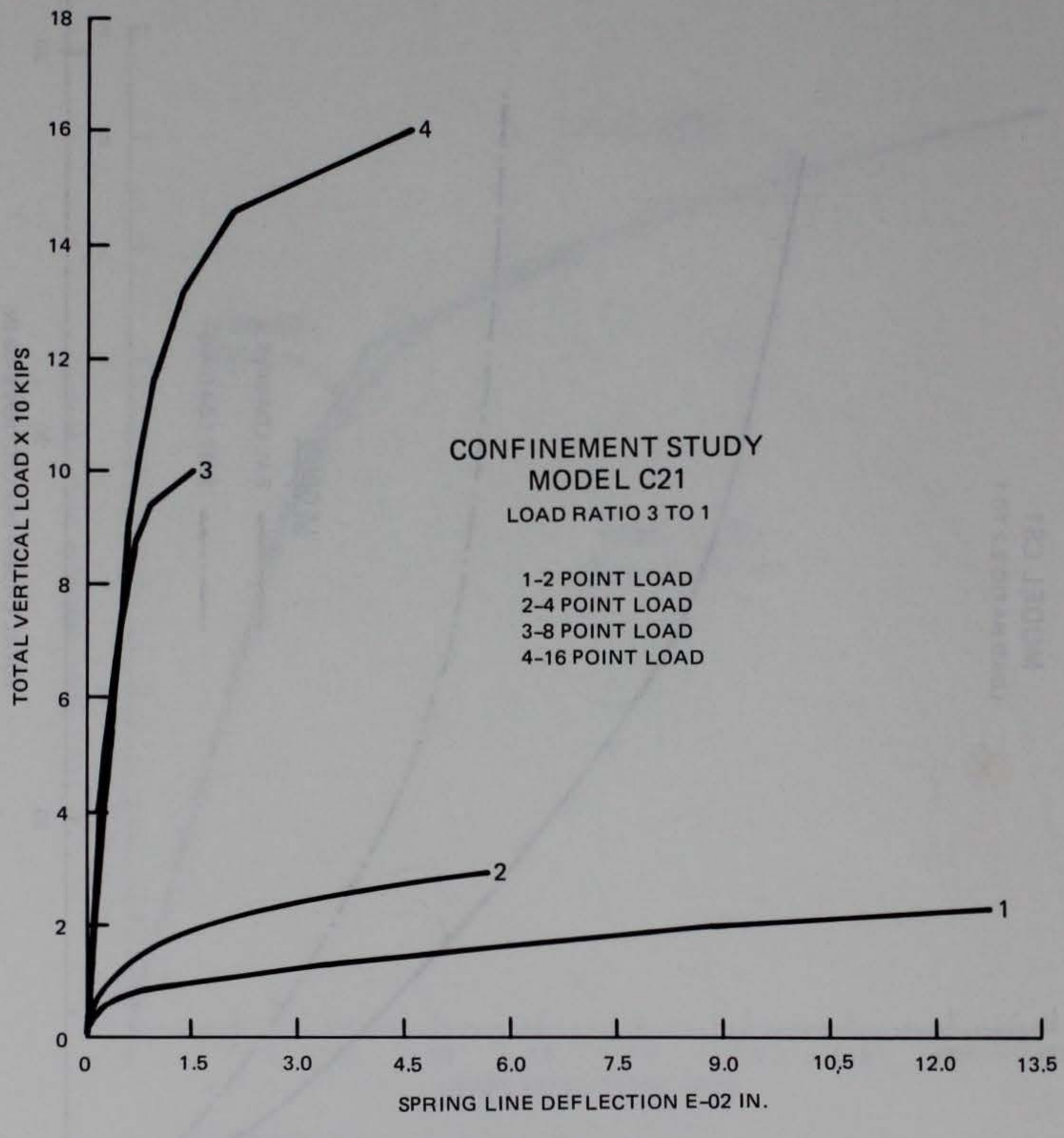

Figure 50. Total load versus crown deflection for Model C21

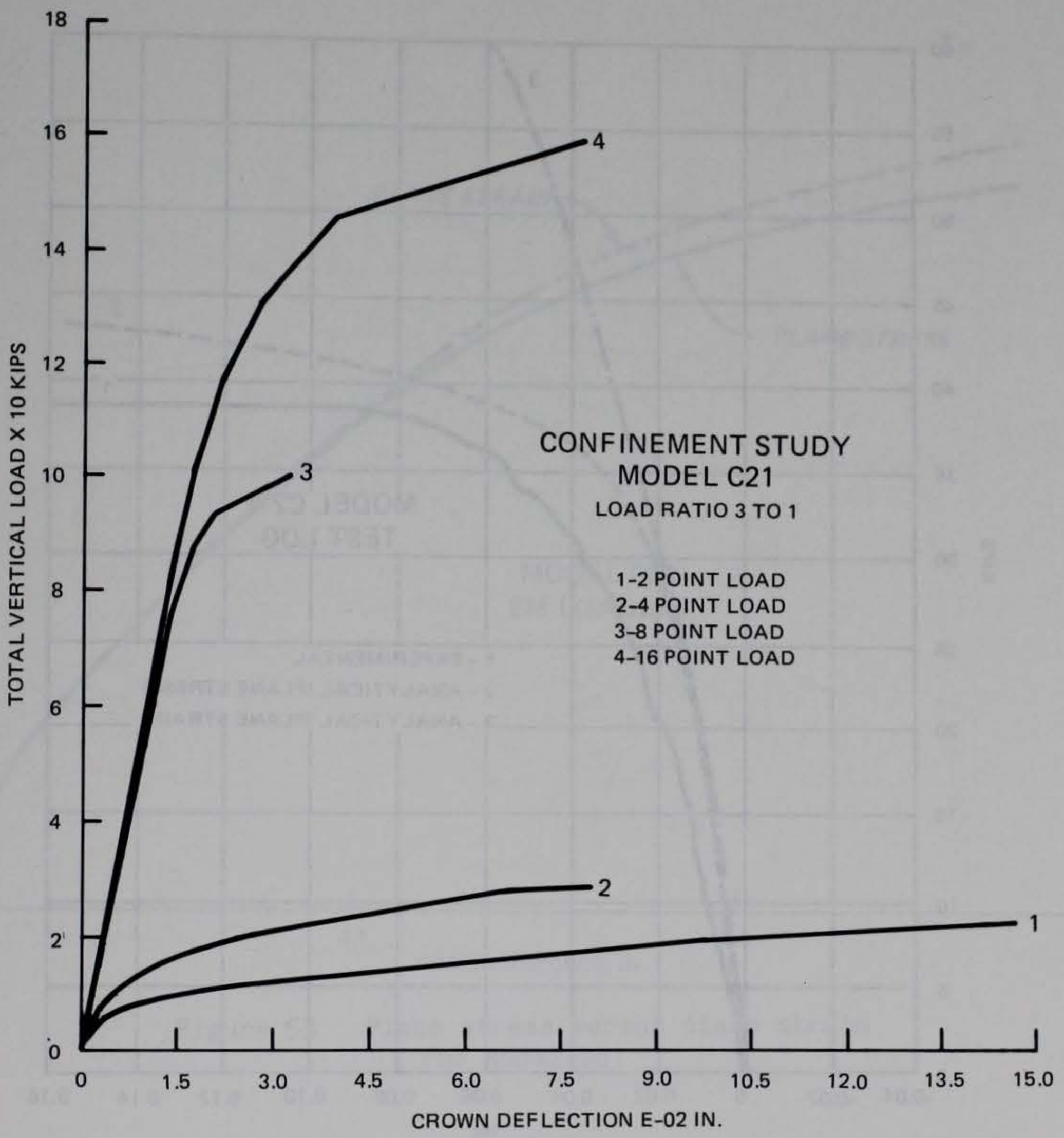

Figure 51. Total load versus springing deflections for Model C21

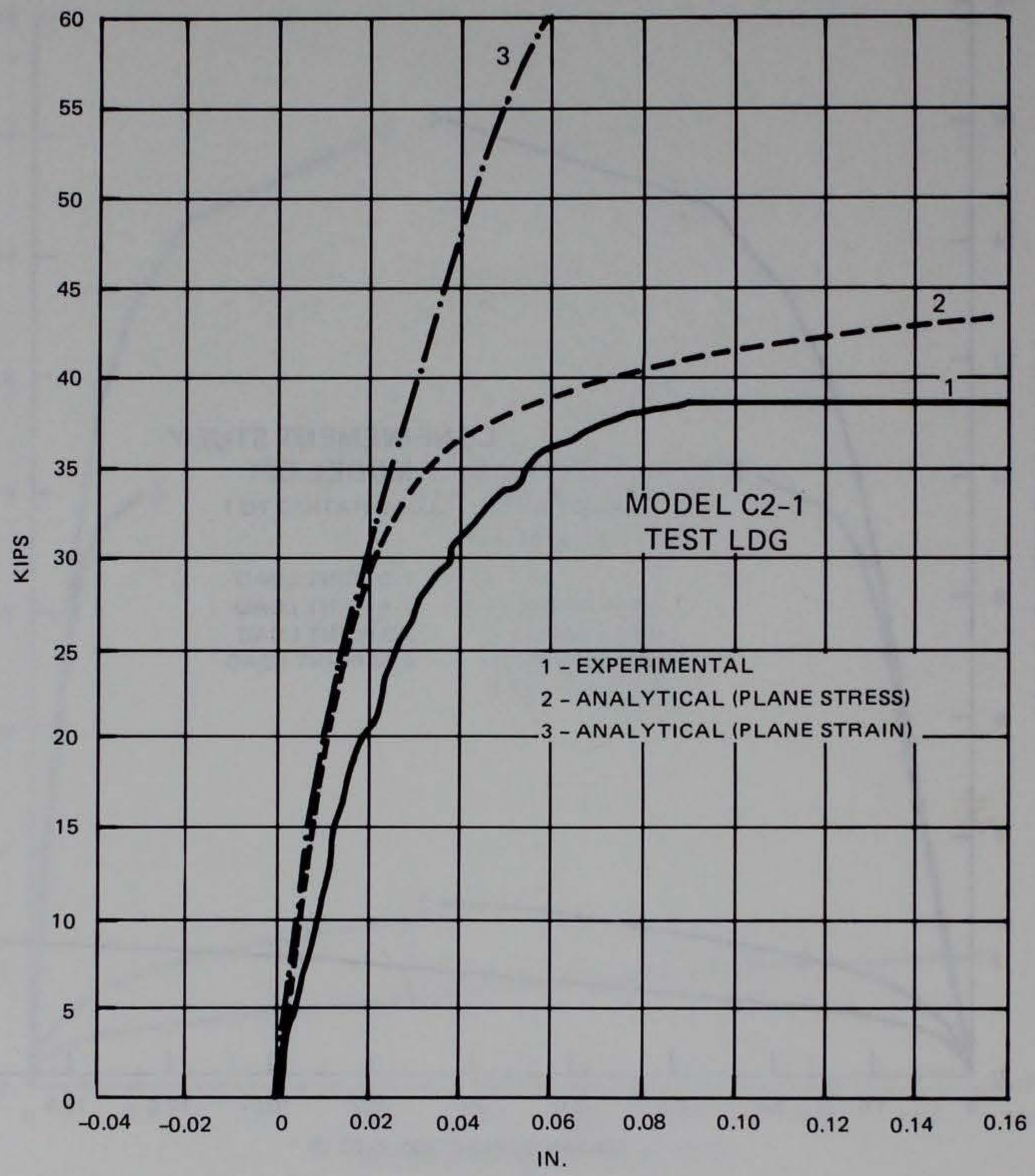

Figure 52. Plane stress versus plane strains for Model C2-1

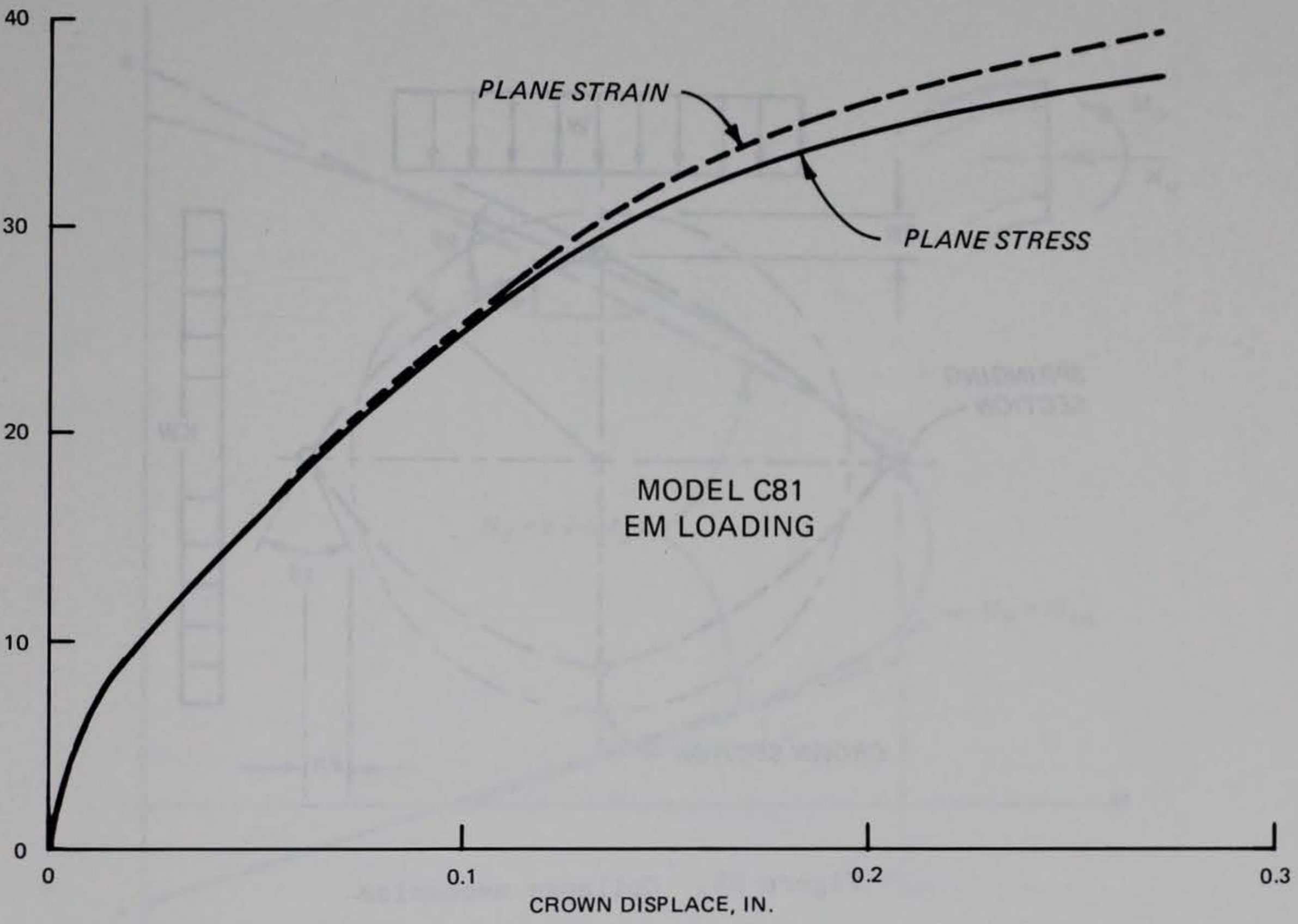

Figure 53. Plane stress versus plane strain for Model C81

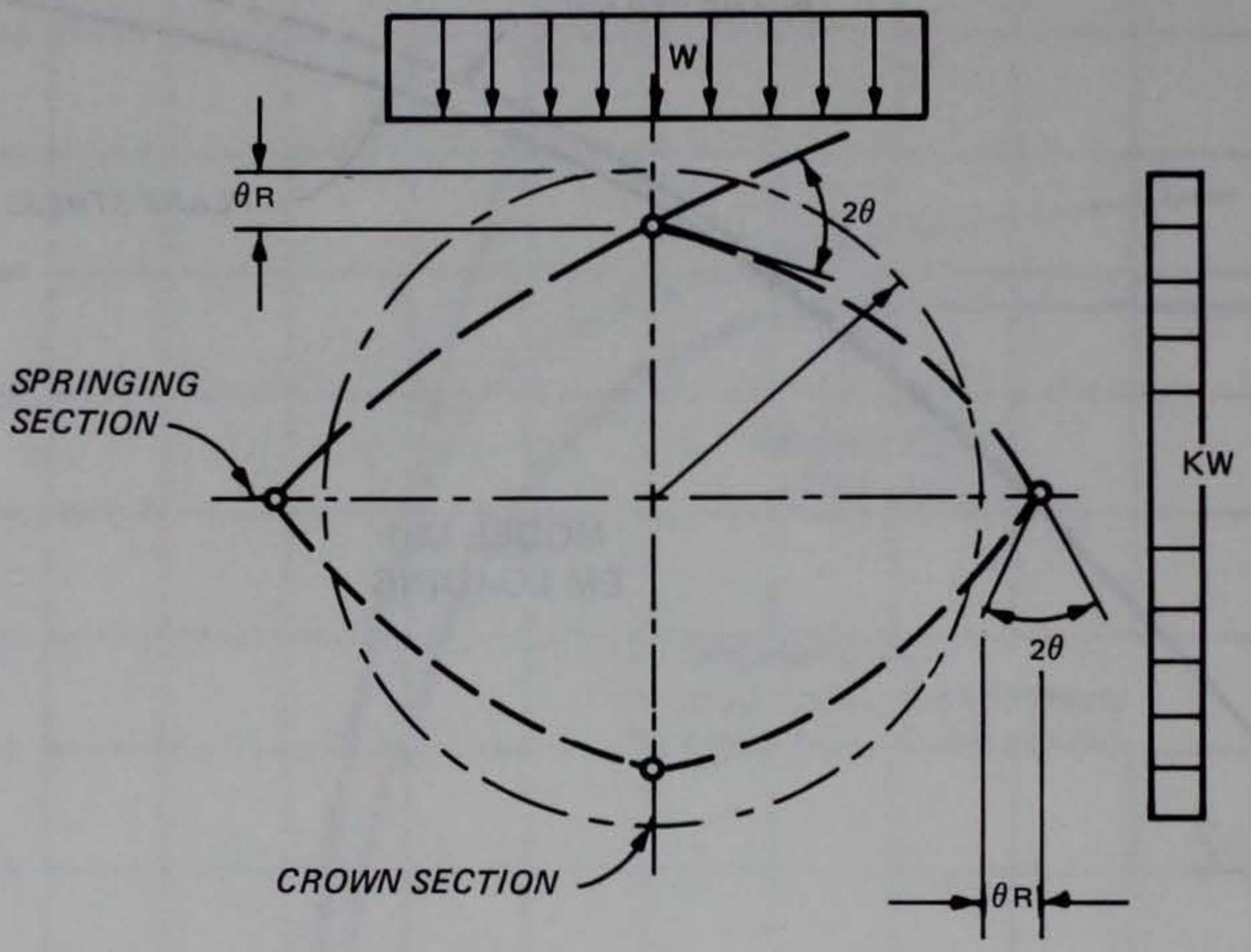

Figure 54. Collapse mechanism

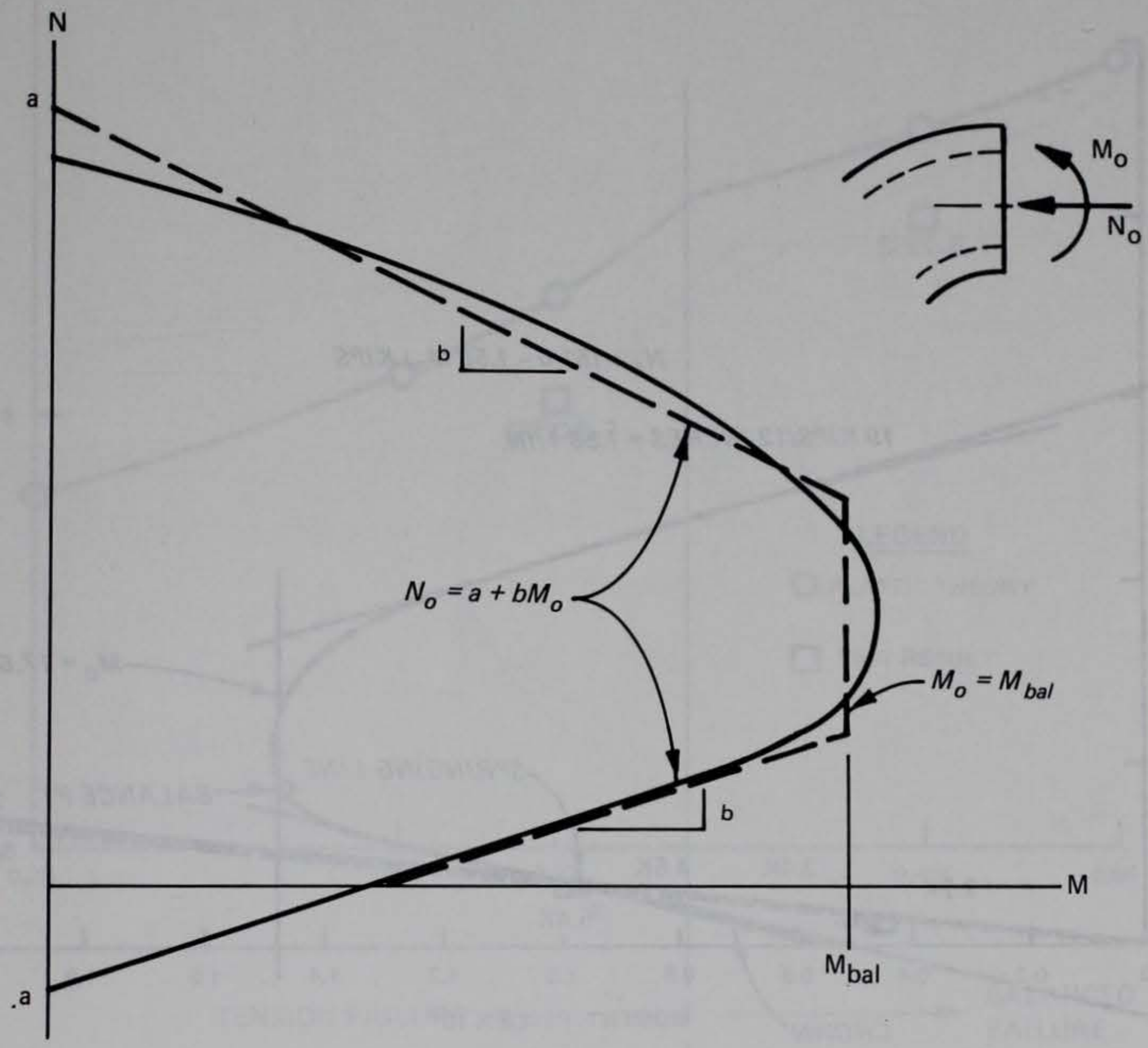

Figure 55. Actual and linearized strength envelope

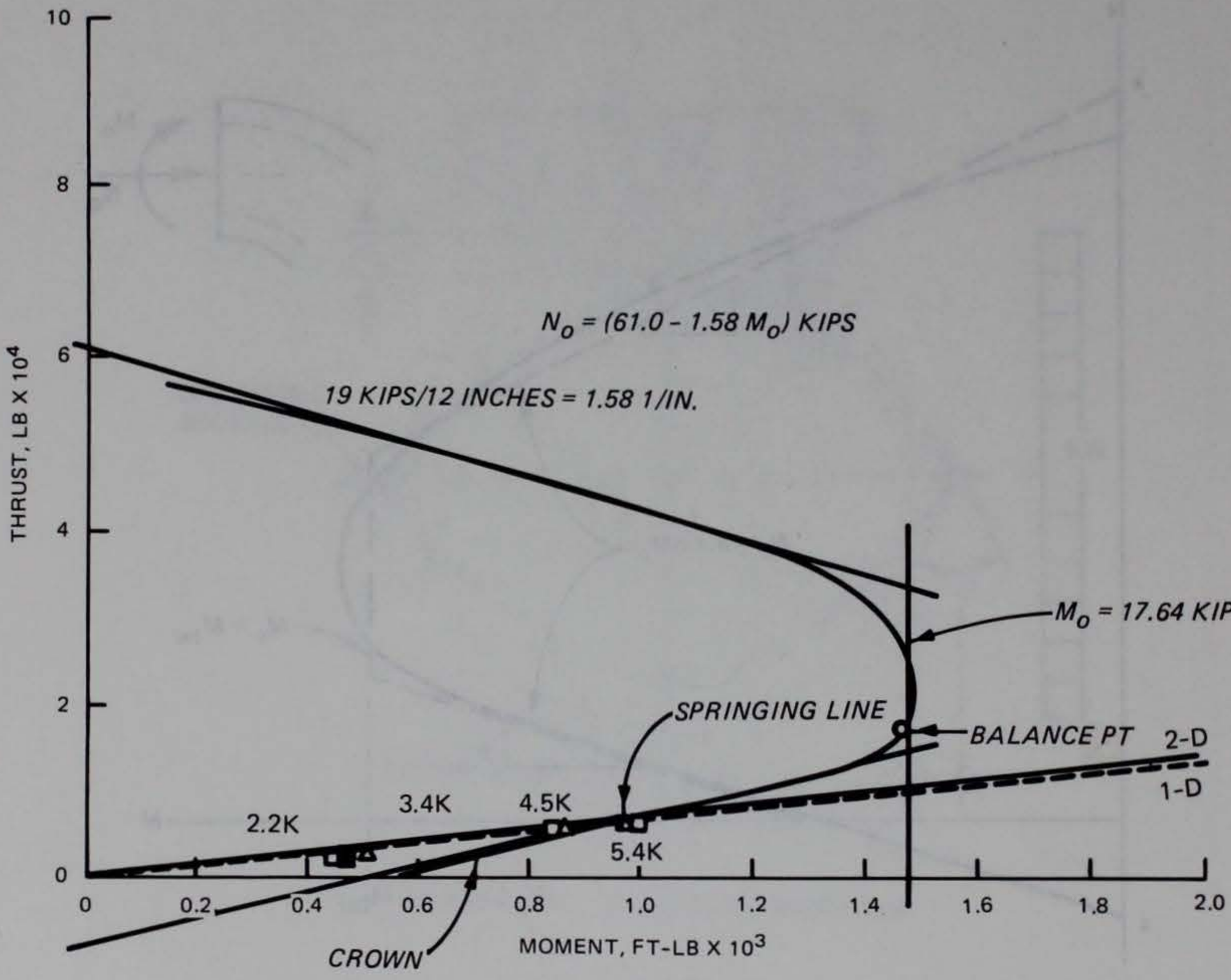

Figure 56. Interaction diagram for Model 8-1

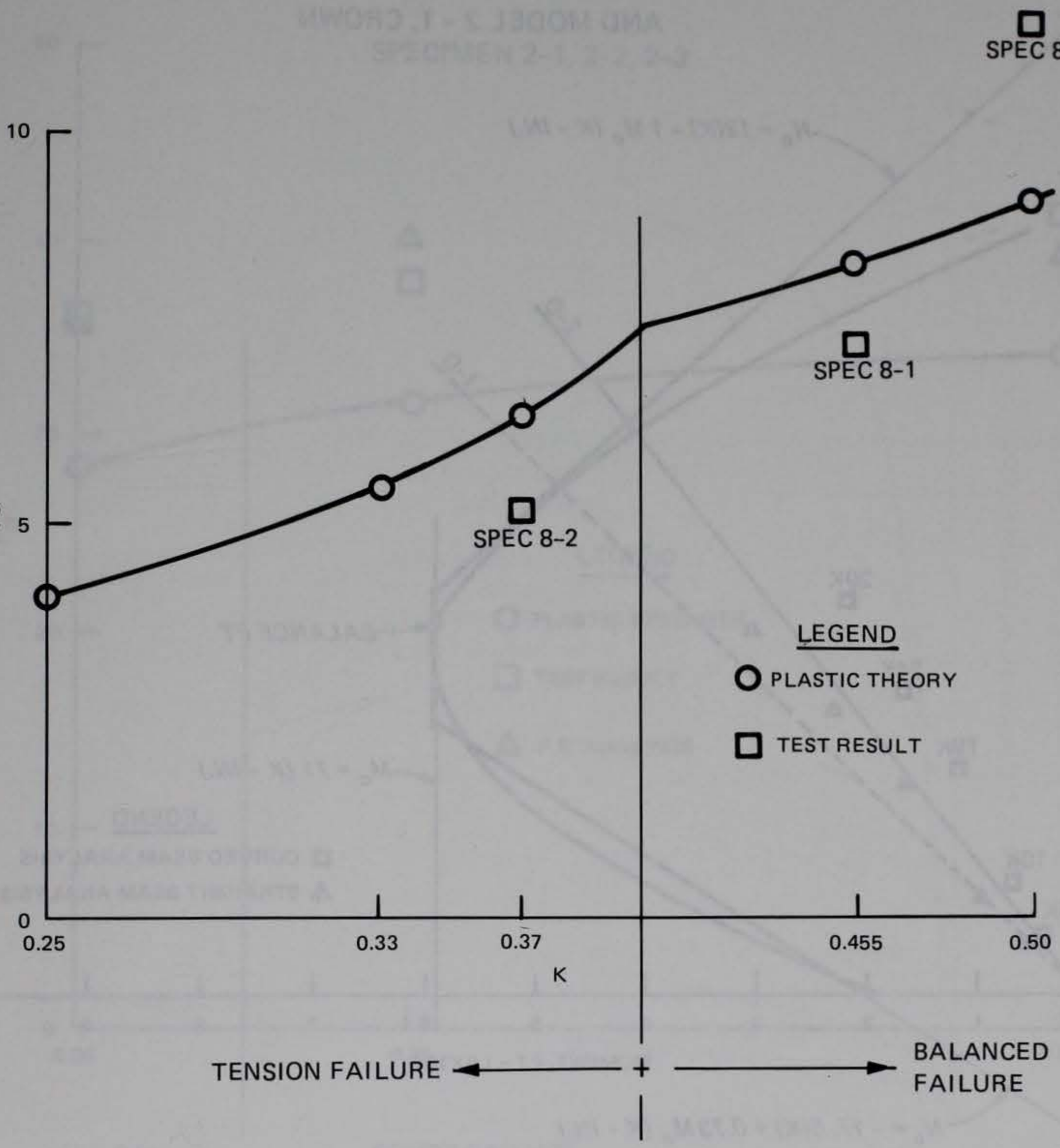

Figure 57. Plastic strength, thin rings

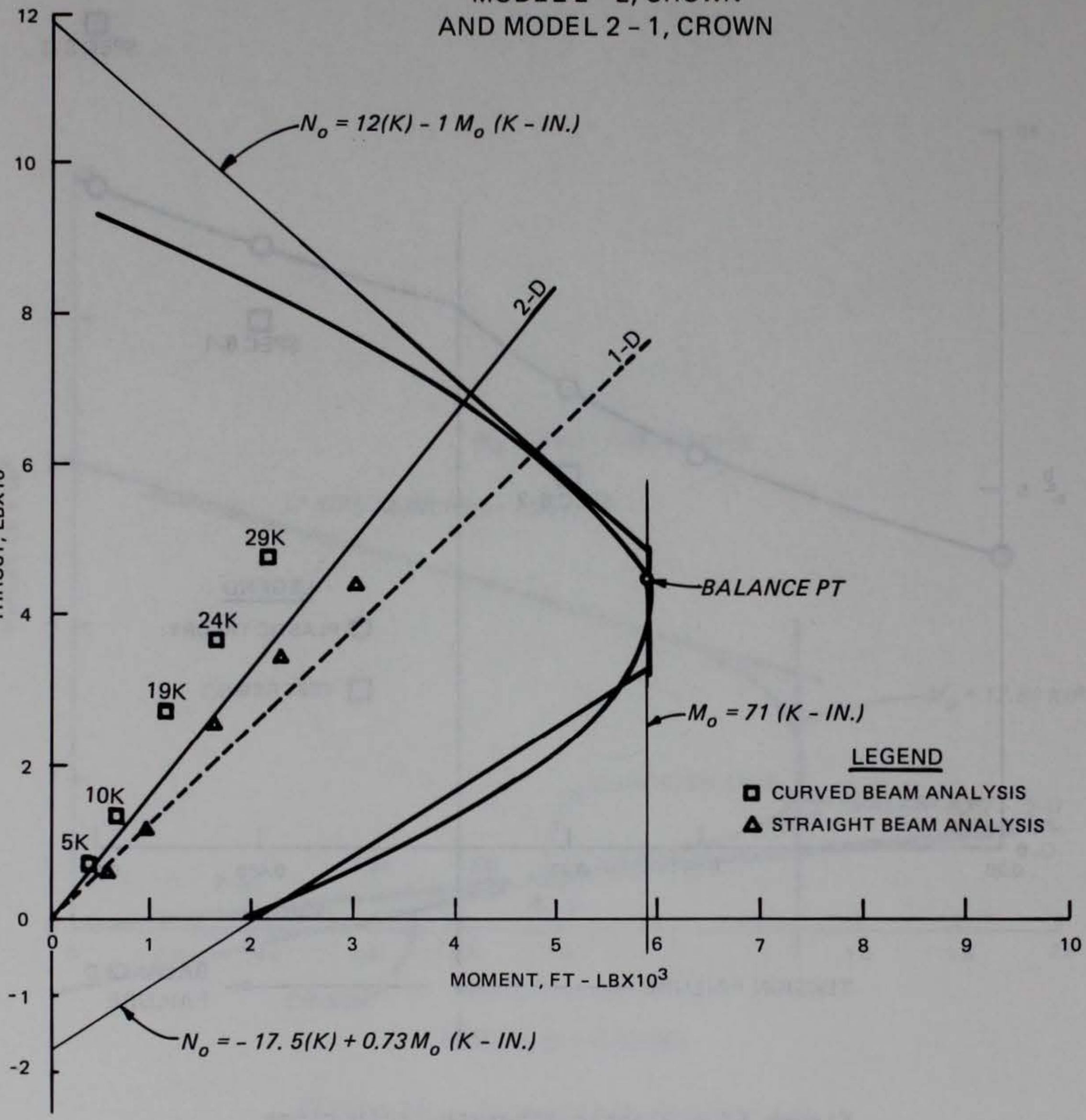

Figure 58. Interaction diagram for Models 2-1 and 2-2

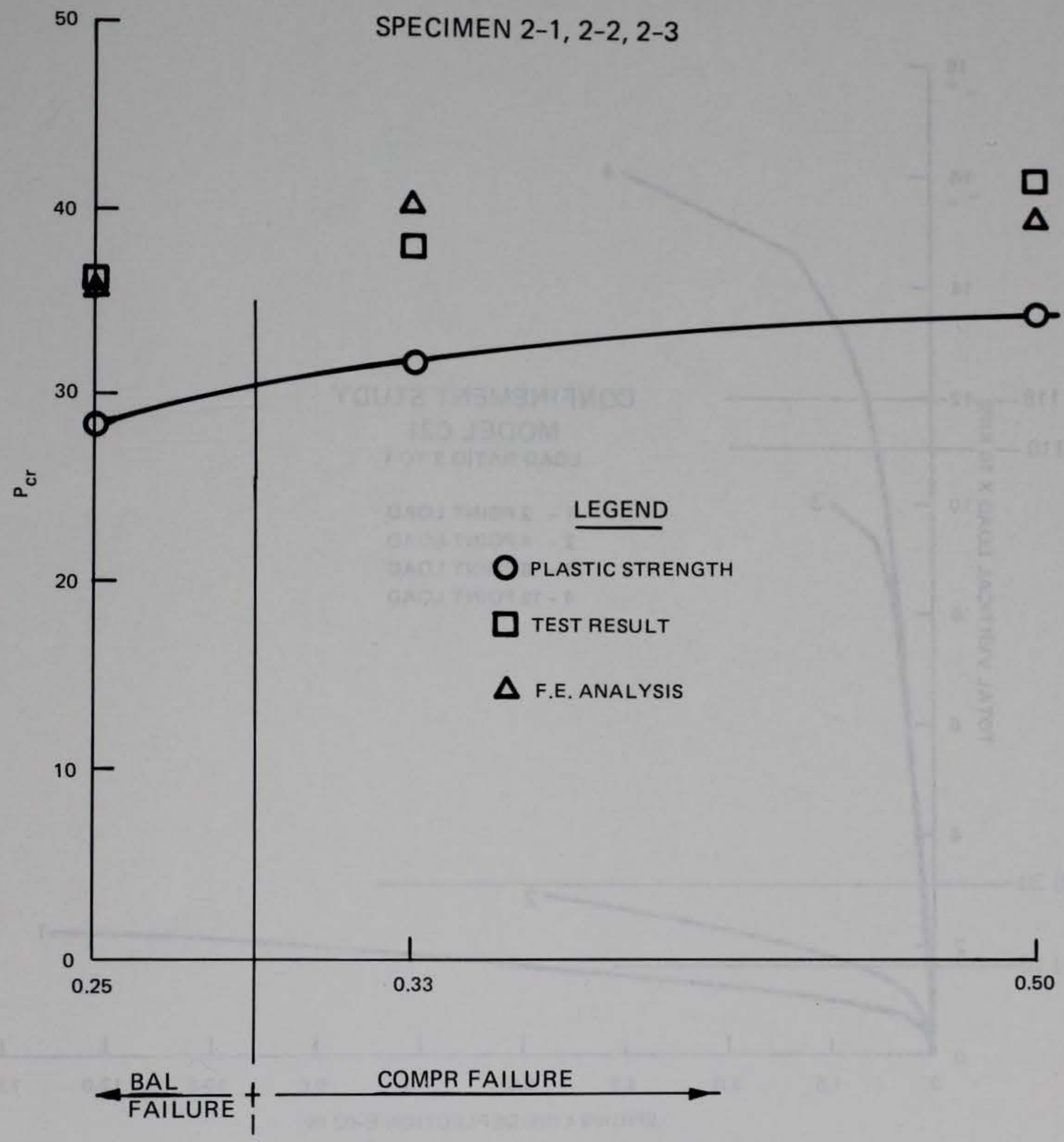

Figure 59. Plastic strength, thick rings

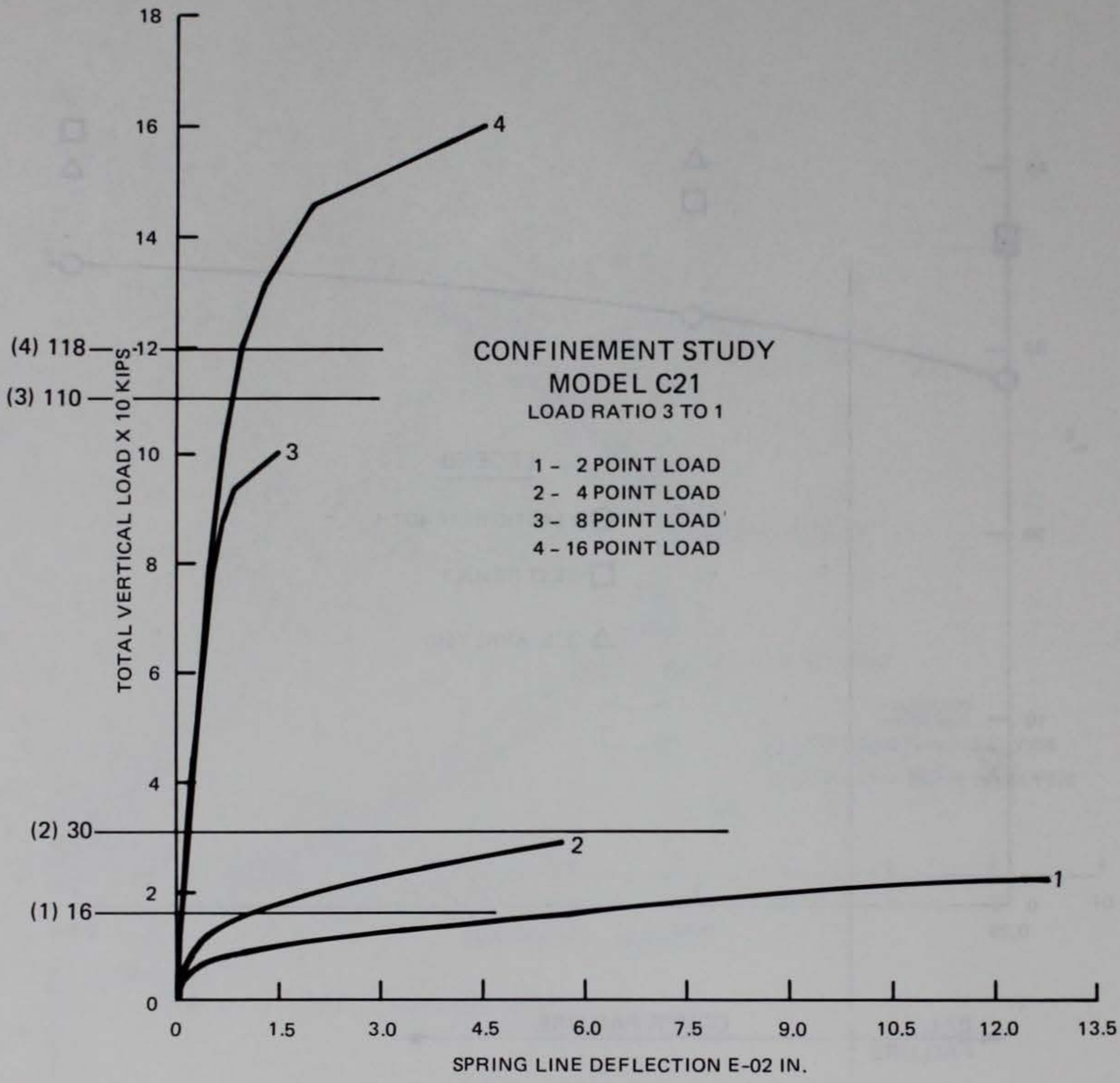

Figure 60. Load versus springline deflection for Model C21